

# **MUELLER MATRIX IMAGING FOR SKIN CANCER DETECTION**

A Thesis

by

ANGELA MICHELLE BALDWIN

Submitted to the Office of Graduate Studies of  
Texas A&M University  
in partial fulfillment of the requirements for the degree of

MASTER OF SCIENCE

May 2004

Major Subject: Biomedical Engineering

# MUELLER MATRIX IMAGING FOR SKIN CANCER DETECTION

A Thesis

by

ANGELA MICHELLE BALDWIN

Submitted to Texas A&M University  
in partial fulfillment of the requirements  
for the degree of

MASTER OF SCIENCE

Approved as to style and content by:

---

Gerard Côté  
(Chair of Committee)

---

Li Hong Wang  
(Member)

---

Henry Taylor  
(Member)

---

Clifford Spiegelman  
(Member)

---

William Hyman  
(Head of Department)

May 2004

Major Subject: Biomedical Engineering

## **ABSTRACT**

Mueller Matrix Imaging for Skin Cancer Detection. (May 2004)

Angela Michelle Baldwin, B.S., Louisiana Tech University

Chair of Advisory Committee: Dr. Gerard Coté

Over one million Americans are afflicted with skin cancer each year. Even though skin cancer has a 95% cure rate, approximately 10,000 people die in the United States each year of this disease. The current ABCDE(F) detection method is not sensitive enough to detect skin cancer in its early stages and requires a biopsy for any suspicious lesions. A lot of unnecessary biopsies, which are painful and costly to the patient, are taken. Therefore, a noninvasive technique is needed that can accurately detect the presence of skin cancer.

In this thesis, an optical approach will be presented that has potential to be a noninvasive skin cancer detection technique. Several morphological and biochemical changes occur as tissue becomes cancerous, and therefore the optical properties of the tissue can be used to detect skin cancer. A Mueller matrix imaging system has been developed by our group that measures the 16 or 36-element Mueller matrix, which completely describes the optical properties of the tissue sample. The system is automated and can collect the Mueller matrix in less than one minute. This system will be used to image Sinclair swine, and data analysis techniques will be employed to determine if the system can distinguish between cancerous and noncancerous tissue. System software improvements will also be made, and a new calibration technique will be presented.

## **DEDICATION**

This thesis is dedicated to my parents, Debra Pemberton and Tad Ryder, and to my husband, Dan Baldwin, and my daughter, Jordan. It is also dedicated to my grandfather, James Russell Noles, and stepfather, Ronnie Pemberton, who could not be here to see me accomplish this.

## ACKNOWLEDGMENTS

I would like to express my gratitude to my committee chair Dr. Gerard Côté for his continued technical support and encouragement throughout this research. I would also like to thank Dr. Cliff Spiegelman for his help with the statistical analysis for this thesis and Dr. Max Amoss for the Sinclair swine. I would also like to thank Justin Baba, a former Ph.D. student in the Optical Biosensing Laboratory, for his help with the data analysis. I would also like to thank all the graduate students in the Optical Biosensing Laboratory for their help and support.

I thank my family, Dan Baldwin and Jordan, my parents, my stepfather, and my grandparents for their support and love. I especially thank my mother, Debra Pemberton, for inspiring me to attain my goals and showing me the importance of education. I would also like to thank my grandfather, James Noles, for being a role model for me.

## TABLE OF CONTENTS

	Page
ABSTRACT .....	iii
DEDICATION .....	iv
ACKNOWLEDGMENTS .....	v
TABLE OF CONTENTS .....	vi
LIST OF FIGURES .....	viii
LIST OF TABLES .....	x
CHAPTER	
I    INTRODUCTION .....	1
II   BACKGROUND.....	4
2.1  Skin.....	4
2.2  Skin Cancer....	7
2.3  Optical Techniques for Skin Cancer Detection.....	10
2.4  Melanoma Morphology of the Sinclair Swine Animal Model.....	14
III  THEORY.....	15
3.1  Polarized Light and Stokes Vectors.....	15
3.2  Mueller Matrix.....	20
3.3  Classification and Regression Tree (CART) Software.....	22
IV  MATERIALS AND METHODS.....	27
4.1  Mueller Matrix Imaging System.....	27
4.1.1  Experimental Setup.....	27
4.1.2  Liquid Crystals.....	29
4.1.3  Polarization Vector.....	31

CHAPTER	Page
4.2	Current System Calibration..... 39
4.2.1	Main Calibration..... 39
4.2.2	Fine Tune the Calibration..... 46
4.3	Sinclair Swine Experiments..... 48
4.3.1	Data Collection..... 48
4.3.2	Data Analysis..... 49
4.4	New Calibration..... 50
V	RESULTS AND DISCUSSION..... 56
5.1	Mueller Matrix Results..... 56
5.2	CART Results..... 66
5.3	New Calibration Verification..... 70
VII	CONCLUSIONS AND FUTURE WORK..... 77
REFERENCES	..... 79
APPENDIX A	..... 83
APPENDIX B	..... 91
APPENDIX C	..... 94
APPENDIX D	..... 96
APPENDIX E	..... 97
APPENDIX F	..... 99
APPENDIX G	..... 117
APPENDIX H	..... 127
VITA	..... 135

## LIST OF FIGURES

FIGURE	Page
1. Anatomy of the Skin.....	5
2. Light as a Transverse Electromagnetic Wave.....	16
3. The Fully Automated Mueller Matrix Polarization Imaging System.....	28
4. Liquid Crystal Variable Rotator Schematic.....	30
5. Liquid Crystal Variable Retarder Construction.....	31
6. Theoretical Results for Rotator(2).....	41
7. Theoretical Results for Rotator(1).....	42
8. Theoretical Results for Retarder(2).....	44
9. Theoretical Results for Retarder(1).....	45
10. Sinclair Swine Model.....	48
11. Rotator2 Calibration Curve.....	52
12. Rotator1 Calibration Curve.....	53
13. Retarder2 Calibration Curve.....	54
14. Retarder1 Calibration Curve.....	55
15. HH Images of Skin Lesions from the Sinclair Swine.....	56
16. Mueller Matrix Images from the Sinclair Swine.....	57
17. Mueller Matrix for Images with Exposure Time 4 secs Obtained using 10 <sup>th</sup> Percentile of Each Image.....	60
18. Mueller Matrix for Images with Exposure Time 4 secs Obtained using 20 <sup>th</sup> Percentile of Each Image.....	60



FIGURE	Page
19. Mueller Matrix for Images with Exposure Time 4 secs Obtained using 30 <sup>th</sup> percentile of each image.....	61
20. Mueller Matrix for Images with Exposure Time 4 secs Obtained using 40 <sup>th</sup> percentile of each image.....	61
21. Mueller Matrix for Images with Exposure Time 4 secs Obtained using 50 <sup>th</sup> percentile of each image.....	62
22. Mueller Matrix for Images with Exposure Time 4 secs Obtained using 60 <sup>th</sup> percentile of each image.....	62
23. Mueller Matrix for Images with Exposure Time 4 secs Obtained using 70 <sup>th</sup> percentile of each image.....	63
24. Mueller Matrix for Images with Exposure Time 4 secs Obtained using 80 <sup>th</sup> percentile of each image.....	63
25. Mueller Matrix for Images with Exposure Time 4 secs Obtained using 90 <sup>th</sup> percentile of each image.....	64
26. Mueller Matrix for Images with Exposure Time 4 secs Obtained using the Mean of Each Image.....	64
27. 10-90 <sup>th</sup> Percentile and Mean Analysis for Raw M11 for Images with Exposure Time of 4 secs.....	65
28. 10-90 <sup>th</sup> Percentile and Mean Analysis for Raw M11 for Images with Exposure Time Less than 4 secs.....	66

## LIST OF TABLES

TABLE	Page
1. Summary of the Derivation of the Standard Polarization States from the General Elliptical Polarization.....	18
2. Mueller Matrix Equations for (a) 16, (b) 36, and (c) 49 Polarization Images.....	21
3. Rotation and Retardance Required to Produce Different Input Polarization States with Input Polarization at $+45^\circ$ .....	33
4. Voltage Settings for Retarder(1) Calibration.....	45
5. Learning Sample Probability.....	67
6. Results from CART Analysis of Data with Exposure Time 4 seconds.....	68
7. Cross Validation Probability.....	68
8. Decision Matrix for Cancer.....	69
9. Decision Matrix for Mole.....	69
10. Relative Importance of the Variables.....	70
11. Mueller Matrix Results for Air .....	71
12. Mueller Matrix Results for Horizontal Polarizer.....	71
13. Mueller Matrix Results for $+45^\circ$ Polarizer.....	72
14. Mueller Matrix after Fine Tune Calibration for Air.....	73
15. Mueller Matrix after Fine Tune Calibration for Horizontal Polarizer.....	74
16. Mueller Matrix after Fine Tune Calibration for $+45^\circ$ Polarizer.....	74
17. Standard Deviation of Each Mueller Matrix Element for Each Sample...	76

## CHAPTER I

### INTRODUCTION

Biological tissues can be characterized by their optical properties, namely the absorption coefficient ( $\mu_a$ ), the scattering coefficient ( $\mu_s$ ) and the anisotropy factor ( $g$ ). The scattering of light in tissues is primarily due to tissue morphology and the absorption of light is due primarily to tissue biochemistry. Skin tissue is known to be birefringent primarily due to the ordered collagen fibers in the tissue. Birefringence in the skin is responsible for the strong randomization of polarized light. The tissue morphology and biochemistry change as tissue becomes cancerous and therefore the optical properties can potentially be used as a means of detecting skin cancer. It is hypothesized that when backscattered light is observed, cancerous tissues, due to unordered collagen fibers, increased size of cell nuclei, and added mitochondria, depolarize light less than non-cancerous tissue. This is because cancerous tissues do not allow the light to penetrate the tissue as deeply and therefore undergo less scattering than non-cancerous tissues. This is the basis for the use of an optical method of noninvasive skin cancer detection used in this thesis.

The American Cancer Society estimates that more than 1 million new cases of basal cell and squamous cell carcinoma will be diagnosed in the United States each year [1]. In 2004 alone, it is estimated that there will be approximately 59,350 new cases of melanoma and an estimated 10,250 deaths attributed to all forms of skin cancer [1]. These figures have increased from the 2003 estimate, which approximated 58,800 new

---

This thesis follows the style and format of the *IEEE Transactions on Biomedical Engineering*.

cases of melanoma and 9,800 deaths [2]. In addition, nearly half of all new cancer cases are skin cancers, which have a 95% cure rate if detected and treated early [3]. The current method of detecting skin cancer is the ABCDEF technique, which stands for Asymmetry, Border, Color, Diameter, Evolutionary change, and Funny-looking lesion [3]. With this technique if a lesion looks suspicious, a biopsy of the suspect lesion is required in order to determine if cancer is present. Many times an unnecessary biopsy, which is very painful and costly to the patient, is taken [3]. Therefore, a technique is needed that can non-invasively and effectively detect skin cancer.

As a tissue becomes cancerous, several morphologic and chemical changes occur that affect the optical properties of the tissue. Uncontrolled growth in cancerous tissue causes the ordered collagen fibers to break down and thus changes the birefringence of the tissue [4]. Also due to increased blood perfusion, cancerous tissue is typically higher in absorption than normal tissue [5]. Finally, cancerous cells are known to change their morphology, such as increased nucleus size or number of mitochondria, which changes the light scattering properties of the tissue [6]. An optical approach, specifically polarimetry, will be used to sense these types of changes and ideally distinguish cancerous from non-cancerous tissue. Polarized light was chosen because it carries information about birefringence, absorption, and scattering simultaneously.

The Automated Mueller Matrix Polarization Imaging System (AMMPIS) developed by our group measures the 16 or 36-element Mueller matrix, which completely describes the optical properties of the sample. This is accomplished by using all combinations of polarized input and output light, including horizontal, vertical,  $\pm 45^\circ$ ,

and right and left circular. The polarization states are created using an input and output arm that both consist of a polarizer, liquid crystal variable rotator, and liquid crystal variable retarder. In order to create the required polarization states, each electro-optic component must be calibrated so that the required voltage can be determined which is a time consuming process. The first goal of this thesis is to improve the calibration technique by using Matlab and Labview software to automate the calibration steps. The second purpose of this thesis is to image Sinclair swine and determine a method of analyzing the images that can differentiate between normal, mole, and cancerous tissue.

## **CHAPTER II**

### **BACKGROUND**

This chapter presents the background necessary to understand this research, and the significance of the problem needed to understand why this research is important. The first section gives a general overview of the skin, and the second section describes the types of skin cancer, their causes, their symptoms, and their current treatments. The third section describes the optical techniques that are currently being investigated and their limitations for skin cancer detection. The final section gives an overview of the melanoma morphology of the Sinclair swine animal model that is used in this research.

#### **2.1 Skin**

The skin is the largest and one of the most versatile organs of the body, and it is vital in maintaining homeostasis. It is a turbid medium that has two distinct tissue layers (Figure 1). The outer layer, called the epidermis, is composed of stratified squamous epithelium. Its thickness ranges from 0.07 mm to 0.12 mm, and it is constantly renewing itself. The epidermis consists of four cell types and five layers. The four cell types are keratinocytes, melanocytes, Merkel cells, and Langerhans cells. Keratinocytes (called squamous cells) produce keratin that helps protect the body, melanocytes produce the dark pigment melanin that provides skin color, Merkel cells associate with a disc-like sensory nerve ending to form the Merkel disc, and Langerhans cells aid in the defense against microorganisms. The five layers are the stratum basale, stratum spinosum, stratum granulosum, stratum lucidum, and stratum corneum. The stratum basale is the

deepest layer, and is composed of a single row of melanocytes and cuboidal or columnar cells that reproduce and grow. The stratum spinosum is the next layer and is composed of many layers of cells with centrally located, large, oval nuclei and developing fibers of keratin. The stratum granulosum is three to five layers of flattened granular cells that contain shrunken fibers of keratin and shriveled nuclei. The stratum lucidum, which is only on the soles and palms and is between the stratum corneum and stratum granulosum, has cells that appear clear and have nuclei, organelles, and cell membranes that are no longer visible. The outer most layer, the stratum corneum, is composed of many layers of keratinized, dead epithelial cells that are flattened and nonnucleated [7].

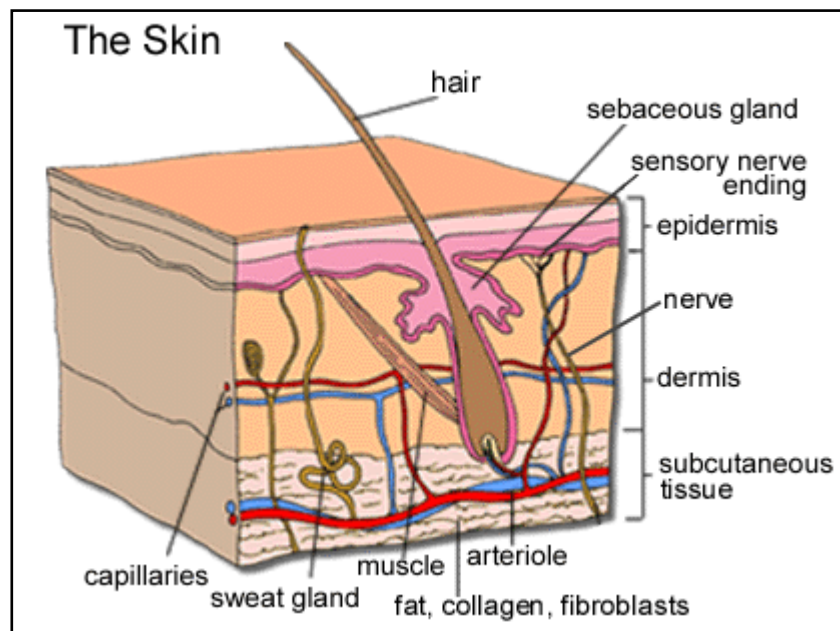


**Figure 1:** Anatomy of the Skin [8]

The inner layer of skin, or dermis, is thicker than the epidermis, and it is made up of connective tissue containing collagen and elastic fibers, epithelial tissue, smooth muscle tissue, nervous tissue, and blood. The average thickness of the dermis is 1-2 mm and varies from 0.5 mm or less on the eyelids to 3 mm on the soles of the feet. The dermis consists of two layers: the papillary layer and the reticular layer. The papillary layer is the outer layer closest to the epidermis and is composed of areolar loose connective tissue. The reticular layer is the deepest and thickest layer. It is made of dense irregular connective tissue containing thick bundles of interlacing collagen fibers and elastic fibers. Beneath the dermis, the hypodermis, which is composed of masses of loose connective and adipose tissues, binds the skin to the underlying organs [7].

Skin is composed of many light scattering and light polarization changing components, including numerous membrane-bound subcellular organelles such as the nuclei, mitochondria, secretory granules, melanosomes, and the highly laminated desmosomes. Another source of light polarization change in the skin is the birefringence of epidermal keratin and dermal collagen. Cancerous tissue is characterized by disordered cell maturation and epithelial architecture, keratin composition, fibrillar packing and loss of cellular orientation, which could influence the transport and remittance of polarized light. Also, differences in nuclei and mitochondrial size and concentration are often seen between normal and cancerous tissues that could be measured using the polarimetric approach.



## 2.2 Skin Cancer

The American Cancer Society estimates that more than 1 million new cases of basal cell and squamous cell carcinomas and approximately 55,100 new cases of melanoma will be diagnosed in the United States each year [1]. In 2004 alone, it is estimated that there will be approximately 10,250 deaths, 7,910 from melanoma and 2,340 from other non-epithelial cancer, attributed to the disease [1]. In addition, nearly half of all new cancer cases are skin cancers, which have a 95% cure rate if detected and treated early [3].

Three main types of skin cancer exist: basal cell carcinoma, squamous cell carcinoma, and melanoma. Basal cell carcinoma is the most common form of skin cancer, affecting more than 800,000 Americans each year [9]. It is also the most common form of all cancers. Basal cell carcinomas arise in the basal cells, which are at the bottom of the epidermis. Squamous cell carcinoma, the second most common skin cancer, afflicts more than 200,000 Americans each year [10]. It arises from the epidermis and resembles the squamous cells that comprise most of the upper layers of the skin. Melanoma is the most serious form of skin cancer. During the past 10 years the number of cases of melanoma has increased more rapidly than that of any other cancer. Early detection of melanoma is crucial to the patient's survival. If melanoma is left undiagnosed, it will metastasize to other parts of the body. Melanoma is a malignant tumor that originates in the melanocytes, the cells that produce the pigment melanin that colors the skin, hair, and eyes. Melanoma falls into four basic categories: superficial spreading melanoma, nodular melanoma, acral lentiginous melanoma, and lentigo

maligna melanoma. Superficial spreading melanoma, which spreads laterally before it invades the deeper tissues, is the most common type and may produce tumors on any part of the body. Nodular melanomas invade deeper tissues earlier than superficial spreading melanomas and tend to have a poorer prognosis. Acral lentiginous melanoma is most commonly found in dark-skinned people and has the poorest prognosis. Lentigo maligna melanoma is the slowest growing form of melanoma and occurs on sun-damaged skin of elderly patients [11].

Squamous cell carcinoma usually appears as a tiny, painless nodule or patch that sometimes is surrounded by a margin of inflammation. The surface of the cancer can be scaly, crusted or wartlike, and its center can form an open sore [10]. Basal cell carcinoma usually appears as a tiny, painless lump with a shiny surface. As the cancer slowly grows, the center of the lump may become sore and produce a crater that bleeds, crusts, or forms a scab [11]. If a lesion is suspect, a biopsy is performed to verify the diagnosis. For squamous cell and basal cell carcinomas, the most common treatment options are excision, curettage and electrodesiccation, cryosurgery, radiation, and Moh's micrographic surgery. Excision is where all visible cancer is cut away together with a 3 to 10 mm margin of healthy tissue and then the skin is stitched closed with sutures. Curettage and electrodesiccation are where all visible cancer is scraped away and then an electric probe is used to kill any remaining microscopic malignant cells. For very small tumors, cryosurgery, which is a technique whereby cancerous cells are killed by freezing them with liquid nitrogen, is used. Radiation destroys the cancer with high-energy rays aimed from outside the body. For cancers on the eyelids, nose, fingers, and other areas, a

technique called Moh's micrographic surgery is used that shaves away the tumor in thin layers and one layer at a time is checked under the microscope in order to preserve as much healthy tissue as possible. Other less common treatments are (1) 5-fluorouracil (Efudex, Fluoroplex), which is an anticancer drug applied directly to the skin, (2) laser therapy, which uses a narrow laser beam to destroy the cancer, (3) chemotherapy, and (4) photodynamic therapy, which kills cancer with chemicals and light. The most effective treatment depends on many factors, including the size and location of the cancer, whether it has recurred, and age and general health of patient [12, 13].

The current method of detecting melanoma is the ABCDEF technique, which stands for Asymmetry, Border, Color, Diameter, Evolutionary change, and Funny-looking lesion [14]. The criteria are as follows: Asymmetry- one side of the lesions is unlike the other side of the lesion, Border-scalloped or blotchy borders or pigment that appears to blend into the surrounding skin, Color-multiple colors or shades, Diameter-sudden increase in size or larger than 6 mm, and Evolutionary change-changes in color, size, symmetry, surface characteristics, pain, bleeding, and tenderness. The last criterion is added to improve the diagnostic sensitivity of the method. It insures a low threshold for biopsy of suspect lesions even if they don't meet the ABCDE criteria. With this technique, a biopsy of the suspect lesion is required in order to determine if cancer is present. If the lesion is cancerous, then it is excised along with a margin of normal-looking skin [15].

### 2.3 Optical Techniques for Skin Cancer Detection

Several optical approaches have been used for the detection of skin cancer. One technique is optical coherence tomography (OCT), which is based on the Michelson interferometer. OCT is a novel tomographic imaging technique with micron scale resolution that can be used to image through highly scattering media, such as tissue [16]. OCT can also be combined with polarization to detect the presence of cancer. Polarization sensitive OCT (PS-OCT) reveals important information about biological tissues such as birefringence, which is related to the collagen of the tissue. Cancer causes the collagen fibers in the tissue to breakdown and therefore this technique could be used to detect this change. PS-OCT measures the Mueller or Jones matrix of the sample, where the latter is possible because OCT only detects the coherent light [17]. The Jones matrix reduces the number of images required and therefore reduces the imaging time. Even though PS-OCT has very high resolution, it has four main problems: (1) a limited depth of field (1-2 mm) [18], (2) slow measurement speed, (3) speckle appearance on images [19], and (4) fiber polarization [20].

Another optical modality for skin cancer detection is fluorescence spectroscopy. This method uses the autofluorescence of the skin to detect changes between normal and cancerous tissue. Brancalion *et al* have shown that endogenous fluorescence due to tryptophan was more intense in both basal cell carcinomas and squamous cell carcinomas than in normal tissue [21]. Another modality that uses fluorescence for skin cancer detection is photodynamic therapy. Photodynamic therapy uses the combination of light and photosensitizers to detect or treat cancer. Photosensitizers are molecules that

have the property of absorbing light energy and using this energy to carry out chemical reactions in cells and body tissues. The most popular photosensitizer is 5-aminolaevulinic acid (ALA), which is a metabolic precursor in the biosynthesis of heme. The immediate precursor to heme in this pathway is protoporphyrin IX (PpIX), which is a natural photosensitizer. With the method, the photosensitizer is applied topically or injected into the blood stream and absorbed by cells all over the body. PpIX is then induced rather selectively in epithelial tumors, which can be visualized after excitation with light. A CCD camera can be used to acquire fluorescence images of the cancerous tissue [22]. This method has several disadvantages. First, it is not cancer specific and therefore even healthy cells take up the photosensitizer. Also, the patient must avoid direct sunlight and bright indoor light for at least 6 weeks because the treatment makes the skin and eyes sensitive to light [23].

Scattered light has also been used for cancer detection. The two types of optical scattering are elastic and inelastic. The elastic scattering can be described using Mie theory (or Rayleigh scattering for particles small compared to the wavelength), which relates the intensity of the scattered radiation with the concentration, size, and shape of the scattering particles. Mourant *et al* have shown that differences in scattering from cells in different stages of growth are due to internal changes of the nucleus. They also found that light scattering is caused by both the nucleus and cytoplasmic structures such as mitochondria [24]. Since tissue undergoes many morphological changes that occur due to changes in size and shape of the cellular and subcellular structures, this method could be used to detect changes in tissue as it becomes cancerous. The disadvantages of

this method are that multiple wavelengths may be required, and its effectiveness is limited in tissues because the effects of many scatters is not known.

The inelastic scattering approach that is used to identify cancer is Raman spectroscopy. Raman measures the molecular specific inelastic scattering of laser light within tissue, which enables the detection of biochemical changes as tissue becomes cancerous [25]. Huang *et al* have shown that Raman signals differ significantly between normal and cancerous tissue, with tumors showing higher percentage signals from nucleic acid, tryptophan, and phenylalanine and lower signals from phospholipids, proline, and valine, compared to normal tissues [26]. Another study found that there were no differences in water content between malignant and benign skin tumors, but the tetrahedral (free) water structure was found to increase in malignant skin tumors and sun-damaged skin relative to normal, healthy skin and benign tumors [27]. Even though this technology shows to be promising for skin cancer detection, the Raman signal in general is very weak and the equipment is bulky and expensive [18]. Also, background fluorescence from the skin inhibits the Raman signal.

Polarized light, the topic of this thesis, is the last optical modality to be discussed. The concept behind this method is that the amount of rotation of polarized light changes with the concentration of an optically active material such as collagen. Collagen fibers begin to breakdown as tissue becomes cancerous and therefore change the amount of rotation of polarized light. Also, changes in size and shape of cellular and subcellular structures cause light to depolarize less in cancerous tissue than in normal tissue. In 1808, E.L. Malus noted the effects of polarization when he noticed that light

was not the same in all directions around its line of travel [28]. In 1812, Biot developed the first known polarimeter and formulated the quantitative laws of polarimetry [29]. Many other advances in the field of polarimetry between the 17<sup>th</sup> and 19<sup>th</sup> century can also be attributed to the works of Bartholinus, Huygens, Brewster, Arago, Newton and Fresnel but will not be described in detail here [29]. In 1976, Bickel et al. advanced polarimetry into the field of biomedical sensing when they described a technique that measured the polarization effects of the forward-scattered light from bacterial suspensions [30]. However, more recently there is a growing interest in the use of backward-scattered polarized light in biomedical applications [31-34]. Hielscher et al [35] introduced the Mueller matrix imaging concept for diffusely backscattered light from turbid media. They have investigated cancerous and noncancerous cell suspensions using this technique, but had to manually insert 49 various polarizer/analyzer combinations that took over 2 hours to produce the Mueller matrix. Pezzaniti et al. have presented data for a mechanical transmission-based 16-EMM polarization imaging system [36]. For their system, it took approximately 3 minutes to sequence through all of the measurements recorded by a 512 X 512 CCD detector [36]. Other semi-automated systems have also been developed that use Mueller matrix imaging [37-39]. This group has developed an Automated Mueller Matrix Polarization Imaging System (AMMPIS) that measures the experimental 16-element Mueller matrix of a sample in near real-time, which is needed for *in vivo* imaging [40]. The system is capable of collecting the Mueller matrix in less time than that of currently developed systems.

## **2.4 Melanoma Morphology of the Sinclair Swine Animal Model**

The Sinclair swine model was established at Texas A&M in the 1970's by Dr. Max Amoss in the College of Veterinary Medicine and have been selectively bred to increase the frequency of Sinclair swine cutaneous melanoma (SSCM) [41]. The model has been considered a useful model for human melanoma and up to 85% of these animals are born with or develop cutaneous melanoma soon after birth [41]. The natural history of the Sinclair swine cutaneous melanoma (SSCM) tumor follows a predictable pattern of growth and spontaneous regression. The SSCM tumor progresses through four phases. The first phase is from birth to around 30 days of age and the tumor is characterized by a rapid increase in melanoma cell numbers. During the second phase, from about 30 to 60 days of age, there is an initial phase of regression marked by infiltration of macrophages and a decrease in melanoma cell numbers. Unique to this model is a third phase, beginning at around 60 days of age, during which surviving melanoma cells undergo rapid clonal expansion. This rapid growth phase usually begins to slow at about 90 days of age when lymphocytes infiltrate the tumor and the final phase of regression is initiated. The fourth phase is total regression of the tumors, which is usually achieved by around 120 days of age. This well characterized model will be used to test the proposed system and guide the analysis of the polarization images.



## CHAPTER III

### THEORY

The fundamental theories underlying this research are described in this chapter. The first section reviews the optical principles involved in polarimetry and the Stokes vector. The relationship between the Stokes vector and the Mueller matrix is discussed in the second section. The final section describes the statistical analysis software that was used in this research to classify the image data taken from the Sinclair swine.

#### 3.1 Polarized Light and Stokes Vectors

Under normal atmospheric conditions, it has been well established that light can be treated as an electromagnetic wave. Light consists of both electric and magnetic waves and therefore has inherent magnitude and phase for each (Figure 2). In terms of the science of polarization and the property of light to be polarized, the magnetic vector is ignored, as it holds no bearing on the polarization phenomenon. Therefore, in discussing the principle of polarization only the electric field of light will be of value. Light is also considered a transverse electromagnetic wave (Figure 2) meaning that the medium is displaced in a direction perpendicular to the motion of the wave. Natural light is termed unpolarized, which has been thought of as a misnomer. Light always has a polarization state; however, natural light has a very fast oscillating polarization state, and therefore appears to not prefer any distinct polarization state. It can be thought of as containing all polarization states over a very short period of time, therefore undetectable by modern detection systems [42].

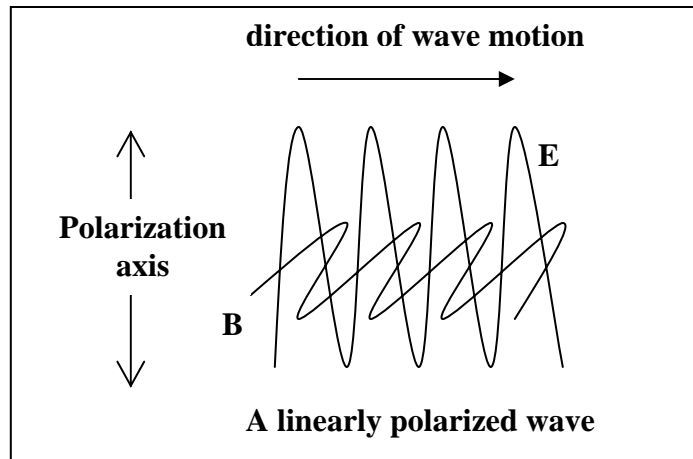


**Figure 2:** Light as a Transverse Electromagnetic Wave

Mathematically, light can be thought of as two orthogonal electric waves oscillating at the same frequency. The set of equations (1) below describe the electric field of monochromatic light propagating in free space (which is by definition polarized).

$$\begin{aligned}
 E &= iE_x + jE_y \\
 E_x &= E_{0x} \cos(\omega t - kz) \\
 E_y &= E_{0y} \cos(\omega t - kz + \varepsilon)
 \end{aligned}
 \tag{1}$$

In these equations,  $E_x$  and  $E_y$  represent the electric fields in the x and y directions respectively,  $E_{0x}$  and  $E_{0y}$  represent the magnitude of the electric fields,  $\omega$  is the frequency of the light,  $k = 2\pi/\lambda$ ,  $t$  is equal to time,  $z$  is the distance in the propagation direction,  $\varepsilon$  is relative phase difference between the waves, and  $\lambda$  is the wavelength of the light.

The polarization state of light can be described as either linear, circular, or elliptical polarization. All possible polarization states of a light wave can be described by applying certain constraints on Equation 2, which is the fundamental elliptical polarization state [42].

$$\frac{E_y^2}{E_{0y}^2} + \frac{E_x^2}{E_{0x}^2} - 2\frac{E_y}{E_{0y}}\frac{E_x}{E_{0x}}\cos\varepsilon = \sin^2\varepsilon \quad (2)$$

where  $E_{0x}$  and  $E_{0y}$  represent the magnitudes of the electric field vector along the orthogonal  $E_x$  and  $E_y$  axes as the light wave propagates along the z-axis with a phase difference of  $\varepsilon = \varepsilon_y - \varepsilon_x$  between the  $E_x$  and  $E_y$  components. Table 1 shows the basic polarization states obtained from Equation 2, and the conditions that are necessary to obtain each [43].

**Table 1:** Summary of the Derivation of the Standard Polarization States from the General Elliptical Polarization

<b>POLARIZATION STATE [Symbol]</b>	<b>CONSTRAINT</b>		<b>EQUATION</b>
	<b>Phase</b>	<b>Amplitude</b>	
<b>Horizontal [H]</b>	$\varepsilon = \pm n\pi$ $n=0, 1, \dots$	$E_y = 0$ $E_o = E_{ox}$	$\mathbf{E} = \mathbf{E}_x + \mathbf{E}_y = \mathbf{E}_x$ $\mathbf{E}_x(z, t) = \hat{\mathbf{i}} E_o \cos(kz - \omega t)$
<b>Vertical [V]</b>	$\varepsilon = \pm n\pi$ $n=0, 1, \dots$	$E_{ox} = 0$ $E_o = E_{oy}$	$\mathbf{E} = \mathbf{E}_x + \mathbf{E}_y = \mathbf{E}_y$ $\mathbf{E}_y(z, t) = \hat{\mathbf{j}} E_o \cos(kz - \omega t)$
<b>Plus 45 deg. [P]</b>	$\varepsilon = \pm n\pi$ $n=0, 1, \dots$	$E_{oy} = E_{ox}$ $= E_o$	$\mathbf{E} = \mathbf{E}_x + \mathbf{E}_y$ $\mathbf{E}(z, t) = (\hat{\mathbf{i}} + \hat{\mathbf{j}}) E_o \cos(kz - \omega t)$
<b>Minus 45 deg. [M]</b>	$\varepsilon = \pm n\pi$ $n=0, 1, \dots$	$E_{oy} = E_{ox}$ $= E_o$	$\mathbf{E} = \mathbf{E}_x + \mathbf{E}_y$ $\mathbf{E}(z, t) = (\hat{\mathbf{i}} - \hat{\mathbf{j}}) E_o \cos(kz - \omega t)$
<b>Right Circular [R]</b>	$\varepsilon = \pm n\pi/2$ $n=1, 2, \dots$	$E_{oy} = E_{ox}$	$\mathbf{E} = E_o[\hat{\mathbf{i}} E_o \cos(kz - \omega t) + \hat{\mathbf{j}} E_o \sin(kz - \omega t)]$
<b>Left Circular [L]</b>	$\varepsilon = \pm n\pi/2$ $n=1, 2, \dots$	$E_{oy} = E_{ox}$	$\mathbf{E} = E_o[\hat{\mathbf{i}} E_o \cos(kz - \omega t) - \hat{\mathbf{j}} E_o \sin(kz - \omega t)]$

The intensity of the polarization vector of light can be completely described by the  $4 \times 1$  Stokes vector as defined below in Equation 3. The polarization state of a beam of light, whether it is natural, totally, or partially polarized, can be described in terms of these quantities.

$$\begin{bmatrix} S_0 \\ S_1 \\ S_2 \\ S_3 \end{bmatrix} = \begin{bmatrix} \langle E_{0x}^2 \rangle_T + \langle E_{0y}^2 \rangle_T \\ \langle E_{0x}^2 \rangle_T - \langle E_{0y}^2 \rangle_T \\ \langle 2E_{0x}E_{0y} \cos \varepsilon \rangle_T \\ \langle 2E_{0x}E_{0y} \sin \varepsilon \rangle_T \end{bmatrix} = \begin{bmatrix} I \\ I_H - I_V \\ I_P - I_M \\ I_R - I_L \end{bmatrix} \quad (3)$$

where  $I$  is the measured intensity value,  $S_0$  is the total detected light intensity, of which  $S_1$  is the portion that corresponds to the difference between linear horizontal and vertical polarization states,  $S_2$  is the portion that corresponds to the difference between the linear  $+45^\circ$  and  $-45^\circ$  polarization states, and  $S_3$  is the portion that corresponds to the difference between the right circular and left circular polarization states [42]. In this equation  $\langle \rangle_T$  refers to time averaging and  $I$  is the detected intensity represented with a subscript for the polarization type it represents (H=horizontal, V=vertical, P=  $+45^\circ$ , M=  $-45^\circ$ , R= right circular, and L= left circular). These measured intensities translate into the Stokes values. All of the values lie between -1 and 1, and they represent the tendency of the measured light to be polarized linearly,  $\pm 45^\circ$ , and right or left-handedness. Using the values of the Stokes vector a value termed the degree of polarization (DOP) can be computed (Equation 4):

$$V = \frac{\sqrt{S_1^2 + S_2^2 + S_3^2}}{S_0} \quad (4)$$

The DOP is 1 for completely polarized light, zero for totally depolarized light, and assumes a fractional value for any case in between.

### 3.2 Mueller Matrix

In 1943, Hans Mueller developed a matrix that relates the Stokes vector of the light impinging on a sample to the Stokes vector leaving the sample [42]. Using the method with the input and output polarization states (Stokes vectors) known, the 4x4 Mueller matrix can be used to describe the polarization properties of a sample. This relationship is shown below in Equation 5 where M is the Mueller matrix and  $S_{out}$  and  $S_{in}$  are the output and input Stokes vectors respectively.

$$S_{out} = \begin{bmatrix} S_0 \\ S_1 \\ S_2 \\ S_3 \end{bmatrix}_{out} = MS_{in} = \begin{bmatrix} M_{11} & M_{12} & M_{13} & M_{14} \\ M_{21} & M_{22} & M_{23} & M_{24} \\ M_{31} & M_{32} & M_{33} & M_{34} \\ M_{41} & M_{42} & M_{43} & M_{44} \end{bmatrix} \begin{bmatrix} S_0 \\ S_1 \\ S_2 \\ S_3 \end{bmatrix}_{in} \quad (5)$$

The Mueller matrix can be calculated using 16, 36, or 49 polarization images, with 36 and 49 images corresponding to an over determined system [43]. Sometimes it is necessary to use more than 16 images to reduce the error due to noise associated with the Mueller matrix calculation [39]. The Mueller matrices are shown in Table 2, where the first term and second terms represent the input and output polarization states respectively. The polarization states are defined as: H=Horizontal, V=Vertical, P=+45°, M=-45°, R=Right circular, L=Left circular, and O=Open (i.e. no polarization).

**Table 2:** Mueller Matrix Equations for (a) 16, (b) 36, and (c) 49 Polarization Images

$M_{11} = HH+HV+VH+VV$	$M_{12} = HH+HV-VH-VV$	$M_{13} = 2PH+2PV-M_{11}$	$M_{14} = 2RH+2RV-M_{11}$
$M_{21} = HH-HV+VH-VV$	$M_{22} = HH-HV-VH+VV$	$M_{23} = 2PH-2PV-M_{21}$	$M_{24} = 2RH-2RV-M_{21}$
$M_{31} = 2HP+2VP-M_{11}$	$M_{32} = 2HP-2VP-M_{12}$	$M_{33} = 4PP-2PH-2PV-M_{31}$	$M_{34} = 4RP-2RH-2RV-M_{31}$
$M_{41} = 2HR+2VR-M_{11}$	$M_{42} = 2HR-2VR-M_{12}$	$M_{43} = 4PR-2PH-2PV-M_{41}$	$M_{44} = 4RR-2RH-2RV-M_{41}$

(a)

$M_{11} = HH+HV+VH+VV$	$M_{12} = HH+HV-VH-VV$	$M_{13} = PH+PV-MH-MV$	$M_{14} = RH+RV-LH-LV$
$M_{21} = HH-HV+VH-VV$	$M_{22} = HH-HV-VH+VV$	$M_{23} = PH-PV-MH+MV$	$M_{24} = RH-RV-LH+LV$
$M_{31} = HP-HM+VP-VM$	$M_{32} = HP-HM-VP+VM$	$M_{33} = PP-PM-MP+MM$	$M_{34} = RP-RM-LP+LM$
$M_{41} = HR-HL+VR-VL$	$M_{42} = HR-HL-VR+VL$	$M_{43} = PR-PL-MR+ML$	$M_{44} = RR-RL-LR+LL$

(b)

$M_{11} = OO$	$M_{12} = HO-VO$	$M_{13} = PO-MO$	$M_{14} = RO-LO$
$M_{21} = OH-OV$	$M_{22} = HH-HV-VH+VV$	$M_{23} = PH-PV-MH+MV$	$M_{24} = RH-RV-LH+LV$
$M_{31} = OP-OM$	$M_{32} = HP-HM-VP+VM$	$M_{33} = PP-PM-MP+MM$	$M_{34} = RP-RM-LP+LM$
$M_{41} = OR-OL$	$M_{42} = HR-HL-VR+VL$	$M_{43} = PR-PL-MR+ML$	$M_{44} = RR-RL-LR+LL$

(c)

If the sample is said to be non-depolarizing, meaning that the input light is polarized and the sample does not depolarize (DOP=1) the light, the Mueller matrix can be simplified into the Jones Matrix shown below in Equation 6, where  $E'$  and  $E$  are the output and input Jones vectors respectively. This, however, does not mean the output must be in the same polarization state as the input, it just needs to be polarized. For example, a coherent laser (vertically polarized) passes through a half wave plate (optical retarder), which rotates the polarization angle of the light but doesn't depolarize the light.

$$\begin{aligned}
 E' &= ME \\
 \begin{pmatrix} E_x' \\ E_y' \end{pmatrix} &= \begin{pmatrix} m_{11} & m_{12} \\ m_{21} & m_{22} \end{pmatrix} \begin{pmatrix} E_x \\ E_y \end{pmatrix} \\
 M &= \text{JonesMatrix}
 \end{aligned} \tag{6}$$

The Jones vector only requires 7 independent measurements, whereas the Mueller matrix needs a minimum of 16 independent measurements [43]. The Mueller matrix is chosen for biomedical applications involving cancer because cancerous tissue is a depolarizing sample.

### 3.3 Classification and Regression Tree (CART) Software

Classification and regression tree (CART) software is used in this thesis to analyze Mueller matrix data taken from Sinclair swine. CART was first introduced by Leo Breiman, Jerome Friedman, Richard Olshen, and Charles Stone in 1984 [44]. CART is a tree structured nonparametric data analysis software that uses tree pruning and cross validation. The CART procedure for growing trees is binary recursive partitioning. It is binary partitioning because parent nodes are always subdivided into two child nodes and recursive because the process is repeated for each subdivision of data continuing until further partitioning is impossible or is limited by some criterion set by the analyst. The keys of a CART analysis are (1) splitting each node in a tree, (2) deciding when a tree is complete, and (3) assigning each terminal node to a class outcome. The first step is splitting each node in a tree and determining the goodness-of-



split. CART uses node impurity, or heterogeneity of a node, to rank candidate splits. If  $Y$  is a categorical dependent variable that takes on values  $j=1, \dots, J$  for which we want to grow a classification tree, each node in the tree will be represented by a symbol  $t$  and will have probability distribution for the values of the dependent variable. Gini impurity criterion, shown in Equation 7, is the default for determining the node impurity [44].

$$i(t) = 1 - S \quad (7)$$

where  $i(t)$  is the impurity of node  $t$  and  $S$  is the sum of squared probabilities  $p(j | t)$  summed over all levels of the dependent variable. Another splitting criterion that can be chosen by the analyst is the Twoing criterion, which is the measure of the difference in probability that a class appears in the left descendant rather than the right descendant node. This criterion is based on class separation rather than node heterogeneity. The Twoing criterion is given in Equation 8 [44].

$$\frac{p_L p_R}{4} \sum_j \left( |p(j | t_L) - p(j | t_R)|^2 \right) \quad (8)$$

where  $p_L$  and  $p_R$  are the probability of going left or right respectively.

The Twoing criterion divides the classes into two groups, gathering similar classes together and attempting to separate the two aggregated groups in the descendant nodes. It thus treats every multi-class split as if it were a two-class problem. The Twoing criterion also reveals class similarities within each node because it separates the data by similar classes [44].

Other splitting criteria are available such as ordered Twoing, forced splitting, and linear combination splits. Ordered Twoing is used when the categorical variables are

ordered and therefore the class label is not arbitrary. This criterion is similar to Twoing except the two class groups are restricted to consist of adjacent classes. Forced splitting is used when the analyst wants to generate a CART tree using specific splitting variables in selected nodes. This can either be done manually when the split value is known or by allowing CART to determine the root node split value. The last splitting criterion is linear combination splits, which is used with data that has a linear structure [44].

Once the best split is found, CART repeats the process for each child node, continuing recursively until further splitting is impossible or is stopped by the analyst. Splitting will be impossible if only one case remains in a particular node or if all the cases in that node are exact copies of each other. Once this maximal tree is obtained, CART examines smaller trees obtained by pruning away branches of the maximal tree. Then the cases in each node are classified. The criterion that is used is the plurality rule, which states that the group with the greatest representation determines the class assignment [44].

Once the maximal tree has been pruned into a set of sub-trees, the best tree is determined by testing each for its error rate or cost. When there is sufficient data (at least 200 cases), this is done by dividing the sample into learning and test sub-samples. The learning sample is used to split the nodes, continuing until the largest tree is grown. The independent test sample is then used to estimate the rate at which cases are misclassified. The misclassification error rate is calculated for the largest tree and also for sub-tree obtained by pruning. The best sub-tree is the one with the lowest or near-lowest cost [44].

If there is insufficient data for a separate test sample (less than 200 cases), CART employs a cross validation technique, in which a maximal tree is grown on the entire learning sample. The learning sample is then divided into 10 roughly equal parts containing smaller distributions for the dependent variable. CART takes the first 9 parts of the data, constructs the largest possible tree, and uses the remaining 1/10 of the data to obtain initial estimates of the error rate of selected sub-trees. The same process is then repeated on another 9/10 of the data while using a different 1/10 part as the test sample. This continues until each part of the data has used as a test sample. The results of the 10 test samples are then combined to form error rates for trees of each possible size. This process gives an accurate estimate of the independent predictive accuracy of the tree [44].

Besides the primary split, two other types of splits, surrogate and competitor, are performed by CART. A competitor is a variable that might have been used instead of the primary split variable. The surrogate split is a splitting rule that closely mimics the action of the primary split. A good surrogate splits the parent node into descendant nodes similar in size and composition to the primary split and also tries to match the primary split on the specific cases that go to the left and right child nodes [44].

The surrogate splits along with the primary splits are used to determine variable importance. This is necessary because variables that are not a primary node splitter may be highly important. Since two variables that contain similar information will be split based on how they perform in a given context, they can not be classified as one important and the other unimportant. Because of this possibility of one variable hiding

the significance of another, CART calculates a variable importance score. The variable importance is the improvement measure attributable to each variable in its role as a surrogate to the primary split. The values of these improvements are summed over each node and totaled, and are scaled relative to the best performing variable. The variable with this highest importance is scored 100, and all other variables will have lower scores ranging downwards towards zero [44].

## CHAPTER IV

### MATERIALS AND METHODS

This chapter presents a detailed description of the Mueller matrix imaging system implemented in this research. The first section presents an overview of the system setup and equipment, and the polarization vector is then traced from the light source to the detector to provide a basis for the calibration procedure. The second section describes the current system calibration procedure and shows the theoretical calibration curves for each electro-optic. The next section describes the *in vivo* Sinclair swine experiments and discusses the image analysis techniques. A new calibration technique is discussed in the final section.

#### 4.1 Mueller Matrix Imaging System

##### 4.1.1 Experimental Setup

The Automated Mueller Matrix Polarization Imaging System, shown in Figure 3, consists of two branches: an input and an output. A 150-watt (Navitar, Rochester, NY), halogen bulb light source is passed through a red 633.8 nm filter (Thermo Oriel, Stratford, CT) with a bandwidth of  $\pm 10.5$  nm and is collimated by a convex lens, focal length 38.1 mm (Newport Corporation, Fountain Valley, CA). This wavelength is chosen because the amount of scatter and absorption in a turbid medium, such as skin, falls off with increasing wavelength in the visible to near-infrared region. The beam is sent through the input branch that consists of a Glan Thompson 100,000:1 linear polarizer (Newport Corporation, Fountain Valley, CA) set at  $+45^\circ$  (to the horizontal) and

two voltage-controlled optical devices, a polarization rotator and a variable retarder (Meadowlark Optics, Frederick, Colorado). These voltage-controlled components allow for the production of the necessary input polarization states. The variable rotator, which rotates the polarization vector of the initially polarized beam, produces all the necessary states of linearly polarized light (horizontal, vertical, and  $\pm 45^\circ$ ), and the variable retarder, which changes the relative phase between the two components of the electric field vector, produces left and right circular polarization states. After passing through the input optics, the polarized light hits the sample and the diffusely reflected light passes through the output optical branch, which consists of the same components as the input branch except in the reverse order with the polarizer set at  $-45^\circ$ . A 508x509, 14-bit CCD camera (Apogee, Auburn, CA) is placed at the end of the output branch and is used to capture the resulting images. Automation of the system is accomplished via a LabVIEW® program that controls the variable rotators, retarders, and the CCD camera.

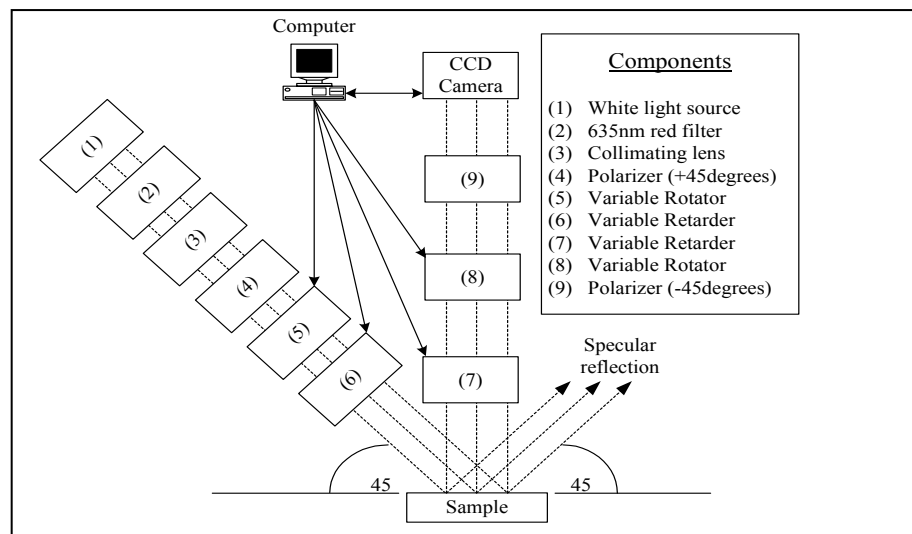


**Figure 3:** The Fully Automated Mueller Matrix Polarization Imaging System [44]

### 4.1.2 Liquid Crystals

The variable rotators and retarders used in this research to modulate the polarized light are liquid crystals, and some background on them will be given here. In 1888, Friedrich Reintzer discovered the first liquid crystal when he noticed that cholesteryl benzoate seemed to have two distinct transition points, one at which the crystal changed into a cloudy liquid and another where it became transparent [42]. Liquid crystals have long cigar-shaped molecules that can move about and lack positional order. However, they do sustain a large-scale orientational order because the molecules strongly interact. The nematic liquid crystals tend to have their molecules parallel even though their positions are fairly random.

Liquid crystal cells are constructed using two pieces of flat glass coated with a transparent conducting metallic film, such as indium tin oxide or fused silica [42,45]. The two pieces of glass are spaced a few microns apart, and the cavity is filled with the liquid crystal. In this configuration, the glass serves as electrodes and a controlling voltage will be applied across them [42]. It is necessary to produce ridges on the interior of each glass window so that the liquid crystal molecules will be parallel to the glass and each other. This can be accomplished by rubbing the surface of the window so that parallel microgrooves are produced.

Liquid crystals are used to make variable rotators and variable retarders, both of which are composed of a liquid crystal variable retarder. The rotator also has a quarter-wave plate within it so that only linear polarization states are produced (Figure 4). The long axis of the liquid crystal molecules defines the extraordinary index, and with no

voltage present, the molecules lie parallel to the windows. This is where maximum retardance occurs. When voltage is applied across the liquid crystal, the molecules tip parallel to the applied electric field, and as voltage increases, the effective birefringence decreases, causing a reduction in retardance (Figure 5) [45]. The retardance  $\Delta\phi$  of a liquid crystal is shown in Equation 9.

$$\Delta\phi(V, T, \lambda_o) = \frac{2\pi}{\lambda_o} d\Delta n(V, T, \lambda_o) \quad (9)$$

where V is applied voltage, T is temperature,  $\lambda_o$  is the vacuum wavelength, d is thickness of crystal, and  $\Delta n$  is the refractive index change. It can be seen from this equation that the retardance is not only dependent on voltage but also on temperature and wavelength. The retardance decreases 0.4% per °C increase and decreases as  $\lambda_o$  increases. The retardance maximum occurs when the voltage is zero and is minimum when the applied voltage is approximately 5-7 volts. At the maximum voltage, the minimum retardance is only about 30 but can be reduced to 0 if a compensator is used [42,45].

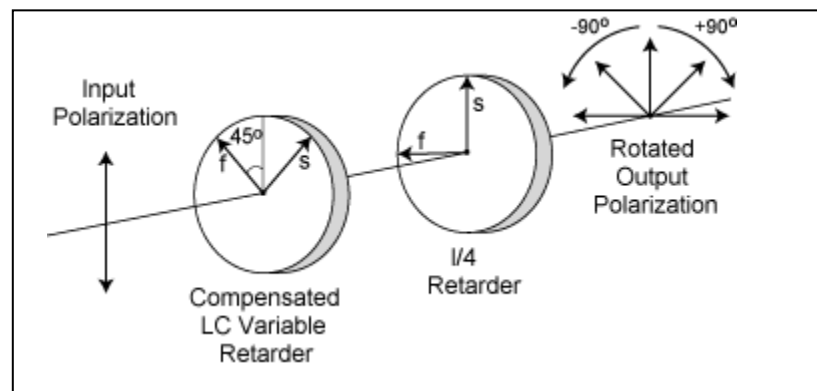


**Figure 4:** Liquid Crystal Variable Rotator Schematic [45]



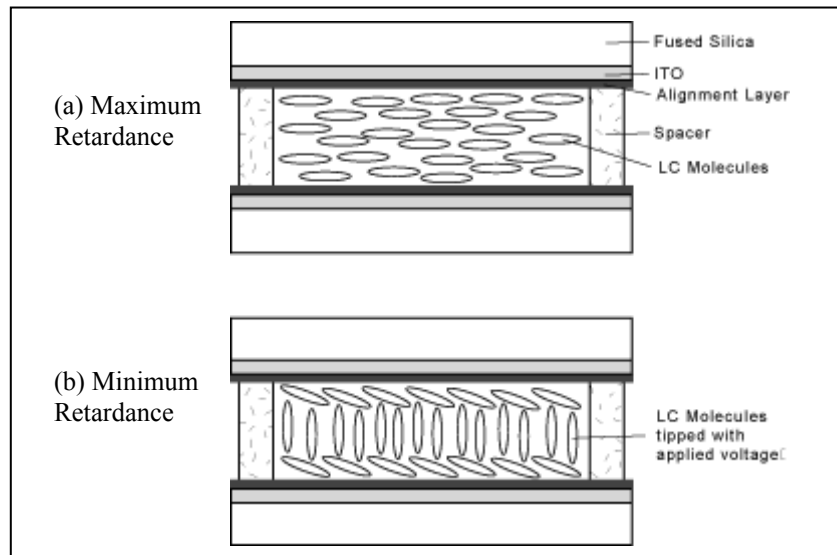


**Figure 5:** Liquid Crystal Variable Retarder Construction [45]

Liquid crystals, as described above, do not require high driving voltages and are therefore easily implemented into a system in which a computer controls them. The drawbacks of using liquid crystals include instability with temperature changes, low modulation frequency compared to other methods (2 kHz), and true rotation can not be obtained. Also, their response time is 5-20 ms, which is longer than other types of polarization modulators such as Pockels cells [45].

#### 4.1.3 Polarization Vector

In order to understand the system calibration procedure, it is important to comprehend the signal being measured. The light is initially linearly polarized by a fixed polarizer at  $+45^\circ$ . The light then passes through a variable retarder that is capable of producing all linear polarization states, including but not limited to horizontal, vertical,

and  $\pm 45^\circ$ . The light then passes through a variable retarder, which is capable of producing right and left circular light. The light then impinges on the sample, and the diffusely reflected light is sent through the output arm. The output arm consists of the same components as the input arm except in reverse order with the polarizer set at  $-45^\circ$ . The output arm is set up in this manner to “unwind” the diffusely reflected light. In order to calculate the 36-element Mueller matrix of a sample, a minimum of 16 independent measurements must be made by producing different combinations of input and output polarization states. According to the Mueller matrix equations given in the theory section, the polarization states that are needed with 36 measurements are horizontal (H), vertical (V),  $+45^\circ$  (P),  $-45^\circ$  (M), right circular (R), and left circular (L). To obtain these polarization states, the three optics in the input arm (and similarly the output arm) must together produce each state. Table 3 below shows the rotation and retardance combinations necessary to produce different input polarization states with input polarization set by polarizer at  $+45^\circ$ . This table is also true for the output polarization states because the direction of light propagation is reversed. This information is needed to calibrate the system because the three input or output optics work together to produce a given polarization state.

**Table 3:** Rotation and Retardance Required to Produce Different Input Polarization States with Input Polarization at  $+45^\circ$

Polarizer	Rotator	Retarder	Output
$+45^\circ$	$0^\circ$	$0^\circ$	$+45^\circ$ (P)
$+45^\circ$	$+45^\circ$	$0^\circ$	Horizontal (H)
$+45^\circ$	$90^\circ$	$0^\circ$	$-45^\circ$ (M)
$+45^\circ$	$135^\circ$	$0^\circ$	Vertical (V)
$+45^\circ$	$+45^\circ$	QWP	Left circular (L)
$+45^\circ$	$135^\circ$	QWP	Right circular (R)

In order to calibrate each electro-optic to produce a desired polarization state, the theoretical model of how each optic acts in the system must be known. This can be done by using Mueller-Stokes calculus to describe the system with each optic's unique Mueller matrix. An ideal linear rotator can be described as follows:

$$\begin{bmatrix} 1 & 0 & 0 & 0 \\ 0 & \cos 2\theta & \sin 2\theta & 0 \\ 0 & -\sin 2\theta & \cos 2\theta & 0 \\ 0 & 0 & 0 & 1 \end{bmatrix} \quad (10)$$

where  $\theta$  is the fast axis.

To calibrate rotator(1), the input polarizer is set to  $+45^\circ$  and the analyzer is changed between horizontal (H), vertical (V),  $+45^\circ$  (P), and  $-45^\circ$  (M). To model the system in this configuration with the fast axis of the rotator changing between 0 and  $\pi$  radians, the Stokes vector for  $+45^\circ$  is multiplied by the rotator Mueller matrix then this

combination is multiplied by the Mueller matrix for H, V, P, or M. This process is shown in Appendix A, and is summarized below where the irradiance is the first component of the Stokes vector.

(1) Horizontal output (Ho)

$$\frac{1}{2} \begin{bmatrix} 1 + \sin 2\theta \\ 1 + \sin 2\theta \\ 0 \\ 0 \end{bmatrix}$$

(2) Vertical output (Vo)

$$\frac{1}{2} \begin{bmatrix} 1 - \sin 2\theta \\ -1 + \sin 2\theta \\ 0 \\ 0 \end{bmatrix}$$

(3) +45° output (Po)

$$\frac{1}{2} \begin{bmatrix} 1 + \cos 2\theta \\ 0 \\ 1 + \cos 2\theta \\ 0 \end{bmatrix}$$

(4) -45° output (Mo)

$$\frac{1}{2} \begin{bmatrix} 1 - \cos 2\theta \\ 0 \\ -1 + \cos 2\theta \\ 0 \end{bmatrix}$$

The irradiance, the first element of the output Stokes vector, is the quantity of interest because it is the measurable quantity. It is measured using the CCD camera. The other three elements of the Stokes vector give information on the polarization state of light, which is not measured by the system. To obtain the theoretical plot for rotator(1), the irradiances are plotted as a function of the fast axis of the rotator. This procedure can be done again for rotator(2) with the difference being that the analyzer is held constant at  $-45^\circ$  but the polarizer is changed between H, V, P, M. The rotator(2) calculations are shown below. The plots for the components are shown in the Results section.

(1) Horizontal input (Hi)

$$\frac{1}{2} \begin{bmatrix} 1 + \sin 2\theta \\ 0 \\ -1 - \sin 2\theta \\ 0 \end{bmatrix}$$

(2) Vertical input (Vi)

$$\frac{1}{2} \begin{bmatrix} 1 - \sin 2\theta \\ 0 \\ -1 + \sin 2\theta \\ 0 \end{bmatrix}$$

(3)  $+45^\circ$  input (Pi)

$$\frac{1}{2} \begin{bmatrix} 1 - \cos 2\theta \\ 0 \\ -1 + \cos 2\theta \\ 0 \end{bmatrix}$$

(4)  $-45^\circ$  input (Mi)

$$\frac{1}{2} \begin{bmatrix} 1 + \cos 2\theta \\ 0 \\ -1 - \cos 2\theta \\ 0 \end{bmatrix}$$

The general equation of the Mueller matrix of an ideal retarder is given in

Equation 11.

$$\begin{bmatrix} 1 & 0 & 0 & 0 \\ 0 & C_2^2 + S_2^2 \cos \delta & S_2 C_2 (1 - \cos \delta) & -S_2 \sin \delta \\ 0 & S_2 C_2 (1 - \cos \delta) & S_2^2 + C_2^2 \cos \delta & C_2 \sin \delta \\ 0 & S_2 \sin \delta & -C_2 \sin \delta & \cos \delta \end{bmatrix} \quad (11)$$

where  $\delta$  is retardance,  $C_2 = \cos 2\theta$ ,  $S_2 = \sin 2\theta$ , and  $\theta$  is fast axis. For the retarder used in this system, the fast axis is  $+45^\circ$ . The Mueller matrix for a retarder with fast axis at  $+45^\circ$  is shown below in Equation 12.

$$\begin{bmatrix} 1 & 0 & 0 & 0 \\ 0 & \cos \delta & 0 & -\sin \delta \\ 0 & 0 & 1 & 0 \\ 0 & \sin \delta & 0 & \cos \delta \end{bmatrix} \quad (12)$$

Mueller Stokes calculus is again used to model the effect of the retarder on the system. Retarder(1) is calibrated by changing the input polarization between H, V, P, and M and setting the output polarization to H. The following shows the calculations for retarder(1).

(1) Horizontal input (Hi)

$$\frac{1}{2} \begin{bmatrix} 1 + \cos \delta \\ 1 + \cos \delta \\ 0 \\ 0 \end{bmatrix}$$

(2) Vertical input (Vi)

$$\frac{1}{2} \begin{bmatrix} 1 - \cos \delta \\ 1 - \cos \delta \\ 0 \\ 0 \end{bmatrix}$$

(3) +45° input (Pi)

$$\frac{1}{2} \begin{bmatrix} 1 \\ 1 \\ 0 \\ 0 \end{bmatrix}$$

(4) -45° input (Mi)

$$\frac{1}{2} \begin{bmatrix} 1 \\ 1 \\ 0 \\ 0 \end{bmatrix}$$

The calculations for retarder(2) produce the same irradiance values as retarder(1). The calculations are shown below, and the plots for retarder(1) and retarder(2) are shown in the Results section.

(1) Horizontal output (Ho)

$$\frac{1}{2} \begin{bmatrix} 1 + \cos \delta \\ 1 + \cos \delta \\ 0 \\ 0 \end{bmatrix}$$

(2) Vertical output (Vo)

$$\frac{1}{2} \begin{bmatrix} 1 - \cos \delta \\ -1 + \cos \delta \\ 0 \\ 0 \end{bmatrix}$$

(3) +45° output (Po)

$$\frac{1}{2} \begin{bmatrix} 1 \\ 1 \\ 0 \\ 0 \end{bmatrix}$$

(4) -45° output (Mo)

$$\frac{1}{2} \begin{bmatrix} 1 \\ 1 \\ 0 \\ 0 \end{bmatrix}$$



## 4.2 Current System Calibration

### 4.2.1 Main Calibration

The Mueller matrix imaging system must be precisely calibrated so that errors are not induced in the measured Mueller matrices. This process is carried out in several steps so that each optic is calibrated separately. When an electro-optic is calibrated, the voltage necessary to produce a specific rotation or retardance is determined. For calibration, the system is setup in transmission mode, and the polarizer and analyzer are placed in the input and output arms respectively and the desired angles ( $+45^\circ$  for polarizer,  $-45^\circ$  for analyzer) are determined. This is accomplished by first setting the polarizer to horizontal and analyzer to vertical so that minimum intensity is found, then the horizontal position for the analyzer is found by subtracting (or adding)  $90^\circ$  to the vertical angle setting. The analyzer horizontal position is verified by detecting maximum intensity. The polarizer is then set to vertical by adding (or subtracting)  $90^\circ$  to the angle setting for horizontal and with the analyzer set to horizontal, the minimum intensity is found. The polarizer and analyzer are also set to vertical and maximum intensity is verified. Now that the horizontal and vertical angles for both the polarizer and analyzer have been determined, the desired angles ( $+45^\circ$  for polarizer,  $-45^\circ$  for analyzer) can be found. The polarizer is then set to  $+45^\circ$  with the analyzer at vertical and horizontal and the half intensity value is verified. The half intensity should be  $(\text{max intensity} + \text{min intensity})/2$ . Next retarder(2) is placed in the output arm to verify polarizer and analyzer settings. If the polarizer and analyzer are set properly then the retarder should have no effect when the analyzer is set to vertical and horizontal and polarizer at  $45^\circ$  ( $P_H = P_V$ ).

The voltages in the Labview program *calibration* are set to go from 0 to 5 Volts in 0.05 increments for channel 2. The Labview program must be changed for each electro-optic so that the program changes the voltage to the desired optic and leaves the voltages to the other optics constant. The Matlab program *cal100.m* (Appendix B) is ran on the images, and the output intensity values are manually copied to Excel. The results are plotted and a straight line should be seen with amplitude of the half intensity value for both PV and PH. If not, then the polarizer and analyzer must be realigned to find the correct angles.

Once the correct angles are found, the analyzer is fixed at  $-45^\circ$ , and retarder(2) is removed. Rotator(2) is then placed into the output arm, and the Labview program is changed so that the channel 3 voltage is varied from 0 to 3 Volts in increments of 0.05. The polarizer is rotated between horizontal, vertical,  $+45^\circ$ , and  $-45^\circ$ , and the Labview program *calibration* is run for each position. The Matlab program *cal60.m* (Appendix C) is ran and the data is copied to Excel so the results can be graphed. The locations of  $H_o$ ,  $V_o$ ,  $P_o$ ,  $M_o$  (output) are then determined by comparing the results to the theoretical graph for rotator 2 shown in Figure 6. According to Figure 6,  $H_o$  occurs when the rotator is rotated by  $3\pi/4$  or when  $P_iM_o$  and  $M_iM_o$  intersect and  $H_i$  is maximum. Therefore, the value for  $H_o$  is found to two decimal places by zooming in at the voltages around the intersection of  $P_iM_o$  and  $M_iM_o$ , and then found to three decimal places by zooming in again. This is done for  $V_o$  (intersection of  $P_iM_o$  and  $M_iM_o$  where  $V_i$  is max),  $P_o$  (intersection of  $H_iM_o$  and  $V_iM_o$  where  $P_i$  is max), and  $M_o$  (intersection of  $H_iM_o$  and  $V_iM_o$  where  $M_i$  is max) so that all are found to three decimal places.

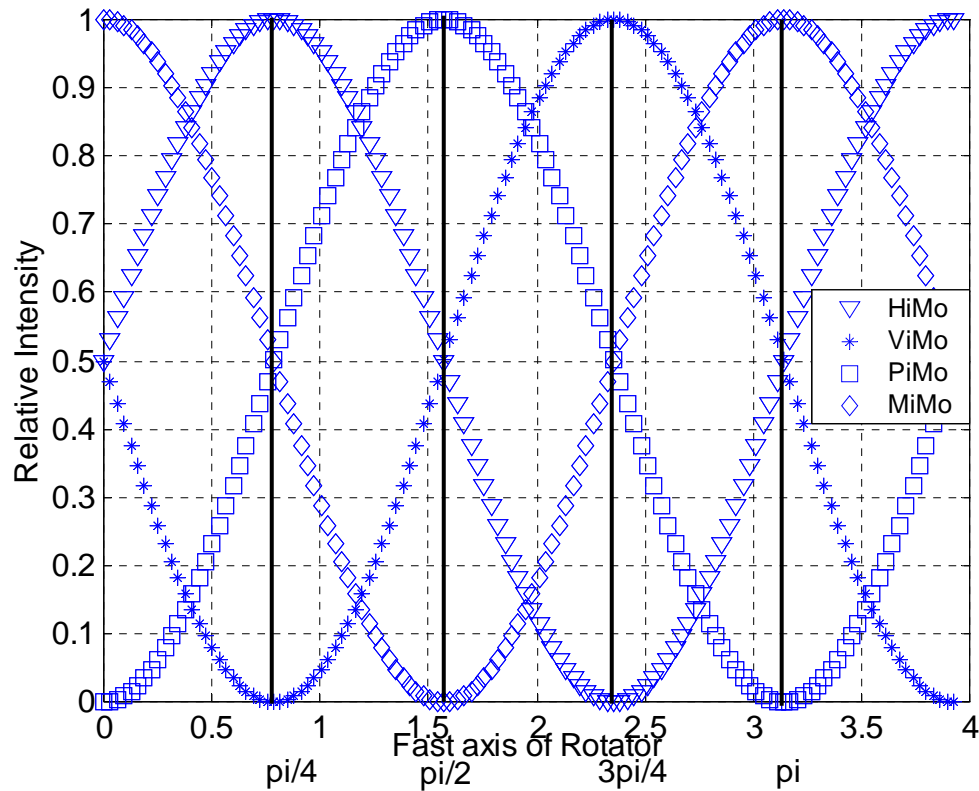


**Figure 6:** Theoretical Results for Rotator(2)

Next rotator(1) is inserted into the input arm and the Labview program is changed so that the voltage to channel 1 is varied from 1-3 Volts in 0.05 increments. The Ho voltage is set in Labview as channel 3, and the data for rotator(1) is taken. This is done three more times, each time changing the channel 3 voltage first to  $V_o$ , then  $P_o$ , and last  $M_o$ . After each set, the Matlab program *cal40.m* (Appendix D) is run, and the intensity values are copied into Excel. A graph of all the cases is made and the Hi, Vi, Pi, and Mi voltages are found to three decimal places the same way the output voltages were found by using Figure 7. In order to obtain horizontal (Hi), vertical (Vi),  $+45^\circ$  (Pi),

and  $-45^\circ$  (Mi) input polarizations, the rotator must rotate the polarized light by  $\pi/4$ ,  $3\pi/4$ ,  $\pi$ , and  $\pi/2$  respectively.

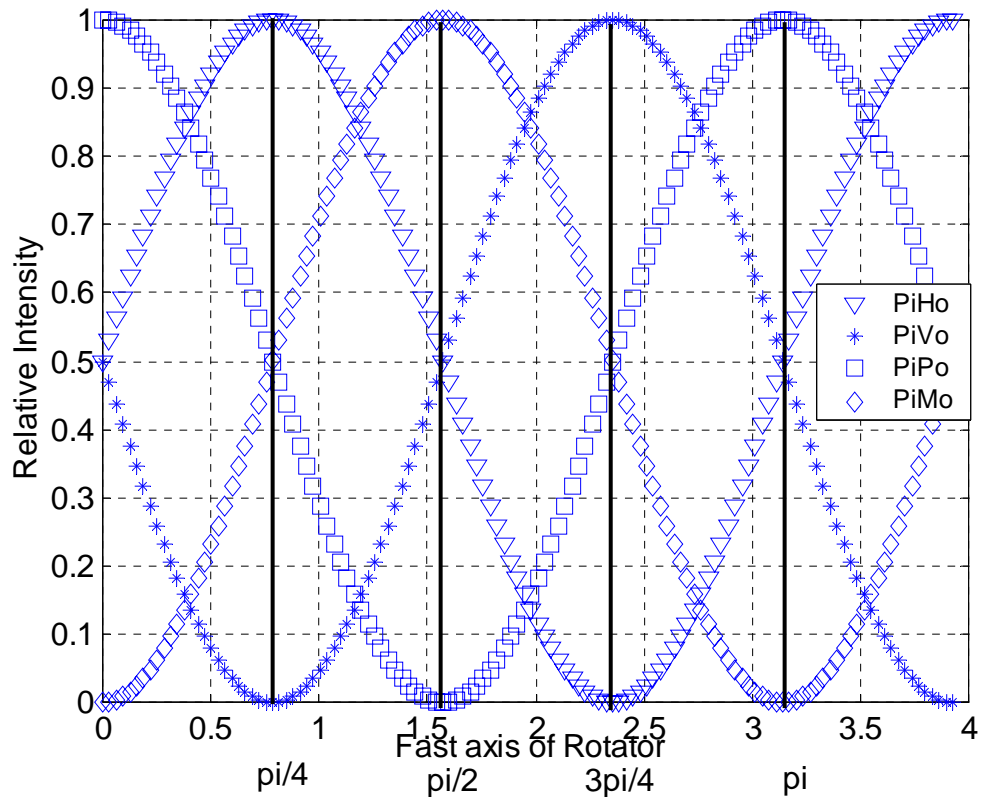


**Figure 7:** Theoretical Results for Rotator(1)

Now that all the voltages necessary to produce the input and output linear polarization states have been found, the next step is to find the circular polarization states. To do this, retarder(2) is inserted into the output arm, and the Labview program is changed so that channel 2 can be varied from 1.5-5.5 Volts in 0.05 increments. In the Labview program, the  $H_i$  voltage is set as channel 0, and the data for  $H_o$ ,  $V_o$ ,  $P_o$ , and  $M_o$  cases taken by changing channel 3 to the corresponding voltage. After each set, the Matlab program *cal80.m* (Appendix E) is ran, and the data is copied into Excel. All the data is plotted on one graph, and the quarter wave plate (QWP) and zero retardance voltages are determined. According to the theoretical graph for the retarder (Figure 8), the QWP occurs when  $H_iH_o$  and  $H_iV_o$  intersect at the half intensity, and zero retardance occurs when  $H_iH_o$  is maximum and  $V_iV_o$  is minimum. As done previously, the voltages are determined to three decimal places by zooming in around the appropriate region. For an ideal retarder, the QWP and zero retardance voltages are equal for both horizontal ( $H_i$ ) and vertical ( $V_i$ ) inputs. Since there is error introduced in the system by misalignments and optic imperfections, the retarders are not ideal and therefore the QWP and zero retardance voltages have to also be found for the vertical input ( $V_i$ ). This is done the same as  $H_i$  except the voltage to channel 0 is set to  $V_i$ .

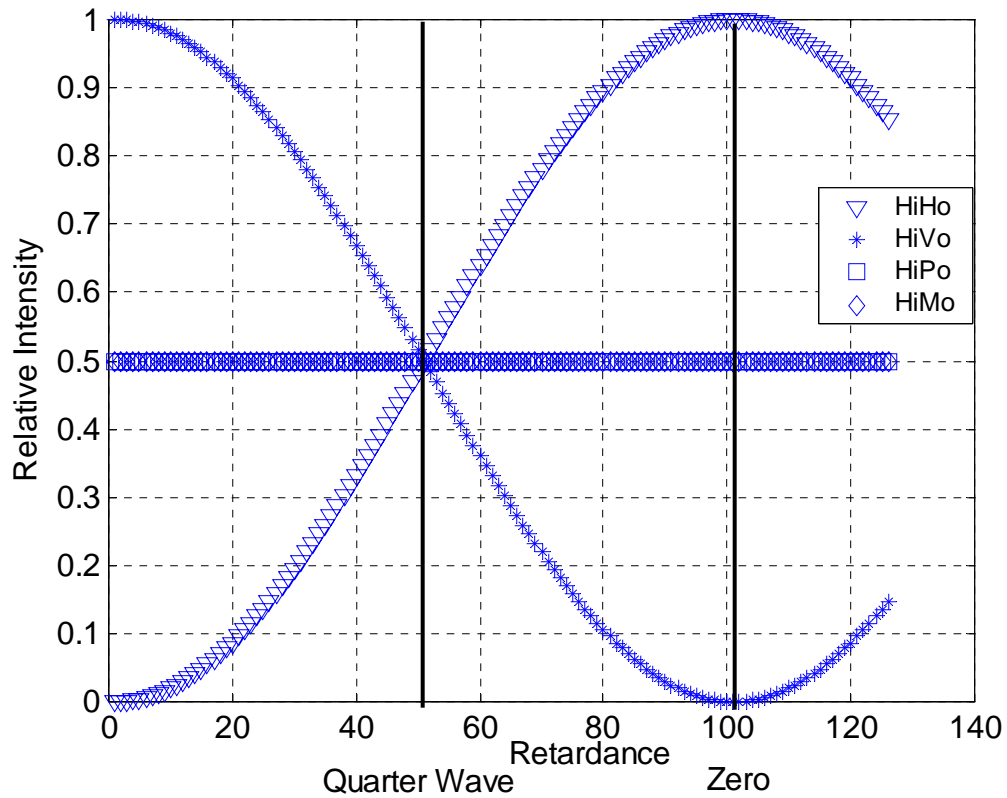


**Figure 8:** Theoretical Results for Retarder(2)

The final step is to calibrate retarder (1). Once it is placed into the input arm, the Labview program is changed so that channel 1 can be incremented by 0.05 Volts from 1.5-5.5 Volts. Channel 0 is set to Hi, channel 2 to zero retardance, and channel 3 to Ho, and retarder(1) calibration data is taken. This is done three more times, each time with channel 0 set to Hi, channel 2 set to zero retardance, and changing channel 3 to Vo, Po, and Mo. Also, this should be done for the output right and left circular cases by setting channel 2 to the QWP voltage and channel 3 to Ho and Vo. Table 4 shows the channel settings for all six cases. From these results, the QWP and zero retardance voltages are

determined to three decimal places for retarder(1) as done previously except using Figure 9.

**Table 4:** Voltage Settings for Retarder(1) Calibration

Channel	$H_i$	$H_i$	$H_i$	$H_i$	$H_i$	$H_i$
Channel 0						
Channel 1	1.5-5.5	1.5-5.5	1.5-5.5	1.5-5.5	1.5-5.5	1.5-5.5
Channel 2	0 retardance	0 retardance	0 retardance	0 retardance	QWP	QWP
Channel 3	$H_o$	$V_o$	$P_o$	$M_o$	$H_o$	$V_o$

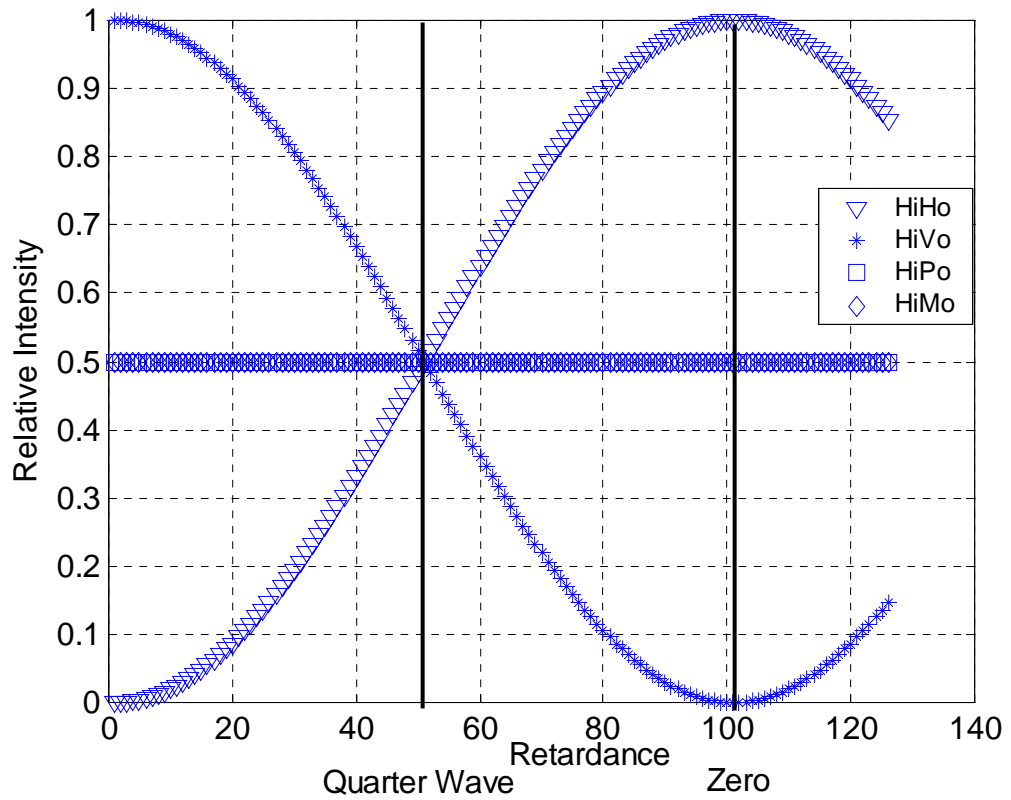


**Figure 9:** Theoretical results for Retarder(1)

### 4.2.2 Fine Tune the Calibration

Once a rough calibration has been obtained, a fine tune calibration is needed. For this calibration, the intensity of each case is observed independently, and the voltages to the rotators and retarders are adjusted so that the appropriate intensity value is achieved. For the cases where input and output are the same polarization state, the intensity is maximum, and when the input and output are 90 degrees out of phase the intensity is minimum. All the other cases the theoretical intensity is maximum plus minimum divided by 2 (half intensity). For each case, there are four variables (voltages) that attribute to the intensity, and in order to determine the correct voltage to adjust, a system model that is a function of the four voltages is needed. The system is modeled using Mueller-Stokes calculus and is shown below in Equations 13 and 14.

$$S_{out} = M' \cdot S_{in} \quad (13)$$

$$M' = M_{Analyzer} \cdot M_{Rotator2} \cdot M_{Retarder2} \cdot M_{sample} \cdot M_{Retarder1} \cdot M_{Rotator1} \quad (14)$$

where  $S_{out}$  and  $S_{in}$  are the output and input Stokes vectors respectively and  $M'$  is the Mueller matrices of all the optical components in the system. For calibration, the system is setup in transmission mode with air as the sample and the initial polarization set to  $+45^\circ$ . The following shows the calculation of  $S_{out}$ , where  $\theta_1$  and  $\theta_2$  are the rotation of rotator 1 and 2 respectively, and  $\delta_1$  and  $\delta_2$  are the retardance of retarder1 and retarder2 respectively.



$$\begin{aligned}
S_{out} = \begin{bmatrix} S_0 \\ S_1 \\ S_2 \\ S_3 \end{bmatrix} &= \frac{1}{2} \begin{bmatrix} 1 & 0 & -1 & 0 \\ 0 & 0 & 0 & 0 \\ -1 & 0 & 1 & 0 \\ 0 & 0 & 0 & 0 \end{bmatrix} \begin{bmatrix} 1 & 0 & 0 & 0 \\ 0 & \cos 2\theta_2 & \sin 2\theta_2 & 0 \\ 0 & -\sin 2\theta_2 & \cos 2\theta_2 & 0 \\ 0 & 0 & 0 & 1 \end{bmatrix} \begin{bmatrix} 1 & 0 & 0 & 0 \\ 0 & 1 & 0 & 0 \\ 0 & 0 & \cos \delta_2 & \sin \delta_2 \\ 0 & 0 & -\sin \delta_2 & \cos \delta_2 \end{bmatrix} \\
&\quad \begin{matrix} -45^\circ \text{ Analyzer} & \text{Rotator 2} & \text{Retarder 2} \\ \begin{bmatrix} 1 & 0 & 0 & 0 \\ 0 & 1 & 0 & 0 \\ 0 & 0 & 1 & 0 \\ 0 & 0 & 0 & 1 \end{bmatrix} & \begin{bmatrix} 1 & 0 & 0 & 0 \\ 0 & 1 & 0 & 0 \\ 0 & 0 & \cos \delta_1 & \sin \delta_1 \\ 0 & 0 & -\sin \delta_1 & \cos \delta_1 \end{bmatrix} & \begin{bmatrix} 1 & 0 & 0 & 0 \\ 0 & \cos 2\theta_1 & \sin 2\theta_1 & 0 \\ 0 & -\sin 2\theta_1 & \cos 2\theta_1 & 0 \\ 0 & 0 & 0 & 1 \end{bmatrix} & \begin{bmatrix} 1 \\ 0 \\ 1 \\ 0 \end{bmatrix} \\
&\quad \begin{matrix} \text{Air} & \text{Retarder 1} & \text{Rotator 1} & +45^\circ \text{ Polarizer} \end{matrix}
\end{aligned}$$

$$S_{out} = \begin{bmatrix} S_0 \\ S_1 \\ S_2 \\ S_3 \end{bmatrix} = \frac{1}{2} \begin{bmatrix} 1 + \sin 2\theta_2 \sin 2\theta_1 - \cos 2\theta_2 \cos 2\theta_1 (\cos \delta_2 \cos \delta_1 - \sin \delta_2 \sin \delta_1) \\ 0 \\ -1 - \sin 2\theta_2 \sin 2\theta_1 + \cos 2\theta_2 \cos 2\theta_1 (\cos \delta_2 \cos \delta_1 - \sin \delta_2 \sin \delta_1) \\ 0 \end{bmatrix}$$

Since the quantity that the system measures is intensity,  $S_0$  is the Stokes parameter of interest, and the output vector can be simplified as shown in Equation 15.

$$S_0 = \frac{1}{2} [1 + \sin 2\theta_2 \sin 2\theta_1 - \cos 2\theta_2 \cos 2\theta_1 (\cos \delta_2 \cos \delta_1 - \sin \delta_2 \sin \delta_1)] \quad (15)$$

This equation can be used to determine the correct voltages to adjust in order to obtain a particular combination of input and output polarization states. See Appendix F for Matlab plots that show the effect of changing each of the four variables for each combination of input and output polarization states.

### 4.3 Sinclair Swine Experiments

#### 4.3.1 Data Collection

Nine Sinclair swine piglets, which are housed at Texas A&M University's Veterinary medicine complex, were used for this study. The Sinclair swine model is shown in Figure 10. An approved animal use protocol controlled their treatment. The pigs were anesthetized with a ketamine/xylezine complex so that they would not be able to move during data collection in order to reduce the error associated with motion artifact.



**Figure 10:** Sinclair Swine Model

A veterinary assistant that was responsible for administering anesthesia and caring for the pigs identified normal skin, benign moles, and melanoma tumors on each

pig. Since the pigs were used in other research, biopsies of the lesions could not be taken. Therefore, the lesions were classified by the veterinary assistant's knowledge of the differences between benign and melanoma lesions. The lesion or normal skin was covered with gel and placed against a glass slide for index of refraction matching, and 36 polarization images were taken. A total of 102 tissue samples, 29 normal, 30 mole, and 43 cancerous lesions, were imaged.

#### **4.3.2 Data Analysis**

Data processing was accomplished by cropping the images to include only pixels within the boundaries of the lesion. These cropped images were then processed using Matlab to calculate the Mueller matrix. In order to compare the Mueller matrices, one numerical value for each Mueller matrix element was used. Two methods of obtaining this value included: (1) the mean and (2) the 10<sup>th</sup>-90<sup>th</sup> percentile intensities of each image. The Mueller matrix for each sample was calculated using both methods, making a total of 10 Mueller matrices for each sample.

In order to separate the data into the three types, normal, mole, and cancer, statistical processing using Classification and Regression Tree (CART) software was performed. The software was used to produce a classification tree, and the importance of each Mueller matrix element in the classification was determined. The 102 cases, each with 10 Mueller matrices, were analyzed using CART. The data was also separated by exposure time and analyzed using CART. Exposure times of 0.06, 0.12, and 4 seconds

were used with 19, 20, 19 samples respectively. The remaining 44 samples could not be divided into large enough groups to do a separate exposure time analysis.

#### **4.4 New Calibration**

Since the calibration procedure described previously is a time consuming and cumbersome process, a new technique has been developed. The new calibration technique is automated and is incorporated into a new Labview program that controls the system (Appendix G). The new Labview program fixes many of the previous software problems such as having to take two images instead of one, and it also has new features such as calculating and displaying the sample Mueller matrix. Within this program, there is a drop down menu on the user interface that gives several options, one of which is calibration. The calibration program allows the user to determine the necessary voltages to be used in the main program for data collection. Before the program can be used to calibrate the system, the zero rotation voltage for rotator1 and the zero retardance voltages for retarder1 and retarder2 must be determined. The zero rotation voltage for rotator1 is determined by first nulling the system with the polarizer at  $+45^\circ$  and the analyzer at  $-45^\circ$ , and then rotator1 is placed between them with its slow axis parallel to the input polarization state. The calibration data that was given from the manufacturer for rotator1 is used to approximate where zero rotation will occur, and then the voltage is varied in a window of about 0.1 volts around that voltage until the system is nulled at minimum intensity. If the system is unable to be nulled, then the polarizer and analyzer angles are not exactly correct and need to be adjusted. This is done by changing the

polarizer and analyzer angles a degree at a time until the system is nulled with rotator1 in place. Once the zero rotation voltage has been determined, the zero retardance voltages for retarder1 and retarder 2 are determined the same way as the rotator1 zero rotation voltage.

Once all the “zero” voltages have been determined, all of the components are aligned using the backreflected beam from a laser with the system in transmission mode. It is important to note here that alignment errors produce large errors in the calibration results, and hence in the Mueller matrix. The zero rotation and retardance voltages are input into the calibration program under the ROTATOR2 tab, and the voltage to rotator2 is set to vary between 1.00 and 2.30 Volts in 0.01 Volt increments. The “Take Images?” button is pressed and the program takes the requested data. The program calculates the  $H_0$ ,  $V_0$ ,  $P_0$ , and  $M_0$  voltages by using the  $P_iM_0$  curve from Figure 3 above, where  $H_0$  and  $V_0$  are calculated as the half intensity voltages,  $P_0$  is the maximum intensity voltage, and  $M_0$  is the minimum intensity voltage. The program calls a Matlab program that searches for the voltages, and it displays them on the screen. Figure 11 shows the rotator2 data acquired using the calibration program with the points of interest enlarged to show the voltages calculated by the Matlab program.

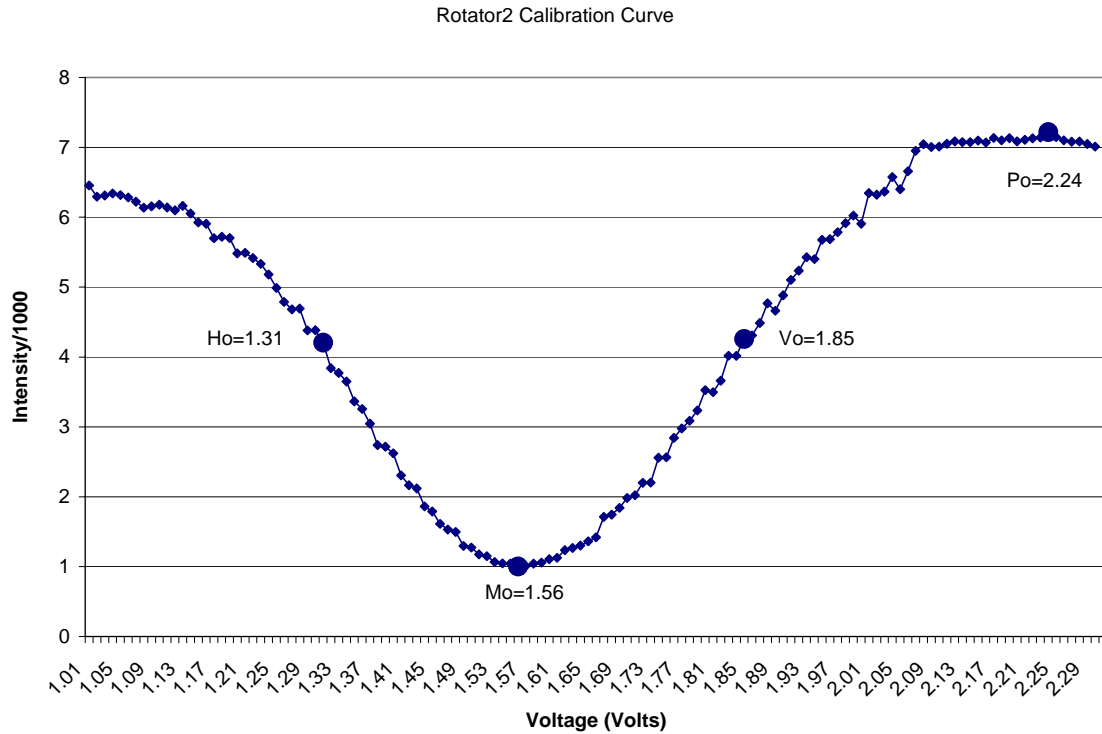


**Figure 11:** Rotator2 Calibration Curve

The next component to calibrate is rotator1. The user then chooses the ROTATOR1 tab and sets the zero rotation voltages for the retarders as done before and sets the Mo voltage for rotator2 obtained from rotator2 calibration. Then the voltage is set to vary between 1.00 and 2.30 Volts in 0.01 Volt increments, and the  $H_i$ ,  $V_i$ ,  $P_i$ , and  $M_i$  voltages are determined as before. Figure 12 shows the data obtained from the rotator1 calibration, where the points chosen by the Matlab program are enlarged.

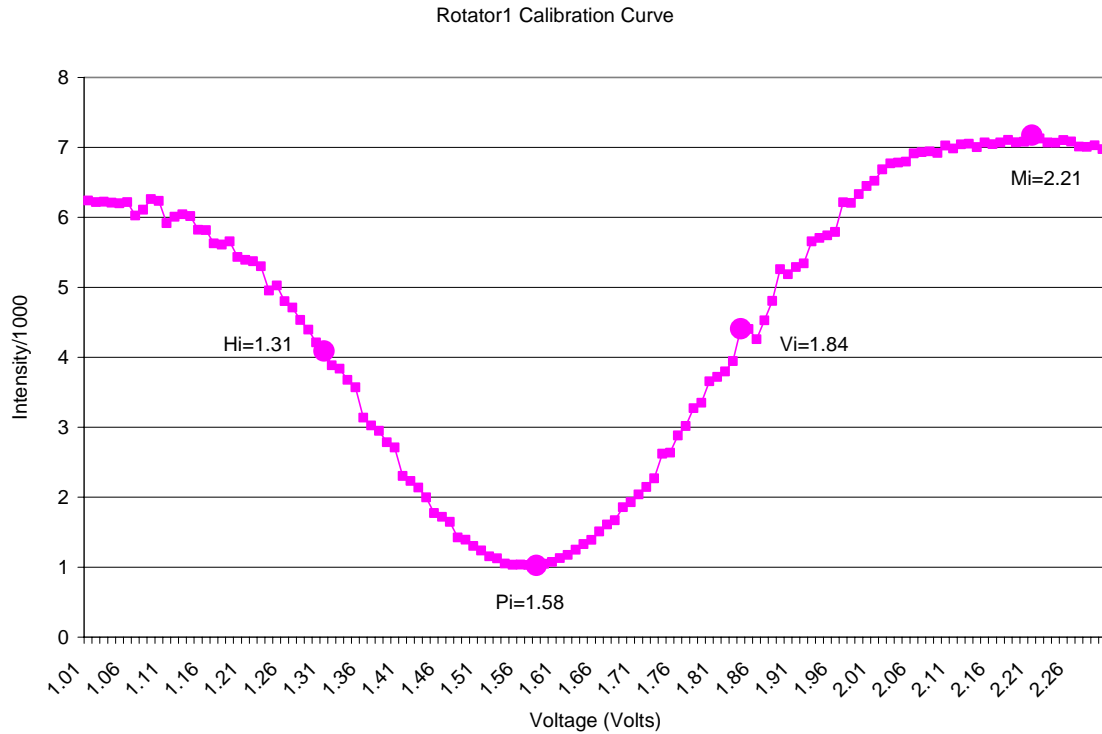


**Figure 12:** Rotator1 Calibration Curve

After all the voltages necessary to produce the linear polarization states have been determined, retarder2 is calibrated by clicking on the RETARDER2 tab in the program and setting the zero retardance voltage for retarder1, the  $H_i$  voltage for rotator1, and the  $V_i$  voltage for rotator2. The retarder2 voltages are set to go from 1.5 to 5.5 in 0.01 increments, and the “Take Images?” button is pressed to collect the data. A Matlab program similar to that for the rotators calculates the quarter wave plate (QWP) voltage for the retarder. This process is repeated again using the  $V_i$  voltage for rotator1 and the  $H_i$  voltage for rotator2. This is done because the experimental QWP voltages for the

horizontal and vertical polarization states are not the same. Figure 13 shows the horizontal and vertical QWP voltages determined using the calibration program.

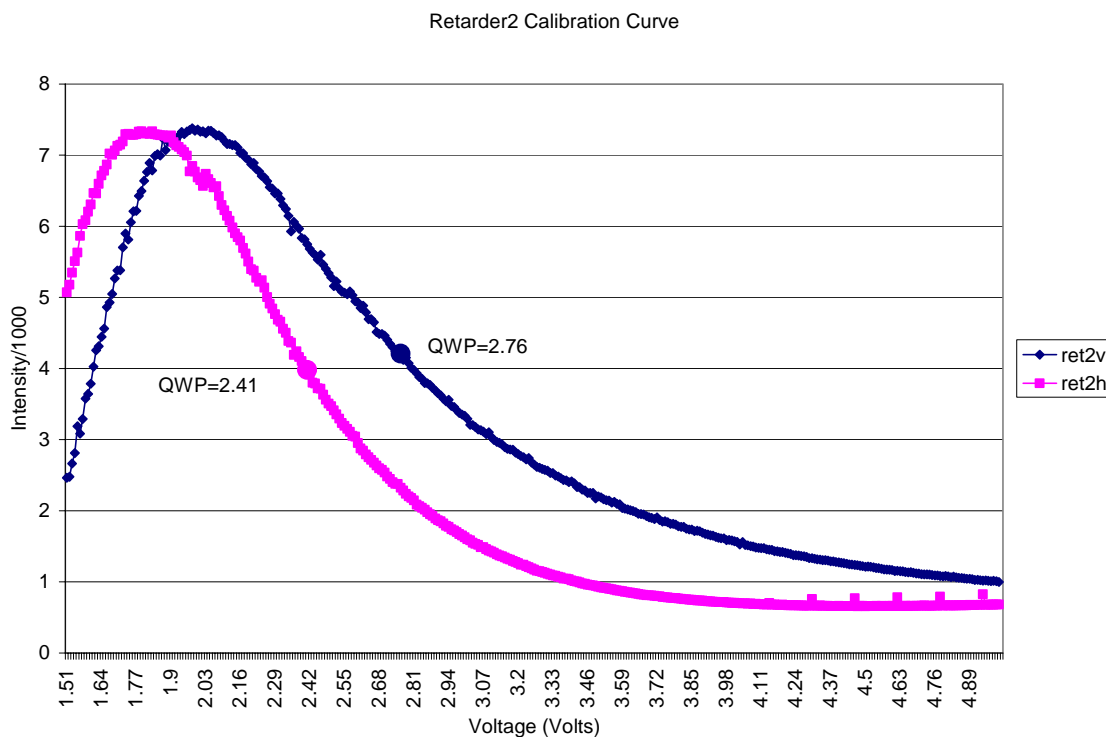


**Figure 13:** Retarder2 Calibration Curve

The last component to be calibrated is retarder1. The RETARDER1 tab is chosen, and the voltages are set to increment by 0.01 Volts from 1.5-5.5 volts. The process used to calibrate retarder2 that was described above is used, and the horizontal and vertical QWP voltages are determined. Figure 14 shows the retarder1 calibration data.



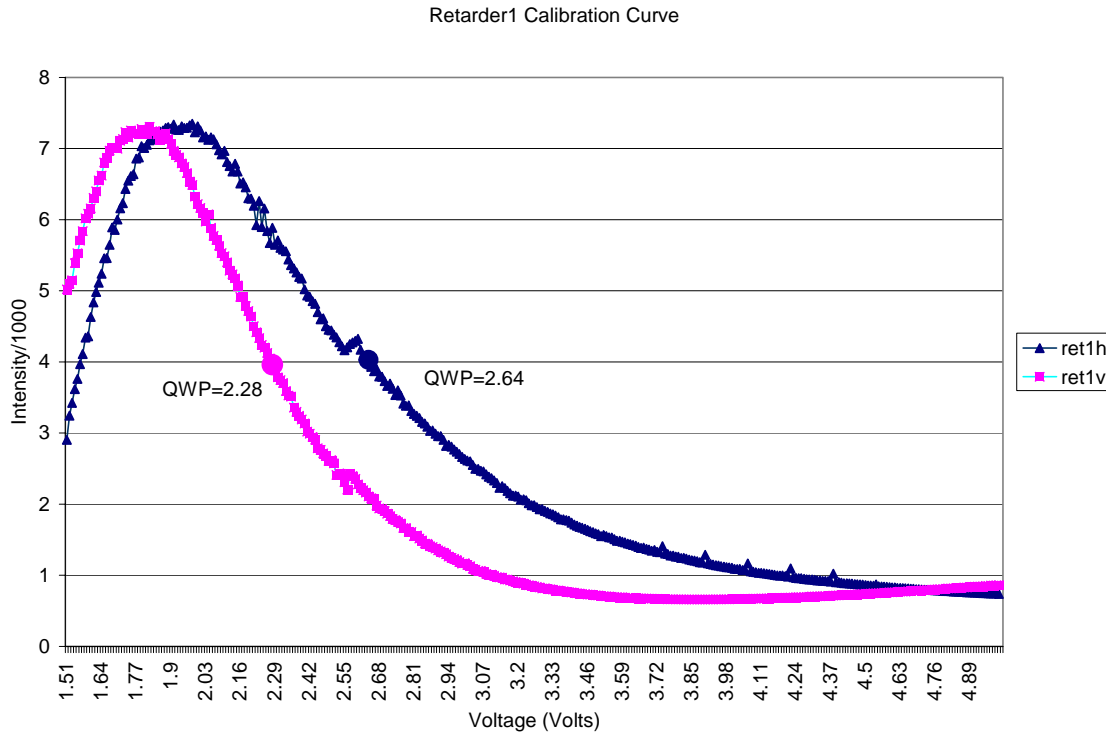


**Figure 14:** Retarder1 Calibration data

Once all of the voltages are determined, the user can close the calibration program by clicking the “OK” button, and can now choose VOLTAGES from the drop down menu. The voltages can be set in the window and will be displayed on the main window for each case of input and output polarization state. Other settings can also be made using the drop down menu such as image save path, number of images to take (16 or 36), and DAQ board settings. Once everything is set and Kestrel Spec Imaging software is opened, the “Acquire Images” button can be pressed to take the polarization images and display the Mueller matrix.

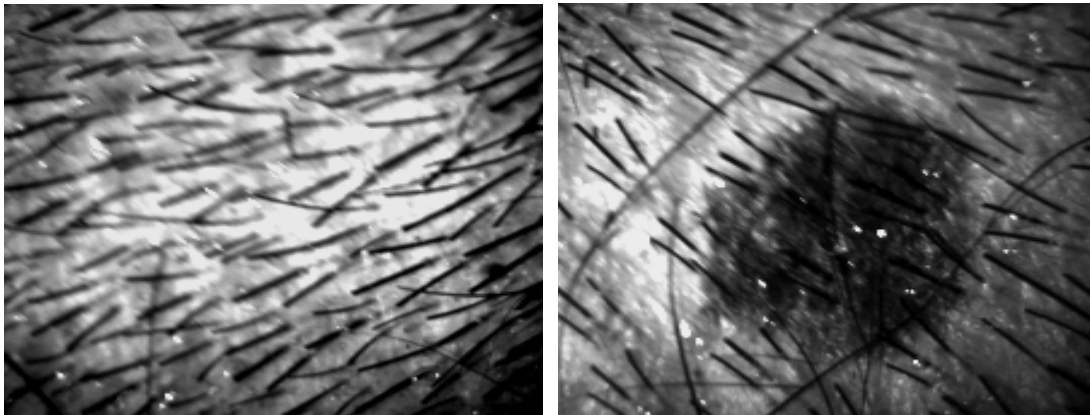
## CHAPTER V

### RESULTS AND DISCUSSION

This chapter reviews and discusses the results obtained during this research. The initial section presents the Mueller matrix image analysis using the mean and percentile intensity values for each image. The second section shows the statistical analysis results for the Mueller matrix data, and gives the variables that are capable of distinguishing between cancerous and noncancerous tissue. The final section gives the new calibration verification results and discusses its potential as a new calibration method.

#### 5.1 Mueller Matrix Results

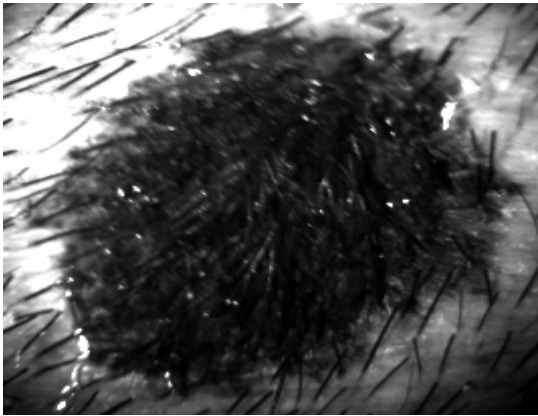
After the data was collected, the Mueller matrix was calculated for each sample. Figure 15 shows the full intensity polarization image, HH, for each skin type.



(a) Normal Skin

(b) Benign Mole

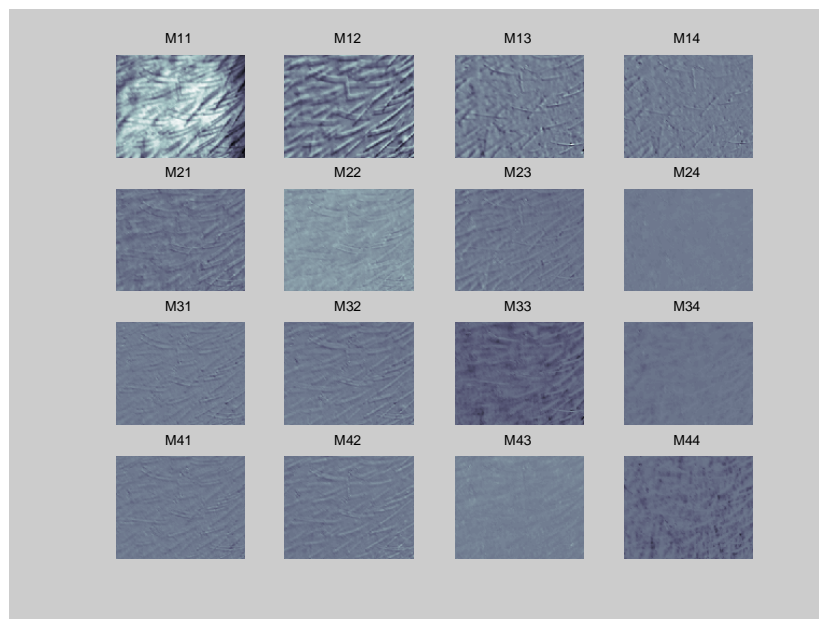
**Figure 15:** HH Images of Skin Lesions from the Sinclair Swine



(c) Cancerous Lesion

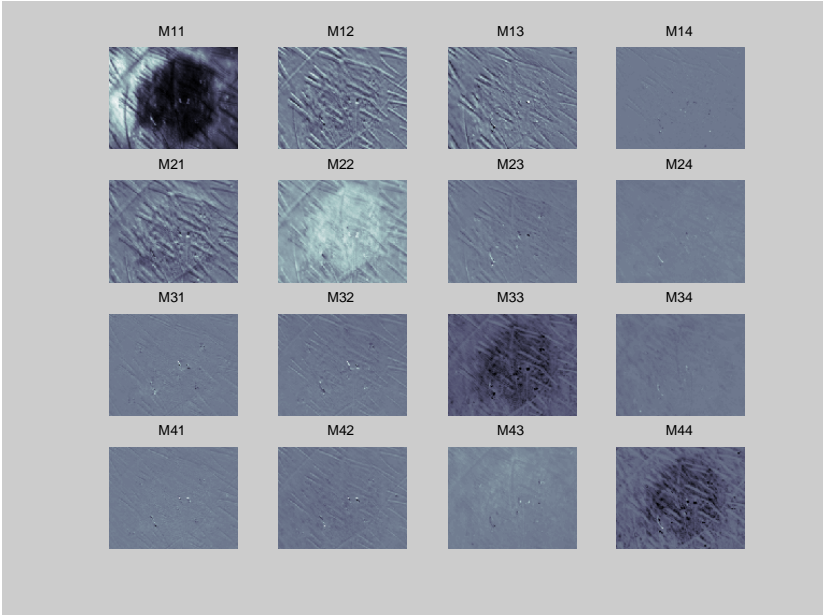
**Figure 15:** Continued

The Mueller matrix images are shown in Figure 16. The images are normalized by the first (M11) image, except the M11 image which was left for comparison.

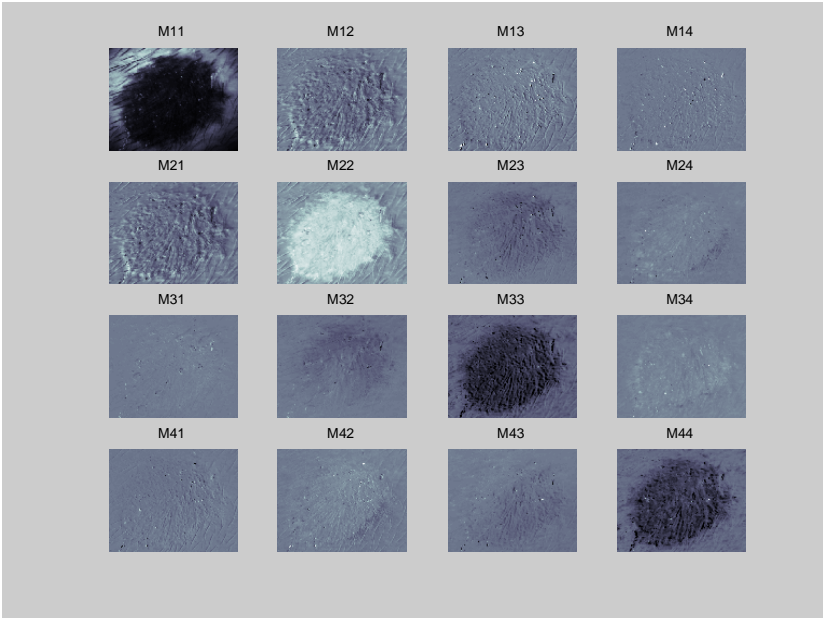


(a) Normal Skin

**Figure 16:** Mueller Matrix Images from the Sinclair Swine



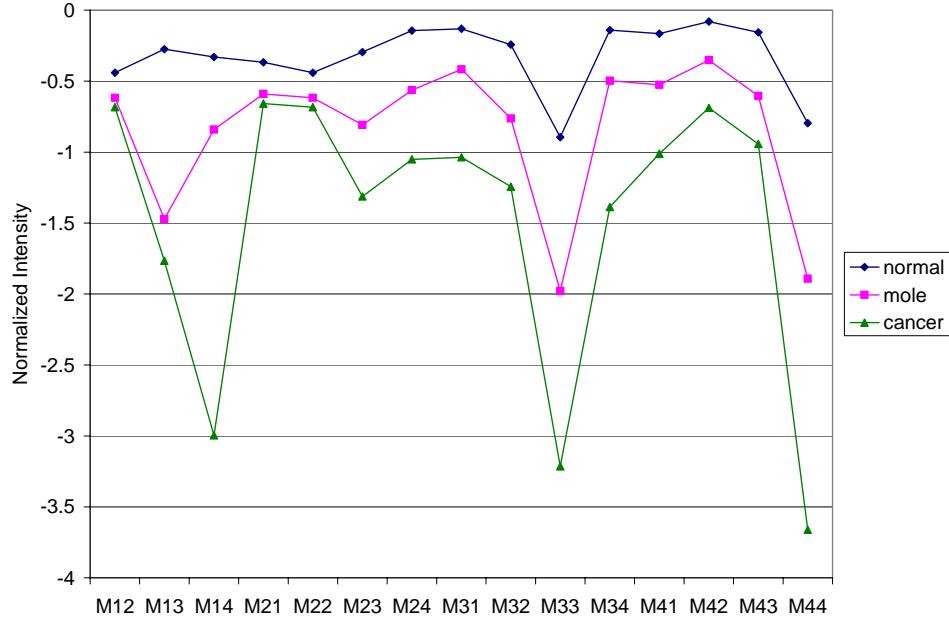
(b) Benign Mole



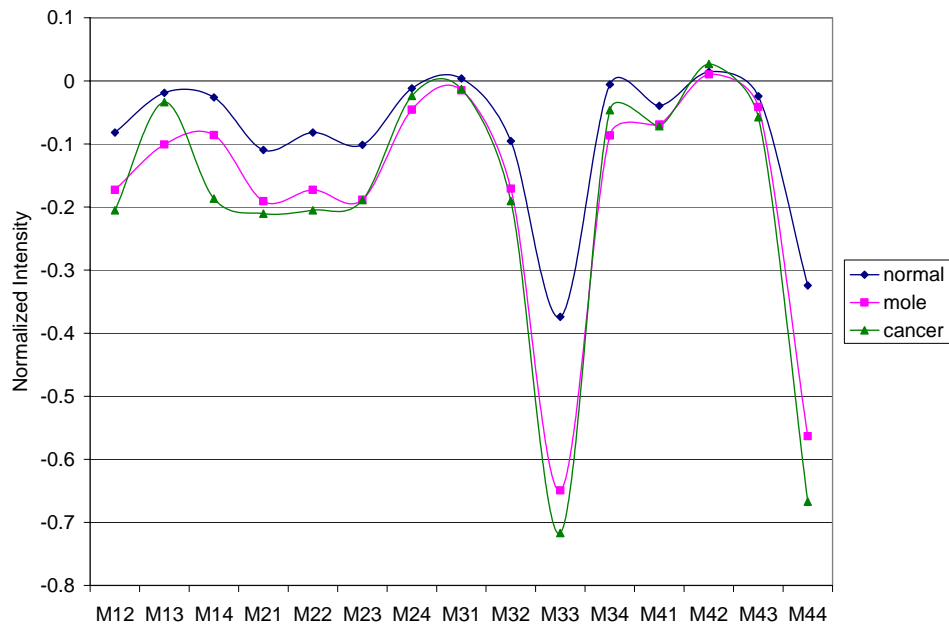
(c) Cancerous Lesion

Figure 16: Continued

From these images alone, it is difficult to distinguish between the tissue types. Therefore, the images were cropped to include only the pixels of the lesion contained within the border, and they were analyzed using both the percentile and mean intensities as described in the previous chapter. The data was analyzed all together and separated by exposure time since exposure time determines the dynamic range of the data. Exposure times of 0.06, 0.12, and 4 seconds were used with 19, 20, and 19 samples respectively for each. The rest of the data was at other exposure times, but not enough data was collected for each to be used. It was determined as will be seen later in the CART analysis that the exposure time not only needs to be constant across the data set, but it must also be large. Therefore, the results of the images with exposure time 4 will be presented, which contained a total of 19 samples -5 normals, 7 moles, 8 cancers. The following plots (Figures 17-26) show the results from this analysis for the images with exposure time of 4 seconds where each line represents the average for each tissue type.



**Figure 17:** Mueller Matrix for Images with Exposure Time 4 secs Obtained using 10<sup>th</sup> Percentile of Each Image



**Figure 18:** Mueller Matrix for Images with Exposure Time 4 secs Obtained using 20<sup>th</sup> Percentile of Each Image

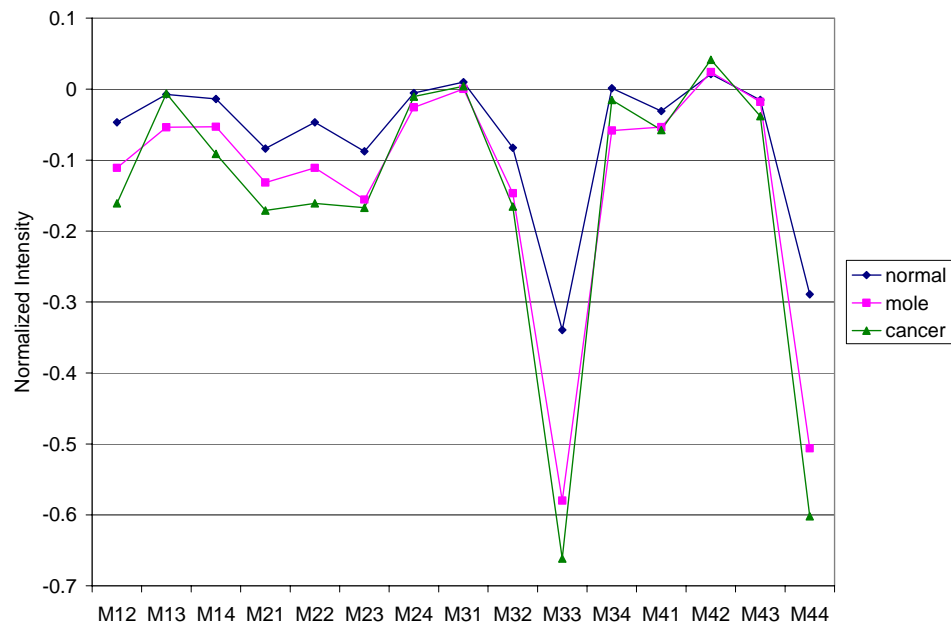


**Figure 19:** Mueller Matrix for Images with Exposure Time 4 secs Obtained using 30<sup>th</sup> Percentile of Each Image

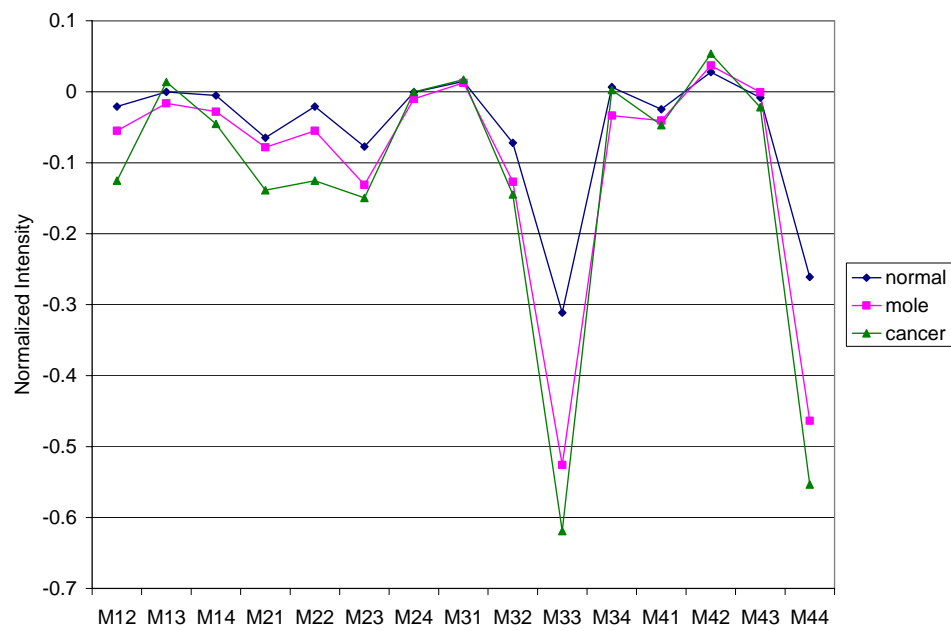


**Figure 20:** Mueller Matrix for Images with Exposure Time 4 secs Obtained using 40<sup>th</sup> Percentile of Each Image

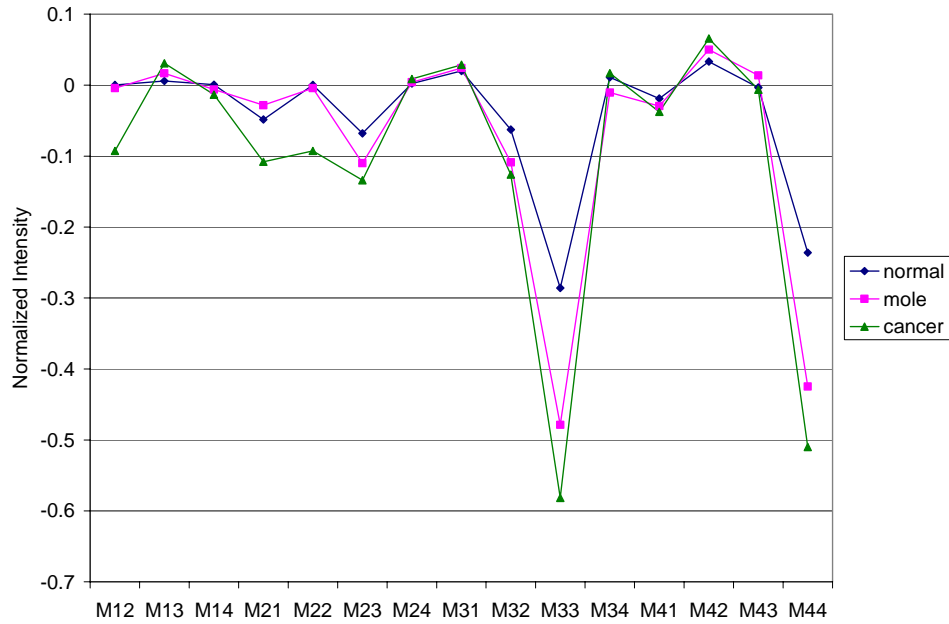


**Figure 21:** Mueller Matrix for Images with Exposure Time 4 secs Obtained using 50<sup>th</sup> Percentile of Each Image

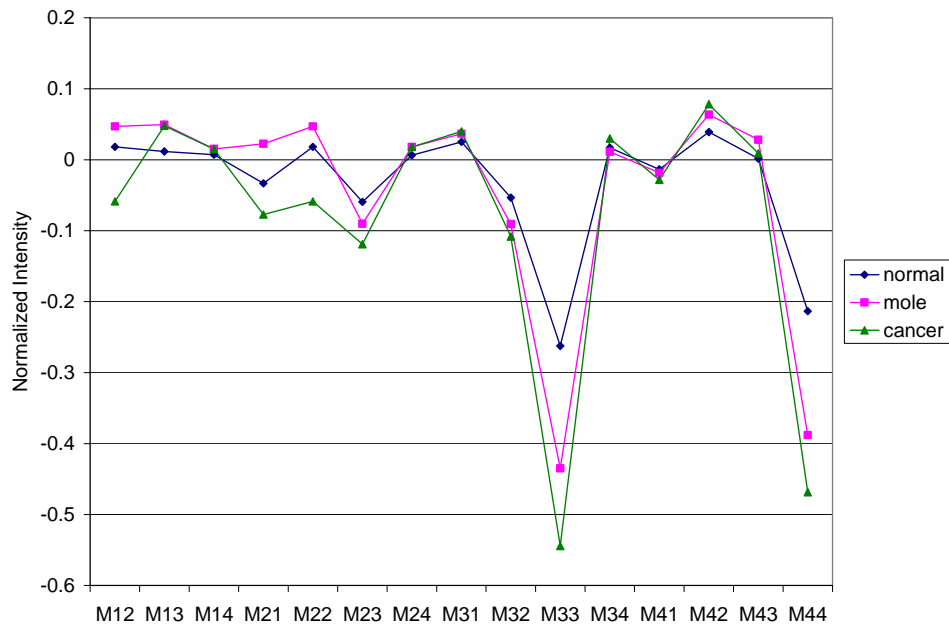


**Figure 22:** Mueller Matrix for Images with Exposure Time 4 secs Obtained using 60<sup>th</sup> Percentile of Each Image



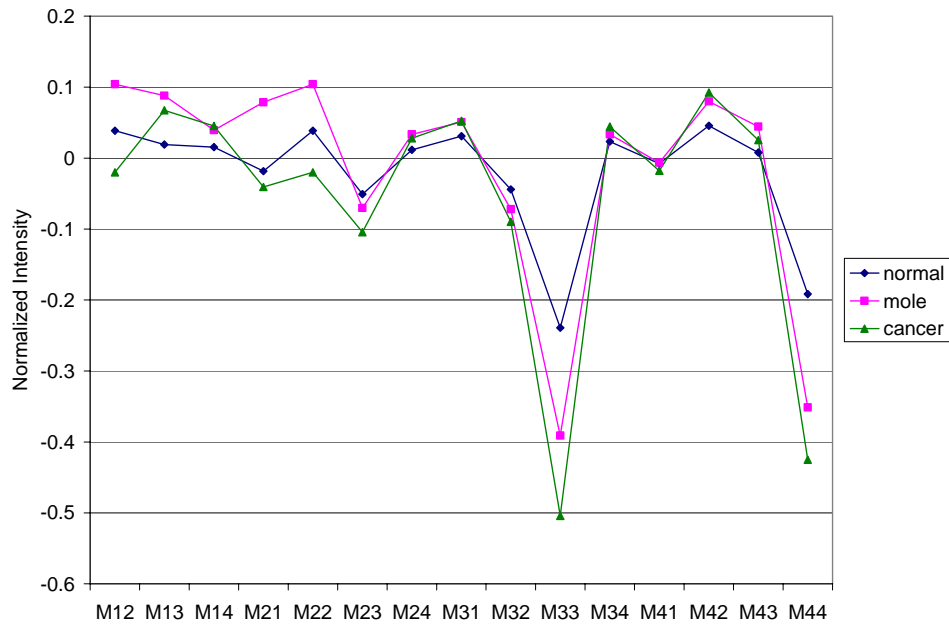


**Figure 23:** Mueller Matrix for Images with Exposure Time 4 secs Obtained using 70<sup>th</sup> Percentile of Each Image

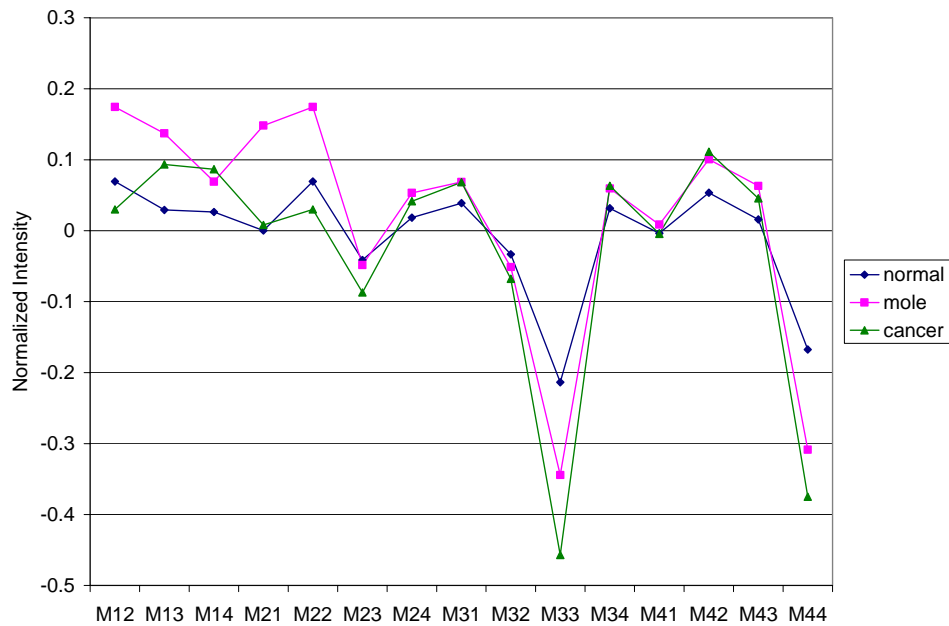


**Figure 24:** Mueller Matrix for Images with Exposure Time 4 secs Obtained using 80<sup>th</sup> Percentile of Each Image

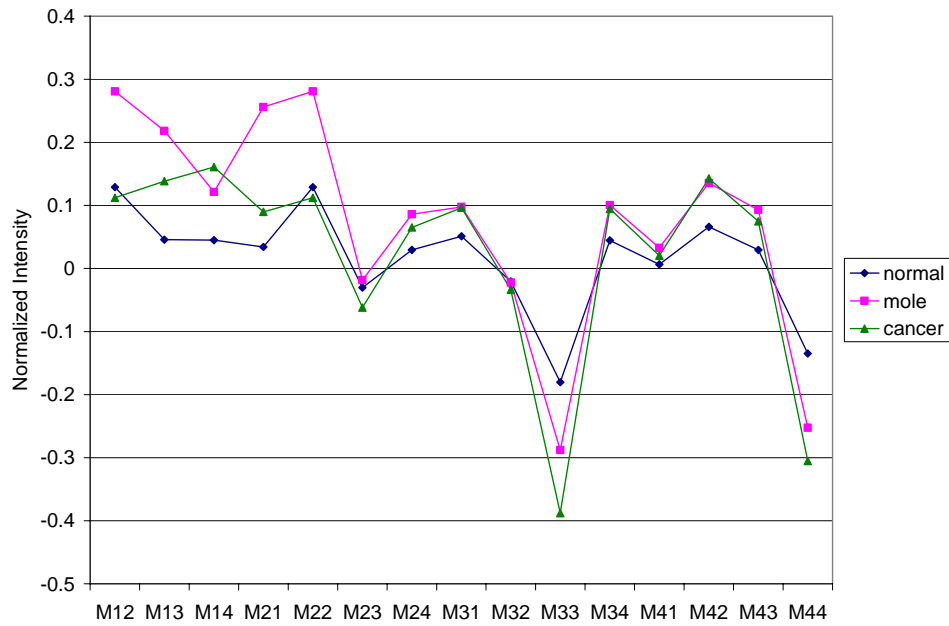


**Figure 25:** Mueller Matrix for Images with Exposure Time 4 secs Obtained using 90<sup>th</sup> Percentile of Each Image

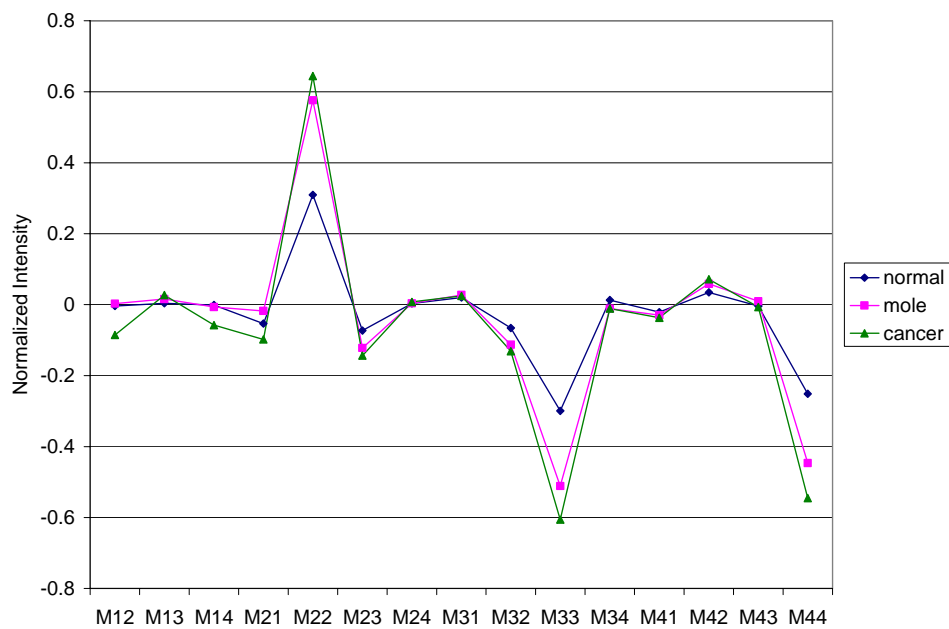


**Figure 26:** Mueller Matrix for Images with Exposure Time 4 secs Obtained using the Mean of Each Image

For the above images  $M_{11}$  was not included because it would be a value of 1 for all cases since the data was normalized by  $M_{11}$ . Therefore, the raw (unnormalized)  $M_{11}$  data was also included in the data analysis and is shown in Figure 27. It can be seen from this plot that the raw  $M_{11}$  value can be used to classify the tissue types. For comparison, the raw  $M_{11}$  plot for the data with exposure time less than 4 is shown in Figure 28. This plot shows that with lower exposure time cancer and moles are indistinguishable.

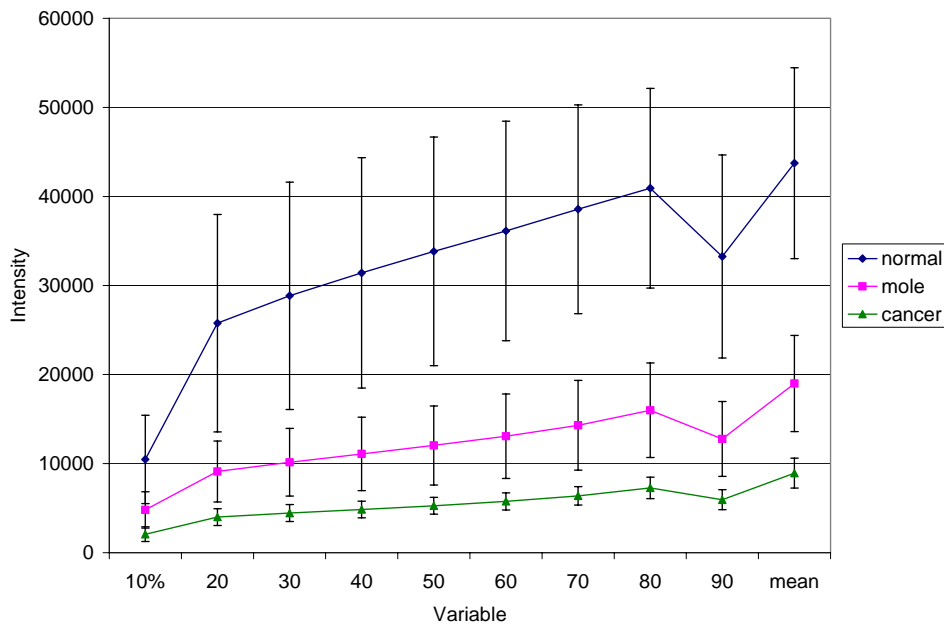


**Figure 27:** 10-90<sup>th</sup> Percentile and Mean Analysis for Raw M11 for Images with Exposure Time of 4 secs

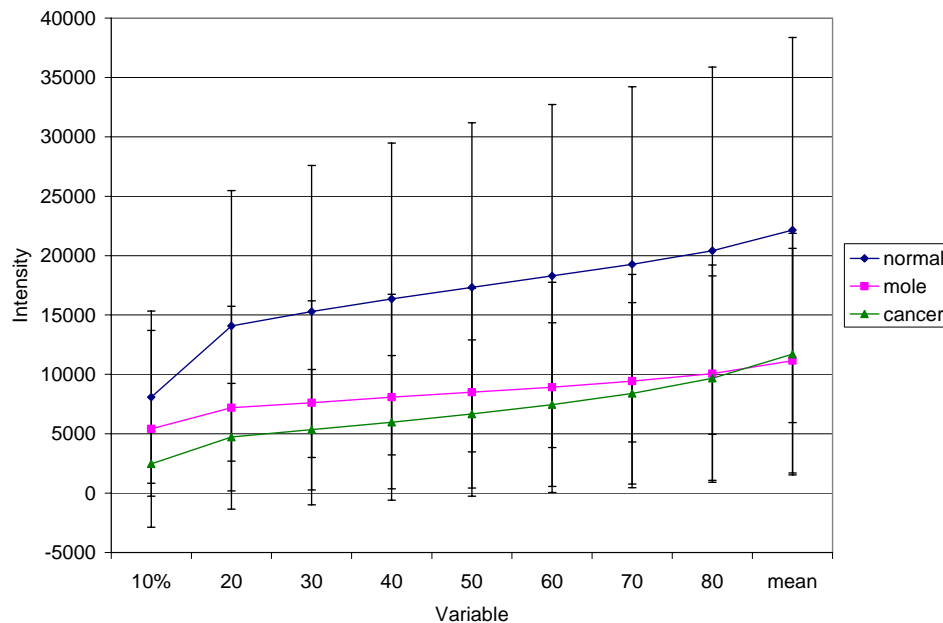


**Figure 28:** 10-90<sup>th</sup> Percentile and Mean Analysis for Raw  $M_{11}$  for Images with Exposure Time Less than 4 seconds

## 5.2 CART Results

The goal of the statistical analysis was to separate the data according into tissue types according to a classification scheme and to identify the importance of each matrix element in the classification. Classification and Regression Tree (CART) software was used to determine the ability of the Mueller matrix imaging system in distinguishing between cancerous and noncancerous tissue. CART uses binary recursive portioning as described in the Theory section to classify the data.

The data was separated by exposure time and a CART analysis was performed on each set. The data was also grouped by exposure times greater than 1 and exposure times greater than 2 to determine if different exposure times could be used together. It was

determined that the data with the largest exposure time, 4 seconds, was accurately classified into the three classes - normal, mole, and cancer. Table 5 shows the classification probability for the data.

**Table 5:** Learning Sample Probability

Actual Class	Predicated Class			Actual Total
	1	2	3	
1-normal	1.000	0.000	0.000	1
2-mole	0.000	1.000	0.000	1
3-cancer	0.000	0.000	1.000	1

Cross validation was performed on the data since there were less than 200 samples. The cross validation classification probability, Table 6, shows classification percentages for each case and provides a numerical analysis of the accuracy of the classification scheme. The classification criteria determined from the classification tree along with the number of misclassified using cross validation are summarized in Table 7 where M11Twenty is the 20% of the  $M_{11}$  matrix element. The full classification tree is displayed in Appendix H.

**Table 6:** Results from CART Analysis of Data with Exposure Time 4 seconds

Sample Type	Classification Pathway			No. <sup>1</sup>	Misclassified	
					# <sup>2</sup>	As <sup>3</sup>
Cancer	M11Twenty <= 5450.00	Node 1		8	0	-
Mole	M11Twenty > 5450.00	M11Twenty <= 15640.50	Node 2	7	5	1
Normal	M11Twenty > 5450.00	M11Twenty > 15640.50	Node 3	4	0	-

Classification: 1=normal, 2=mole, 3=cancer.

<sup>1</sup>No. indicates the number of cases classified by the specific path

<sup>2</sup># indicates the number of each case that was misclassified

<sup>3</sup>As indicates what the misclassified cases were actually classified as

**Table 7:** Cross Validation Probability

Actual Class	Predicated Class			Actual Total
	1	2	3	
1-normal	1.000	0.000	0.000	1
2-mole	0.714	0.286	0.000	1
3-cancer	0.000	0.000	1.000	1

From the cross validation probability table above, a 2x2 decision matrix for cancer was made (Table 8). From the table it can be seen that cancer was correctly diagnosed for all of the samples. The sensitivity, defined as true positive divided by the sum of true positive and false negative, and the specificity, which is defined as true negative divided by the sum of true negative and false positive, can be determined using Table 8. The sensitivity is calculated to be 100.0%, and the specificity is determined to be 100.0%.

**Table 8:** Decision Matrix for Cancer

True Positive 8	False Positive 0
False Negative 0	True Negative 11

A similar matrix can be made for moles, which is shown in Table 9. The sensitivity for moles is 28.6%, and the specificity is 100%. The 5 moles that were misclassified were classified as normal tissue, which does not present a problem in detecting cancer.

**Table 9:** Decision Matrix for Mole

True Positive 2	False Positive 0
False Negative 5	True Negative 12

The CART analysis also determines the importance of each variable in the classification. Table 10 shows the relative variable importance, where the variables with zero importance are not listed.

**Table 10:** Relative Importance of the Variables

<b>Variable</b>	<b>Relative Importance</b>
M11Twenty	100.000
M11Thirty	100.000
M11Forty	100.000
M11Fifty	100.000
M11Sixty	100.000
M11Seventy	100.000

### **5.3 New Calibration Verification**

To verify the new calibration procedure, the Mueller matrix for several known samples was calculated using the Mueller matrix imaging system with both a rough and fine tune calibration. The known samples used were air, a polarizer oriented at horizontal, and a polarizer oriented at  $+45^\circ$ . The Mueller matrix was taken 10 times for each sample to show system repeatability, and the mean and standard deviation were calculated. The experimental and theoretical Mueller matrices for each sample using a rough calibration are shown below in Tables 11-13.



Table 11: Mueller Matrix Results for Air

Experimental			
1	0.0097	0.0136	0.0034
-0.031	<b>0.9214</b>	-0.008	0.0136
0.0734	0.0395	0.9263	-0.026
0.018	-0.004	-0.018	0.924
Theoretical			
1	0	0	0
0	1	0	0
0	0	1	0
0	0	0	1
Absolute Error			
0.00	0.97	1.36	0.34
-3.09	<b>7.86</b>	-0.82	1.36
7.34	3.95	7.37	-2.58
1.80	-0.38	-1.82	7.60

Table 12: Mueller Matrix Results for Horizontal Polarizer

Experimental			
1	0.9267	0.0729	-0.026
0.9349	<b>0.9116</b>	0.0721	-0.021
-0.083	-0.084	0.0073	-0.087
0.0332	0.0435	0.0061	-0.077
Theoretical			
1	1	0	0
1	1	0	0
0	0	0	0
0	0	0	0
Absolute Error			
0.00	7.33	7.29	-2.61
6.51	<b>8.84</b>	7.21	-2.05
-8.25	-8.44	0.73	-8.66
3.32	4.35	0.61	-7.67

**Table 13:** Mueller Matrix Results for +45° Polarizer

Experimental			
1	<b>-0.088</b>	1.0036	0.0105
-0.035	-0.007	-0.029	0.0026
0.9676	0.0176	0.9212	-0.01
-0.06	-0.004	0.0248	-0.057
Theoretical			
1	0	1	0
0	0	0	0
1	0	1	0
0	0	0	0
Absolute Error			
0.00	<b>-8.82</b>	-0.36	1.05
-3.45	-0.71	-2.86	0.26
3.24	1.76	7.88	-1.02
-5.95	-0.36	2.48	-5.65

The results show that the maximum absolute error for air was 7.86%, which occurred in the  $M_{22}$  element. For the horizontal polarizer, the maximum absolute error was 8.84% in the  $M_{22}$  element. The final sample, +45° polarizer, had a maximum absolute error of 8.82 in the  $M_{12}$  element. Even though this error is within reasonable range, the calibration was fine tuned using the system model in Equation 15 and Appendix F to determine if the error could be reduced. With this method, each element of the Mueller matrix is analyzed to determine the images that are responsible for the error. Then the intensity of those images is examined and compared with theoretical values. The plots in Appendix F are used to determine the voltages to change so that the experimental intensity is approximately equal to the theoretical intensity. For example for the  $M_{22}$  element of air, the equation for  $M_{22}$  from the theory section was used to

determine that the images HH, HV, VH, and VV needed to be examined. For the VV image, the plots in Appendix F show that the rotator voltages are responsible for the irradiance, and therefore were changed until the correct intensity (maximum) was found. This process was repeated for the other three images (HH, VH, and HV), and then another matrix element was examined in the same manner. The polarization images were taken again, and the Mueller matrix was calculated. The results after fine tuning are shown in Tables 14-16 below.

**Table 14:** Mueller Matrix after Fine Tune Calibration for Air

Experimental			
1	-0.005	<b>0.0183</b>	0.0093
-0.002	0.9907	0.0178	0.0036
0.015	0.011	0.9819	-0.016
0.013	0.0095	0.0127	0.9996
Theoretical			
1	0	0	0
0	1	0	0
0	0	1	0
0	0	0	1
Absolute Error			
0.00	-0.47	<b>1.83</b>	0.93
-0.15	0.93	1.78	0.36
1.50	1.10	1.81	-1.59
1.30	0.95	1.27	0.04

**Table 15:** Mueller Matrix after Fine Tune Calibration for Horizontal Polarizer

Experimental			
1	0.9866	0.0152	-0.013
0.9962	0.9885	0.0053	-0.008
-0.013	-0.016	-0.006	<b>-0.017</b>
0.0093	0.0042	-0.003	-0.015
Theoretical			
1	1	0	0
1	1	0	0
0	0	0	0
0	0	0	0
Absolute Error			
0.00	1.34	1.52	-1.32
0.38	1.15	0.53	-0.82
-1.26	-1.58	-0.57	<b>-1.74</b>
0.93	0.42	-0.29	-1.49

**Table 16:** Mueller Matrix after Fine Tune Calibration for +45° Polarizer

Experimental			
1	0.0066	0.9905	0.0182
-0.013	0.0056	-0.013	-0.003
<b>0.9812</b>	0.0043	0.9827	-0.014
-0.009	-0.006	0.0185	-0.007
Theoretical			
1	0	1	0
0	0	0	0
1	0	1	0
0	0	0	0
Absolute Error			
0.00	0.66	0.95	1.82
-1.29	0.56	-1.34	-0.29
<b>1.88</b>	0.43	1.73	-1.41
-0.94	-0.62	1.85	-0.68

The maximum absolute error after fine tuning was found to be 1.83 for air, 1.74 for the horizontal polarizer, and 1.88 for the  $+45^\circ$  polarizer. Fine tuning is capable of reducing the error by 6 - 7%. The new calibration method was shown to be accurate and a viable method to replace the old, time consuming technique.

The error in the sample Mueller matrices is due to several issues. First, the optics are not perfect and therefore introduce error in the system. Also, since a broadband red filter is used, light at other wavelengths gets through which causes error in the retardance. The system also shows preferential polarization in the vertical direction, which causes intensity differences that create error in the Mueller matrix. The liquid crystals are temperature sensitive, and therefore their rotation/retardance varies as a function of the room temperature. A temperature monitor/controller is needed to ensure that the liquid crystals are maintained at a constant temperature. Also, the computer used to drive the system does not have sufficient RAM. It only has 128MB of RAM, which causes problems with the systems performance in terms of acquiring and saving images.

To demonstrate the repeatability of the system, the Mueller matrix was taken 10 times, and the standard deviation of each case was calculated and is shown below in Table 17. The maximum standard deviation was 0.0078, 0.0072, and 0.0089 for air, horizontal polarizer, and the  $+45^\circ$  polarizer respectively. The standard deviation shows that the repeatability of the system is good, and therefore the calibration held over ten runs of the system.

Table 17: Standard Deviation of Each Mueller Matrix Element for Each Sample

	Air	Hpolarizer	Ppolarizer
M11	0.0000	0.0000	0.0000
M12	0.0045	0.0051	0.0041
M13	0.0074	0.0047	<b>0.0089</b>
M14	0.0031	0.0028	0.0084
M21	0.0046	0.0031	0.0046
M22	0.0019	0.0034	0.0038
M23	0.0042	0.0047	0.0047
M24	<b>0.0078</b>	<b>0.0072</b>	0.0076
M31	0.0047	0.0050	0.0026
M32	0.0038	0.0059	0.0051
M33	0.0052	0.0041	0.0077
M34	0.0062	0.0039	0.0087
M41	0.0049	0.0049	0.0059
M42	0.0048	0.0050	0.0044
M43	0.0069	0.0062	0.0066
M44	0.0045	0.0062	0.0070

## CHAPTER VI

### CONCLUSIONS AND FUTURE WORK

The American Cancer Society estimates that more than 1 million new cases of basal cell and squamous cell carcinomas and approximately 55,100 new cases of melanoma will be diagnosed in the United States each year [1]. If the cancer is detected in its early stages, it has a 95% cure rate, but current detection methods cannot adequately detect the presence of cancer. These methods are painful and costly to the patient and are not guaranteed effective. Therefore, the work done for this thesis was an optical approach for skin cancer detection in hopes of overcoming the problems with current detection methods.

The two main purposes of this thesis were to analyze Sinclair swine data taken using the Mueller matrix imaging system, and to redesign the calibration procedure for the system. The Sinclair swine data was analyzed to determine the ability of the system to distinguish between cancerous and noncancerous tissue. The results, shown previously, show that the system is capable of distinguishing between cancer, mole, and normal tissue as long as the exposure time is constant for the data set and the dynamic range is large. The Raw  $M_{11}$  images with exposure time of 4 seconds were able to correctly classify all of the cancers and only misclassified 5 moles as normal skin.

The system calibration procedure was redesigned because the previous technique took nearly a day to complete. The new procedure takes about half the time and is just as accurate. A fine tune calibration should be done in conjunction with the new calibration technique to reduce the error associated with calibrating all of the optics together.

Future investigations will be directed to improve the system electronics. The electro-optics require a 2 kHz square-wave, and very specific voltages to produce different polarization states. These voltages should be very accurate, and therefore circuitry should be designed to do this. The voltages supplied from the DAQ should be measured and compared across days.

Other future work should be focused on monitoring and controlling the liquid crystal's temperature. Meadowlark Optics, the liquid crystal manufacturer, sells a temperature sensor for the liquid crystals for accurate monitoring of the operating temperature. A temperature sensor is recommended, but ideally it would work in conjunction with a temperature regulator.

The system stability is another issue in question. To quantify the stability of the system, the calibration program should be run several times, and the voltages used to produce the polarization states should be recorded. The voltages should also be compared over days.

Using the new calibration procedure and data analysis tools, more Sinclair swine or other animal data should be collected to obtain a larger data set. The CART analysis should again be performed so that the ability of the system to classify the tissue types over a large sample is validated. The system should then be made portable so that it can be used for clinical studies. The system should also be able to distinguish between skin cancer types, and thus work in this area is also needed. Although, much work is still needed before the system is ready for clinical studies, progress has been made towards attaining this goal.



## REFERENCES

- [1] American Cancer Society, "Skin Cancer Facts & Figures 2004", American Cancer Society, Pub. No. 5008.04, 2004.
- [2] American Cancer Society, "Cancer Facts and Figures 2003" 2003. American Cancer Society, Pub. No. 5008.03, 2003.
- [3] Melanoma Net. (2002, December). Common Skin Cancers Other than Melanoma. American Academy of Dermatology, Schaumburg, IL. [Online]. Available: [http://www.skincarephysicians.com/melanomanet/SkinCancers\\_December.htm](http://www.skincarephysicians.com/melanomanet/SkinCancers_December.htm)
- [4] S. Jacques, J. Roman, and K. Lee, "Imaging superficial tissues with polarized light," *Lasers in Surgery and Medicine*, vol. 26, pp. 119-129, 2000.
- [5] M. Mehrubeoglu, N. Kehtarnavaz, G. Marquez, M. Duvic, and L.-H. Wang, "Skin lesion classification using diffuse reflectance spectroscopic imaging with oblique incidence," *Applied Optics*, vol. 41, no. 1, pp. 182-192, 2002.
- [6] B. Beauvoit, S. Evans, and T. Jenkins, "Correlation between the light scattering and the mitochondrial content of normal tissues and transplantable rodent tumors," *Analytical Biochemistry*, vol. 226, pp. 167-174, 1995.
- [7] G. Yao and L.V. Wang, "Two-dimensional depth resolved Mueller matrix characterization of biological tissue by optical coherence tomography," *Optics Letters*, vol. 24, no. 8, pp. 537-539, 1999.
- [8] Loyola University Health System. (2003, December). Anatomy of the Skin. Loyola University Health System, Maywood, IL. [Online]. Available: <http://www.luhs.org/health/topics/skin/anatomy.htm>
- [9] The Skin Cancer Foundation, "Basal Cell Carcinoma: The Most Common Skin Cancer" The Skin Cancer Foundation, Item ID. BR-7, 2003.
- [10] The Skin Cancer Foundation, "Squamous Cell Carcinoma: The Second Most Common Skin Cancer" The Skin Cancer Foundation, Item ID. BR-9, 2003.
- [11] The Skin Cancer Foundation, "Types and Descriptions of Skin Cancers" The Skin Cancer Foundation, Item ID. BR-3, 2003, 2003.
- [12] Aetna IntelliHealth. (2002, November). Squamous Cell Carcinoma. Aetna, Hartford, CT. [Online]. Available: <http://www.intelihealth.com/IH/ihtIH/WSIHW000/8297/24556/211186.html?d=dmtHealthAZ>

- [13] Aetna IntelliHealth. (2003, June). Basal Cell Carcinoma. Aetna, Hartford, CT. [Online]. Available: <http://www.intelihealth.com/IH/ih/IH/WSIHW000/8297/24556/211185.html?d=dmtHealthAZ#info>
- [14] B. Hazen. (1999, November). The clinical diagnosis of early malignant melanoma: expansion of the ABCD criteria to improve diagnostic sensitivity. *Dermatology Online Journal*. [Online]. 5(2), pp. 3. Available: <http://dermatology.cdlib.org/>
- [15] Aetna IntelliHealth (2004, January). Melanoma. Aetna, Hartford, CT. [Online]. Available: <http://www.intelihealth.com/IH/ih/IH/WSIHW000/8297/24556/211187.html?d=dmtHealthAZ>
- [16] K. Yu and L. Ji, "How to optimize OCT," *Optics Express*, vol. 9, no. 1, pp. 24-35, 2001.
- [17] S. Jiao and L. Wang, "Two-dimensional depth-resolved Mueller matrix of biological tissues measured with double-beam polarization sensitive optical coherence tomography," *Optics Letters*, vol. 27, no. 2, pp. 101-103, 2002.
- [18] G. Cote, R.M. Lec, M.V. Pishko, "Emerging biomedical sensing technologies and their applications," *IEEE Sensors Journal*, vol. 3, no. 3, pp. 251-266, 2003.
- [19] M. Bashkansky and J. Reintjes, "Statistics and reduction of speckle in optical coherence tomography," *Optics Letters*, vol. 25, no. 8, pp. 545-547, 2000.
- [20] S. Jiao and W. Yu, "Optical fiber based Mueller optical coherence tomography," *Optics Letters*, vol. 28, no. 4, pp. 1206-1208, 2003.
- [21] L. Bvancaleon, A. Durkin, J. Tu, G. Menaker, J. Fallon, and N. Kollias, "In vivo fluorescence spectroscopy of non melanoma skin cancer," *Photochemistry and Photobiology*, vol. 73, no. 2, pp. 178-183, 2000.
- [22] R.M. Szeimies and M. Landthaler, "Photodynamic therapy and fluorescence diagnosis of skin cancers," *Cancer Research*, vol. 160, pp. 240-245, 2002.
- [23] Cancer Information Service. (1999, August). Photodynamic Therapy. National Cancer Institute, Bethesda, MD. [Online]. Available: [http://cis.nci.nih.gov/fact/7\\_7.htm](http://cis.nci.nih.gov/fact/7_7.htm)

- [24] J. R. Mourant, M. Canpola, C. Brocker, O. Esponda-Ramos, T.M. Johnson, A. Matanock, K. Stetter, and J.P. Freyer, "Light scattering from cells: the contribution of the nucleus and the effects of proliferative status," *Journal of Biomedical Optics*, vol. 5, no. 2, pp. 131-137, 2000.
- [25] N. Stone, C. Kendall, J. Smith, P. Crow, H. Barr, "Raman spectroscopy for identification of epithelial cancers," *Faraday Discussions*, vol. 126, pp. 141-157, 2004.
- [26] Z.W. Huang, A. McWilliams, H. Lui, D.I. McLean, S. Lam, and H. Zeng., "Near-infrared Raman spectroscopy for optical diagnosis of lung cancer," *International Journal of Cancer*, vol. 107, no. 6, pp. 1047-1052, 2003.
- [27] M. Gniadecka, O.F. Nielsen, and H.C. Wulf, "Water content and structure in malignant and benign skin tumors," *Journal of Molecular Structure*, vol. 661, pp. 405-410, 2003.
- [28] R. Schaffer. (1998, November). An Introduction to Optical Rotation Polarimetry. National Institute of Standards and Technology, Gaithersburg, MD. [Online]. Available: <http://museum.nist.gov/panels/bates/intro.htm>
- [29] J. Alcoz. (2003, December). The Discovery. Aflash Photonics, Hollywood Park, TX. [Online]. Available: <http://polarization.com/history/history.html>
- [30] W.S. Bickel, J.F. Davidson, D.R. Huffman, and R. Kilkson, "Application of polarization effects in light scattering: a new biophysical tool," in *Proc. Natl. Acad. Sci. USA*, vol. 73, 1976, pp. 486.
- [31] K. Sokolov, R. Drezek, K. Gossage, and R. Richards-Kortum, "Reflectance spectroscopy with polarized light: is it sensitive to cellular and nuclear morphology," *Optics Express*, vol. 5, 1999.
- [32] M. Dogariu and T. Asakura, "Photon pathlength distribution from polarized backscattering in random media," *Opt. Eng.*, vol. 35, pp. 2234, 1996.
- [33] A.H. Hielscher, A.A. Eick, J.R. Mourant, D. Shen, J.P. Freyer, and I.J. Bigio, "Diffuse backscattering Mueller matrices of highly scattering media," *Opt. Express*, vol. 1, pp. 441, 1997.
- [34] F. Delplancke, "Automated high-speed Mueller matrix scatterometer," *Appl. Opt.*, vol. 36, pp. 5388, 1997.
- [35] A. Hielscher, SPIE Proceedings 2976, Biomed. Sensing, Imaging & Tracking Tech. II, 1997.

- [36] J. L. Pezzaniti and R. A. Chipman, "Mueller matrix imaging polarimetry," *Opt. Eng.*, vol. 34, pp. 1558-1568, 1995.
- [37] L. Jacques and R.J. Ramella-Roman, "Propagation of polarized light beams through biological tissues," in *Proc. SPIE 3914*, pp. 345, 2000.
- [38] J. M. Bueno, "Polarimetry using liquid-crystal variable retarders: theory and calibration," *J. Opt. A, Pure Appl. Opt.*, vol. 2, pp. 216-222, 2000.
- [39] M. Mujat and A. Dogariu, "Real-time measurement of the polarization transfer function," *Appl. Opt.*, vol. 40, pp. 34-44, 2001.
- [40] J.R. Chung, J.S. Baba, A.H. DeLaughter, and G.L. Coté, "Development and use of a novel automated Mueller matrix polarization imaging system for in-vivo imaging of lesions," in *SPIE Proc, Optical Biopsy IV*, vol. 4613, pp. 111-117, 2002.
- [41] M. Amoss (2003, December). TAMU Sinclair Swine Model of Malignant Melanoma, Department of Veterinary Physiology and Pharmacology, Texas A&M University, College Station, TX. [Online]. Available: <http://www.cvm.tamu.edu/SSCM/>
- [42] E. Hecht, *Optics*, 4<sup>th</sup> ed., New York: Addison Wesley, 2002.
- [43] J. S. Baba, *The Use of Polarized Light for Biomedical Applications*, Ph.D. Dissertation, Texas A&M University, College Station, TX 77843, 2003.
- [44] D. Steinberg and P. Colla, *CART: A Supplementary Module for SYSTAT*. San Diego, CA: Salford Systems, 1995.
- [45] "Polarization Control with Liquid Crystals", *2001-2003 Meadowlark Optics Catalog*. Frederick, CO: Meadowlark Optics, 2001.

## APPENDIX A

### CALIBRATION EQUATIONS

#### Rotator1

(1) Horizontal output (Ho)

$$\frac{1}{2} \begin{bmatrix} 1 & 1 & 0 & 0 \\ 1 & 1 & 0 & 0 \\ 0 & 0 & 0 & 0 \\ 0 & 0 & 0 & 0 \end{bmatrix} \begin{bmatrix} 1 & 0 & 0 & 0 \\ 0 & \cos 2\theta & \sin 2\theta & 0 \\ 0 & -\sin 2\theta & \cos 2\theta & 0 \\ 0 & 0 & 0 & 1 \end{bmatrix} \begin{bmatrix} 1 \\ 0 \\ 1 \\ 0 \end{bmatrix}$$

*Horizontal Polarizer*                      *Rotator*                      *Polarizer at +45*

$$\equiv \frac{1}{2} \begin{bmatrix} 1 & 1 & 0 & 0 \\ 1 & 1 & 0 & 0 \\ 0 & 0 & 0 & 0 \\ 0 & 0 & 0 & 0 \end{bmatrix} \begin{bmatrix} 1 \\ \sin 2\theta \\ \cos 2\theta \\ 0 \end{bmatrix} \equiv \frac{1}{2} \begin{bmatrix} 1 + \sin 2\theta \\ 1 + \sin 2\theta \\ 0 \\ 0 \end{bmatrix}$$

(2) Vertical output (Vo)

$$\frac{1}{2} \begin{bmatrix} 1 & -1 & 0 & 0 \\ -1 & 1 & 0 & 0 \\ 0 & 0 & 0 & 0 \\ 0 & 0 & 0 & 0 \end{bmatrix} \begin{bmatrix} 1 & 0 & 0 & 0 \\ 0 & \cos 2\theta & \sin 2\theta & 0 \\ 0 & -\sin 2\theta & \cos 2\theta & 0 \\ 0 & 0 & 0 & 1 \end{bmatrix} \begin{bmatrix} 1 \\ 0 \\ 1 \\ 0 \end{bmatrix}$$

*Vertical Polarizer*                      *Rotator*                      *Polarizer at +45*

$$\equiv \frac{1}{2} \begin{bmatrix} 1 & -1 & 0 & 0 \\ -1 & 1 & 0 & 0 \\ 0 & 0 & 0 & 0 \\ 0 & 0 & 0 & 0 \end{bmatrix} \begin{bmatrix} 1 \\ \sin 2\theta \\ \cos 2\theta \\ 0 \end{bmatrix} \equiv \frac{1}{2} \begin{bmatrix} 1 - \sin 2\theta \\ -1 + \sin 2\theta \\ 0 \\ 0 \end{bmatrix}$$

(3) +45° output (Po)

$$\frac{1}{2} \begin{bmatrix} 1 & 0 & 1 & 0 \\ 0 & 0 & 0 & 0 \\ 1 & 0 & 1 & 0 \\ 0 & 0 & 0 & 0 \end{bmatrix} \begin{bmatrix} 1 & 0 & 0 & 0 \\ 0 & \cos 2\theta & \sin 2\theta & 0 \\ 0 & -\sin 2\theta & \cos 2\theta & 0 \\ 0 & 0 & 0 & 1 \end{bmatrix} \begin{bmatrix} 1 \\ 0 \\ 1 \\ 0 \end{bmatrix}$$

*+45° Polarizer                      Rotator                      Polarizer at +45*

$$\equiv \frac{1}{2} \begin{bmatrix} 1 & 0 & 1 & 0 \\ 0 & 0 & 0 & 0 \\ 1 & 0 & 1 & 0 \\ 0 & 0 & 0 & 0 \end{bmatrix} \begin{bmatrix} 1 \\ \sin 2\theta \\ \cos 2\theta \\ 0 \end{bmatrix} \equiv \frac{1}{2} \begin{bmatrix} 1 + \cos 2\theta \\ 0 \\ 1 + \cos 2\theta \\ 0 \end{bmatrix}$$

(4) -45° output (Mo)

$$\frac{1}{2} \begin{bmatrix} 1 & 0 & -1 & 0 \\ 0 & 0 & 0 & 0 \\ -1 & 0 & 1 & 0 \\ 0 & 0 & 0 & 0 \end{bmatrix} \begin{bmatrix} 1 & 0 & 0 & 0 \\ 0 & \cos 2\theta & \sin 2\theta & 0 \\ 0 & -\sin 2\theta & \cos 2\theta & 0 \\ 0 & 0 & 0 & 1 \end{bmatrix} \begin{bmatrix} 1 \\ 0 \\ 1 \\ 0 \end{bmatrix}$$

*-45° Polarizer                      Rotator                      Polarizer at +45*

$$\equiv \frac{1}{2} \begin{bmatrix} 1 & 0 & -1 & 0 \\ 0 & 0 & 0 & 0 \\ -1 & 0 & 1 & 0 \\ 0 & 0 & 0 & 0 \end{bmatrix} \begin{bmatrix} 1 \\ \sin 2\theta \\ \cos 2\theta \\ 0 \end{bmatrix} \equiv \frac{1}{2} \begin{bmatrix} 1 - \cos 2\theta \\ 0 \\ -1 + \cos 2\theta \\ 0 \end{bmatrix}$$

**Rotator2**

(1) Horizontal input (Hi)

$$\frac{1}{2} \begin{bmatrix} 1 & 0 & -1 & 0 \\ 0 & 0 & 0 & 0 \\ -1 & 0 & 1 & 0 \\ 0 & 0 & 0 & 0 \end{bmatrix} \begin{bmatrix} 1 & 0 & 0 & 0 \\ 0 & \cos 2\theta & \sin 2\theta & 0 \\ 0 & -\sin 2\theta & \cos 2\theta & 0 \\ 0 & 0 & 0 & 1 \end{bmatrix} \begin{bmatrix} 1 \\ 1 \\ 0 \\ 0 \end{bmatrix}$$

*Polarizer at  $-45^\circ$                       Rotator                      Horizontal Polarizer*

$$\equiv \frac{1}{2} \begin{bmatrix} 1 & 0 & -1 & 0 \\ 0 & 0 & 0 & 0 \\ -1 & 0 & 1 & 0 \\ 0 & 0 & 0 & 0 \end{bmatrix} \begin{bmatrix} 1 \\ \cos 2\theta \\ -\sin 2\theta \\ 0 \end{bmatrix} \equiv \frac{1}{2} \begin{bmatrix} 1 + \sin 2\theta \\ 0 \\ -1 - \sin 2\theta \\ 0 \end{bmatrix}$$

(2) Vertical input (Vi)

$$\frac{1}{2} \begin{bmatrix} 1 & 0 & -1 & 0 \\ 0 & 0 & 0 & 0 \\ -1 & 0 & 1 & 0 \\ 0 & 0 & 0 & 0 \end{bmatrix} \begin{bmatrix} 1 & 0 & 0 & 0 \\ 0 & \cos 2\theta & \sin 2\theta & 0 \\ 0 & -\sin 2\theta & \cos 2\theta & 0 \\ 0 & 0 & 0 & 1 \end{bmatrix} \begin{bmatrix} 1 \\ -1 \\ 0 \\ 0 \end{bmatrix}$$

*Polarizer at  $-45^\circ$                       Rotator                      Vertical Polarizer*

$$\equiv \frac{1}{2} \begin{bmatrix} 1 & 0 & -1 & 0 \\ 0 & 0 & 0 & 0 \\ -1 & 0 & 1 & 0 \\ 0 & 0 & 0 & 0 \end{bmatrix} \begin{bmatrix} 1 \\ -\cos 2\theta \\ \sin 2\theta \\ 0 \end{bmatrix} \equiv \frac{1}{2} \begin{bmatrix} 1 - \sin 2\theta \\ 0 \\ -1 + \sin 2\theta \\ 0 \end{bmatrix}$$

(3) +45° input (Pi)

$$\frac{1}{2} \begin{bmatrix} 1 & 0 & -1 & 0 \\ 0 & 0 & 0 & 0 \\ -1 & 0 & 1 & 0 \\ 0 & 0 & 0 & 0 \end{bmatrix} \begin{bmatrix} 1 & 0 & 0 & 0 \\ 0 & \cos 2\theta & \sin 2\theta & 0 \\ 0 & -\sin 2\theta & \cos 2\theta & 0 \\ 0 & 0 & 0 & 1 \end{bmatrix} \begin{bmatrix} 1 \\ 0 \\ 1 \\ 0 \end{bmatrix}$$

*Polarizer at -45°                      Rotator                      Polarizer at +45*

$$\equiv \frac{1}{2} \begin{bmatrix} 1 & 0 & -1 & 0 \\ 0 & 0 & 0 & 0 \\ -1 & 0 & 1 & 0 \\ 0 & 0 & 0 & 0 \end{bmatrix} \begin{bmatrix} 1 \\ \sin 2\theta \\ \cos 2\theta \\ 0 \end{bmatrix} \equiv \frac{1}{2} \begin{bmatrix} 1 - \cos 2\theta \\ 0 \\ -1 + \cos 2\theta \\ 0 \end{bmatrix}$$

(4) -45° input (Mi)

$$\frac{1}{2} \begin{bmatrix} 1 & 0 & -1 & 0 \\ 0 & 0 & 0 & 0 \\ -1 & 0 & 1 & 0 \\ 0 & 0 & 0 & 0 \end{bmatrix} \begin{bmatrix} 1 & 0 & 0 & 0 \\ 0 & \cos 2\theta & \sin 2\theta & 0 \\ 0 & -\sin 2\theta & \cos 2\theta & 0 \\ 0 & 0 & 0 & 1 \end{bmatrix} \begin{bmatrix} 1 \\ 0 \\ -1 \\ 0 \end{bmatrix}$$

*Polarizer at -45°                      Rotator                      Polarizer at -45*

$$\equiv \frac{1}{2} \begin{bmatrix} 1 & 0 & -1 & 0 \\ 0 & 0 & 0 & 0 \\ -1 & 0 & 1 & 0 \\ 0 & 0 & 0 & 0 \end{bmatrix} \begin{bmatrix} 1 \\ -\sin 2\theta \\ -\cos 2\theta \\ 0 \end{bmatrix} \equiv \frac{1}{2} \begin{bmatrix} 1 + \cos 2\theta \\ 0 \\ -1 - \cos 2\theta \\ 0 \end{bmatrix}$$



**Retarder1**

(1) Horizontal input (Hi)

$$\frac{1}{2} \begin{bmatrix} 1 & 1 & 0 & 0 \\ 1 & 1 & 0 & 0 \\ 0 & 0 & 0 & 0 \\ 0 & 0 & 0 & 0 \end{bmatrix} \begin{bmatrix} 1 & 0 & 0 & 0 \\ 0 & \cos \delta & 0 & -\sin \delta \\ 0 & 0 & 1 & 0 \\ 0 & \sin \delta & 0 & \cos \delta \end{bmatrix} \begin{bmatrix} 1 \\ 1 \\ 0 \\ 0 \end{bmatrix}$$

*Horizontal Polarizer*                      *Retarder*                      *Horizontal Polarizer*

$$\equiv \frac{1}{2} \begin{bmatrix} 1 & 1 & 0 & 0 \\ 1 & 1 & 0 & 0 \\ 0 & 0 & 0 & 0 \\ 0 & 0 & 0 & 0 \end{bmatrix} \begin{bmatrix} 1 \\ \cos \delta \\ 0 \\ \sin \delta \end{bmatrix} \equiv \frac{1}{2} \begin{bmatrix} 1 + \cos \delta \\ 1 + \cos \delta \\ 0 \\ 0 \end{bmatrix}$$

(2) Vertical input (Vi)

$$\frac{1}{2} \begin{bmatrix} 1 & 1 & 0 & 0 \\ 1 & 1 & 0 & 0 \\ 0 & 0 & 0 & 0 \\ 0 & 0 & 0 & 0 \end{bmatrix} \begin{bmatrix} 1 & 0 & 0 & 0 \\ 0 & \cos \delta & 0 & -\sin \delta \\ 0 & 0 & 1 & 0 \\ 0 & \sin \delta & 0 & \cos \delta \end{bmatrix} \begin{bmatrix} 1 \\ -1 \\ 0 \\ 0 \end{bmatrix}$$

*Horizontal Polarizer*                      *Retarder*                      *Vertical Polarizer*

$$\equiv \frac{1}{2} \begin{bmatrix} 1 & 1 & 0 & 0 \\ 1 & 1 & 0 & 0 \\ 0 & 0 & 0 & 0 \\ 0 & 0 & 0 & 0 \end{bmatrix} \begin{bmatrix} 1 \\ -\cos \delta \\ 0 \\ \sin \delta \end{bmatrix} \equiv \frac{1}{2} \begin{bmatrix} 1 - \cos \delta \\ 1 - \cos \delta \\ 0 \\ 0 \end{bmatrix}$$

(3) +45° input (Pi)

$$\frac{1}{2} \begin{bmatrix} 1 & 1 & 0 & 0 \\ 1 & 1 & 0 & 0 \\ 0 & 0 & 0 & 0 \\ 0 & 0 & 0 & 0 \end{bmatrix} \begin{bmatrix} 1 & 0 & 0 & 0 \\ 0 & \cos \delta & 0 & -\sin \delta \\ 0 & 0 & 1 & 0 \\ 0 & \sin \delta & 0 & \cos \delta \end{bmatrix} \begin{bmatrix} 1 \\ 0 \\ 1 \\ 0 \end{bmatrix}$$

*Horizontal Polarizer*                      *Retarder*                      *Polarizer at +45°*

$$\equiv \frac{1}{2} \begin{bmatrix} 1 & 1 & 0 & 0 \\ 1 & 1 & 0 & 0 \\ 0 & 0 & 0 & 0 \\ 0 & 0 & 0 & 0 \end{bmatrix} \begin{bmatrix} 1 \\ 0 \\ 1 \\ 0 \end{bmatrix} \equiv \frac{1}{2} \begin{bmatrix} 1 \\ 1 \\ 0 \\ 0 \end{bmatrix}$$

(4) -45° input (Mi)

$$\frac{1}{2} \begin{bmatrix} 1 & 1 & 0 & 0 \\ 1 & 1 & 0 & 0 \\ 0 & 0 & 0 & 0 \\ 0 & 0 & 0 & 0 \end{bmatrix} \begin{bmatrix} 1 & 0 & 0 & 0 \\ 0 & \cos \delta & 0 & -\sin \delta \\ 0 & 0 & 1 & 0 \\ 0 & \sin \delta & 0 & \cos \delta \end{bmatrix} \begin{bmatrix} 1 \\ 0 \\ -1 \\ 0 \end{bmatrix}$$

*Horizontal Polarizer*                      *Retarder*                      *Polarizer at -45°*

$$\equiv \frac{1}{2} \begin{bmatrix} 1 & 1 & 0 & 0 \\ 1 & 1 & 0 & 0 \\ 0 & 0 & 0 & 0 \\ 0 & 0 & 0 & 0 \end{bmatrix} \begin{bmatrix} 1 \\ 0 \\ -1 \\ 0 \end{bmatrix} \equiv \frac{1}{2} \begin{bmatrix} 1 \\ 1 \\ 0 \\ 0 \end{bmatrix}$$

**Retarder2**

(1) Horizontal output (Ho)

$$\frac{1}{2} \begin{bmatrix} 1 & 1 & 0 & 0 \\ 1 & 1 & 0 & 0 \\ 0 & 0 & 0 & 0 \\ 0 & 0 & 0 & 0 \end{bmatrix} \begin{bmatrix} 1 & 0 & 0 & 0 \\ 0 & \cos \delta & 0 & -\sin \delta \\ 0 & 0 & 1 & 0 \\ 0 & \sin \delta & 0 & \cos \delta \end{bmatrix} \begin{bmatrix} 1 \\ 1 \\ 0 \\ 0 \end{bmatrix}$$

*Horizontal Polarizer*                      *Retarder*                      *Horizontal Polarizer*

$$\equiv \frac{1}{2} \begin{bmatrix} 1 & 1 & 0 & 0 \\ 1 & 1 & 0 & 0 \\ 0 & 0 & 0 & 0 \\ 0 & 0 & 0 & 0 \end{bmatrix} \begin{bmatrix} 1 \\ \cos \delta \\ 0 \\ \sin \delta \end{bmatrix} \equiv \frac{1}{2} \begin{bmatrix} 1 + \cos \delta \\ 1 + \cos \delta \\ 0 \\ 0 \end{bmatrix}$$

(2) Vertical output (Vo)

$$\frac{1}{2} \begin{bmatrix} 1 & -1 & 0 & 0 \\ -1 & 1 & 0 & 0 \\ 0 & 0 & 0 & 0 \\ 0 & 0 & 0 & 0 \end{bmatrix} \begin{bmatrix} 1 & 0 & 0 & 0 \\ 0 & \cos \delta & 0 & -\sin \delta \\ 0 & 0 & 1 & 0 \\ 0 & \sin \delta & 0 & \cos \delta \end{bmatrix} \begin{bmatrix} 1 \\ 1 \\ 0 \\ 0 \end{bmatrix}$$

*Vertical Polarizer*                      *Retarder*                      *Horizontal Polarizer*

$$\equiv \frac{1}{2} \begin{bmatrix} 1 & -1 & 0 & 0 \\ -1 & 1 & 0 & 0 \\ 0 & 0 & 0 & 0 \\ 0 & 0 & 0 & 0 \end{bmatrix} \begin{bmatrix} 1 \\ \cos \delta \\ 0 \\ \sin \delta \end{bmatrix} \equiv \frac{1}{2} \begin{bmatrix} 1 - \cos \delta \\ -1 + \cos \delta \\ 0 \\ 0 \end{bmatrix}$$

(3) +45° output (Po)

$$\frac{1}{2} \begin{bmatrix} 1 & 0 & 1 & 0 \\ 0 & 0 & 0 & 0 \\ 1 & 0 & 1 & 0 \\ 0 & 0 & 0 & 0 \end{bmatrix} \begin{bmatrix} 1 & 0 & 0 & 0 \\ 0 & \cos \delta & 0 & -\sin \delta \\ 0 & 0 & 1 & 0 \\ 0 & \sin \delta & 0 & \cos \delta \end{bmatrix} \begin{bmatrix} 1 \\ 1 \\ 0 \\ 0 \end{bmatrix}$$

*Polarizer at +45°*                      *Retarder*                      *Horizontal Polarizer*

$$\equiv \frac{1}{2} \begin{bmatrix} 1 & 0 & 1 & 0 \\ 0 & 0 & 0 & 0 \\ 1 & 0 & 1 & 0 \\ 0 & 0 & 0 & 0 \end{bmatrix} \begin{bmatrix} 1 \\ \cos \delta \\ 0 \\ \sin \delta \end{bmatrix} \equiv \frac{1}{2} \begin{bmatrix} 1 \\ 1 \\ 0 \\ 0 \end{bmatrix}$$

(4) -45° output (Mo)

$$\frac{1}{2} \begin{bmatrix} 1 & 0 & -1 & 0 \\ 0 & 0 & 0 & 0 \\ -1 & 0 & 1 & 0 \\ 0 & 0 & 0 & 0 \end{bmatrix} \begin{bmatrix} 1 & 0 & 0 & 0 \\ 0 & \cos \delta & 0 & -\sin \delta \\ 0 & 0 & 1 & 0 \\ 0 & \sin \delta & 0 & \cos \delta \end{bmatrix} \begin{bmatrix} 1 \\ 1 \\ 0 \\ 0 \end{bmatrix}$$

*Polarizer at -45°*                      *Retarder*                      *Horizontal Polarizer*

$$\equiv \frac{1}{2} \begin{bmatrix} 1 & 0 & -1 & 0 \\ 0 & 0 & 0 & 0 \\ -1 & 0 & 1 & 0 \\ 0 & 0 & 0 & 0 \end{bmatrix} \begin{bmatrix} 1 \\ \cos \delta \\ 0 \\ \sin \delta \end{bmatrix} \equiv \frac{1}{2} \begin{bmatrix} 1 \\ 1 \\ 0 \\ 0 \end{bmatrix}$$

**APPENDIX B****MATLAB PROGRAM CAL100.M**

```
T0=fitsread('test0.fit');T1=fitsread('test1.fit');
T2=fitsread('test2.fit');T3=fitsread('test3.fit');
T4=fitsread('test4.fit');T5=fitsread('test5.fit');
T6=fitsread('test6.fit');T7=fitsread('test7.fit');
T8=fitsread('test8.fit');T9=fitsread('test9.fit');
T10=fitsread('test10.fit');T11=fitsread('test11.fit');
T12=fitsread('test12.fit');T13=fitsread('test13.fit');
T14=fitsread('test14.fit');T15=fitsread('test15.fit');
T16=fitsread('test16.fit');T17=fitsread('test17.fit');
T18=fitsread('test18.fit');T19=fitsread('test19.fit');
T20=fitsread('test20.fit');T21=fitsread('test21.fit');
T22=fitsread('test22.fit');T23=fitsread('test23.fit');
T24=fitsread('test24.fit');T25=fitsread('test25.fit');
T26=fitsread('test26.fit');T27=fitsread('test27.fit');
T28=fitsread('test28.fit');T29=fitsread('test29.fit');
T30=fitsread('test30.fit');T31=fitsread('test31.fit');
T32=fitsread('test32.fit');T33=fitsread('test33.fit');
T34=fitsread('test34.fit');T35=fitsread('test35.fit');
T36=fitsread('test36.fit');T37=fitsread('test37.fit');
T38=fitsread('test38.fit');T39=fitsread('test39.fit');
T40=fitsread('test40.fit');T41=fitsread('test41.fit');
T42=fitsread('test42.fit');T43=fitsread('test43.fit');
T44=fitsread('test44.fit');T45=fitsread('test45.fit');
T46=fitsread('test46.fit');T47=fitsread('test47.fit');
T48=fitsread('test48.fit');T49=fitsread('test49.fit');
T50=fitsread('test50.fit');T51=fitsread('test51.fit');
T52=fitsread('test52.fit');T53=fitsread('test53.fit');
T54=fitsread('test54.fit');T55=fitsread('test55.fit');
T56=fitsread('test56.fit');T57=fitsread('test57.fit');
T58=fitsread('test58.fit');T59=fitsread('test59.fit');
T60=fitsread('test60.fit');T61=fitsread('test61.fit');
T62=fitsread('test62.fit');T63=fitsread('test63.fit');
T64=fitsread('test64.fit');T65=fitsread('test65.fit');
T66=fitsread('test66.fit');T67=fitsread('test67.fit');
T68=fitsread('test68.fit');T69=fitsread('test69.fit');
T70=fitsread('test70.fit');T71=fitsread('test71.fit');
T72=fitsread('test72.fit');T73=fitsread('test73.fit');
T74=fitsread('test74.fit');T75=fitsread('test75.fit');
T76=fitsread('test76.fit');T77=fitsread('test77.fit');
T78=fitsread('test78.fit');T79=fitsread('test79.fit');
T80=fitsread('test80.fit');T81=fitsread('test81.fit');
T82=fitsread('test82.fit');T83=fitsread('test83.fit');
T84=fitsread('test84.fit');T85=fitsread('test85.fit');
T86=fitsread('test86.fit');T87=fitsread('test87.fit');
T88=fitsread('test88.fit');T89=fitsread('test89.fit');
T90=fitsread('test90.fit');T91=fitsread('test91.fit');
T92=fitsread('test92.fit');T93=fitsread('test93.fit');
T94=fitsread('test94.fit');T95=fitsread('test95.fit');
```

```
T96=fitsread('test96.fit');T97=fitsread('test97.fit');
T98=fitsread('test98.fit');T99=fitsread('test99.fit');
T100=fitsread('test100.fit');

T0=double(T0);t0=mean(mean(T0));T1=double(T1);t1=mean(mean(T1));
T2=double(T2);t2=mean(mean(T2));T3=double(T3);t3=mean(mean(T3));
T4=double(T4);t4=mean(mean(T4));T5=double(T5);t5=mean(mean(T5));
T6=double(T6);t6=mean(mean(T6));T7=double(T7);t7=mean(mean(T7));
T8=double(T8);t8=mean(mean(T8));T9=double(T9);t9=mean(mean(T9));
T10=double(T10);t10=mean(mean(T10));T11=double(T11);t11=mean(mean(T11));
T12=double(T12);t12=mean(mean(T12));T13=double(T13);t13=mean(mean(T13));
T14=double(T14);t14=mean(mean(T14));T15=double(T15);t15=mean(mean(T15));
T16=double(T16);t16=mean(mean(T16));T17=double(T17);t17=mean(mean(T17));
T18=double(T18);t18=mean(mean(T18));T19=double(T19);t19=mean(mean(T19));
T20=double(T20);t20=mean(mean(T20));T21=double(T21);t21=mean(mean(T21));
T22=double(T22);t22=mean(mean(T22));T23=double(T23);t23=mean(mean(T23));
T24=double(T24);t24=mean(mean(T24));T25=double(T25);t25=mean(mean(T25));
T26=double(T26);t26=mean(mean(T26));T27=double(T27);t27=mean(mean(T27));
T28=double(T28);t28=mean(mean(T28));T29=double(T29);t29=mean(mean(T29));
T30=double(T30);t30=mean(mean(T30));T31=double(T31);t31=mean(mean(T31));
T32=double(T32);t32=mean(mean(T32));T33=double(T33);t33=mean(mean(T33));
T34=double(T34);t34=mean(mean(T34));T35=double(T35);t35=mean(mean(T35));
T36=double(T36);t36=mean(mean(T36));T37=double(T37);t37=mean(mean(T37));
T38=double(T38);t38=mean(mean(T38));T39=double(T39);t39=mean(mean(T39));
T40=double(T40);t40=mean(mean(T40));T41=double(T41);t41=mean(mean(T41));
T42=double(T42);t42=mean(mean(T42));T43=double(T43);t43=mean(mean(T43));
T44=double(T44);t44=mean(mean(T44));T45=double(T45);t45=mean(mean(T45));
T46=double(T46);t46=mean(mean(T46));T47=double(T47);t47=mean(mean(T47));
T48=double(T48);t48=mean(mean(T48));T49=double(T49);t49=mean(mean(T49));
T50=double(T50);t50=mean(mean(T50));T51=double(T51);t51=mean(mean(T51));
T52=double(T52);t52=mean(mean(T52));T53=double(T53);t53=mean(mean(T53));
T54=double(T54);t54=mean(mean(T54));T55=double(T55);t55=mean(mean(T55));
T56=double(T56);t56=mean(mean(T56));T57=double(T57);t57=mean(mean(T57));
T58=double(T58);t58=mean(mean(T58));T59=double(T59);t59=mean(mean(T59));
T60=double(T60);t60=mean(mean(T60));T61=double(T61);t61=mean(mean(T61));
T62=double(T62);t62=mean(mean(T62));T63=double(T63);t63=mean(mean(T63));
T64=double(T64);t64=mean(mean(T64));T65=double(T65);t65=mean(mean(T65));
T66=double(T66);t66=mean(mean(T66));T67=double(T67);t67=mean(mean(T67));
T68=double(T68);t68=mean(mean(T68));T69=double(T69);t69=mean(mean(T69));
T70=double(T70);t70=mean(mean(T70));T71=double(T71);t71=mean(mean(T71));
T72=double(T72);t72=mean(mean(T72));T73=double(T73);t73=mean(mean(T73));
T74=double(T74);t74=mean(mean(T74));T75=double(T75);t75=mean(mean(T75));
T76=double(T76);t76=mean(mean(T76));T77=double(T77);t77=mean(mean(T77));
T78=double(T78);t78=mean(mean(T78));T79=double(T79);t79=mean(mean(T79));
T80=double(T80);t80=mean(mean(T80));T81=double(T81);t81=mean(mean(T81));
T82=double(T82);t82=mean(mean(T82));T83=double(T83);t83=mean(mean(T83));
T84=double(T84);t84=mean(mean(T84));T85=double(T85);t85=mean(mean(T85));
T86=double(T86);t86=mean(mean(T86));T87=double(T87);t87=mean(mean(T87));
T88=double(T88);t88=mean(mean(T88));T89=double(T89);t89=mean(mean(T89));
T90=double(T90);t90=mean(mean(T90));T91=double(T91);t91=mean(mean(T91));
T92=double(T92);t92=mean(mean(T92));T93=double(T93);t93=mean(mean(T93));
T94=double(T94);t94=mean(mean(T94));T95=double(T95);t95=mean(mean(T95));
T96=double(T96);t96=mean(mean(T96));T97=double(T97);t97=mean(mean(T97));
T98=double(T98);t98=mean(mean(T98));T99=double(T99);t99=mean(mean(T99));
```

```
T100=double(T100);t100=mean(mean(T100));
```

```
RAW=[t0;t1;t2;t3;t4;t5;t6;t7;t8;t9;  
      t10;t11;t12;t13;t14;t15;t16;t17;t18;t19;  
      t20;t21;t22;t23;t24;t25;t26;t27;t28;t29;  
      t30;t31;t32;t33;t34;t35;t36;t37;t38;t39;  
      t40;t41;t42;t43;t44;t45;t46;t47;t48;t49;  
      t50;t51;t52;t53;t54;t55;t56;t57;t58;t59;  
      t60;t61;t62;t63;t64;t65;t66;t67;t68;t69;  
      t70;t71;t72;t73;t74;t75;t76;t77;t78;t79;  
      t80;t81;t82;t83;t84;t85;t86;t87;t88;t89;  
      t90;t91;t92;t93;t94;t95;t96;t97;t98;t99;  
      t100]
```

## APPENDIX C

### MATLAB PROGRAM CAL60.M

```

T0=fitsread('test0.fit');T1=fitsread('test1.fit');
T2=fitsread('test2.fit');T3=fitsread('test3.fit');
T4=fitsread('test4.fit');T5=fitsread('test5.fit');
T6=fitsread('test6.fit');T7=fitsread('test7.fit');
T8=fitsread('test8.fit');T9=fitsread('test9.fit');
T10=fitsread('test10.fit');T11=fitsread('test11.fit');
T12=fitsread('test12.fit');T13=fitsread('test13.fit');
T14=fitsread('test14.fit');T15=fitsread('test15.fit');
T16=fitsread('test16.fit');T17=fitsread('test17.fit');
T18=fitsread('test18.fit');T19=fitsread('test19.fit');
T20=fitsread('test20.fit');T21=fitsread('test21.fit');
T22=fitsread('test22.fit');T23=fitsread('test23.fit');
T24=fitsread('test24.fit');T25=fitsread('test25.fit');
T26=fitsread('test26.fit');T27=fitsread('test27.fit');
T28=fitsread('test28.fit');T29=fitsread('test29.fit');
T30=fitsread('test30.fit');T31=fitsread('test31.fit');
T32=fitsread('test32.fit');T33=fitsread('test33.fit');
T34=fitsread('test34.fit');T35=fitsread('test35.fit');
T36=fitsread('test36.fit');T37=fitsread('test37.fit');
T38=fitsread('test38.fit');T39=fitsread('test39.fit');
T40=fitsread('test40.fit');T41=fitsread('test41.fit');
T42=fitsread('test42.fit');T43=fitsread('test43.fit');
T44=fitsread('test44.fit');T45=fitsread('test45.fit');
T46=fitsread('test46.fit');T47=fitsread('test47.fit');
T48=fitsread('test48.fit');T49=fitsread('test49.fit');
T50=fitsread('test50.fit');T51=fitsread('test51.fit');
T52=fitsread('test52.fit');T53=fitsread('test53.fit');
T54=fitsread('test54.fit');T55=fitsread('test55.fit');
T56=fitsread('test56.fit');T57=fitsread('test57.fit');
T58=fitsread('test58.fit');T59=fitsread('test59.fit');
T60=fitsread('test60.fit');

T0=double(T0);t0=mean(mean(T0));T1=double(T1);t1=mean(mean(T1));
T2=double(T2);t2=mean(mean(T2));T3=double(T3);t3=mean(mean(T3));
T4=double(T4);t4=mean(mean(T4));T5=double(T5);t5=mean(mean(T5));
T6=double(T6);t6=mean(mean(T6));T7=double(T7);t7=mean(mean(T7));
T8=double(T8);t8=mean(mean(T8));T9=double(T9);t9=mean(mean(T9));
T10=double(T10);t10=mean(mean(T10));T11=double(T11);t11=mean(mean(T11))
T12=double(T12);t12=mean(mean(T12));T13=double(T13);t13=mean(mean(T13))
T14=double(T14);t14=mean(mean(T14));T15=double(T15);t15=mean(mean(T15))
T16=double(T16);t16=mean(mean(T16));T17=double(T17);t17=mean(mean(T17))
T18=double(T18);t18=mean(mean(T18));T19=double(T19);t19=mean(mean(T19))
T20=double(T20);t20=mean(mean(T20));T21=double(T21);t21=mean(mean(T21))
T22=double(T22);t22=mean(mean(T22));T23=double(T23);t23=mean(mean(T23))
T24=double(T24);t24=mean(mean(T24));T25=double(T25);t25=mean(mean(T25))
T26=double(T26);t26=mean(mean(T26));T27=double(T27);t27=mean(mean(T27))
T28=double(T28);t28=mean(mean(T28));T29=double(T29);t29=mean(mean(T29))

```



```
T30=double(T30);t30=mean(mean(T30));T31=double(T31);t31=mean(mean(T31))
T32=double(T32);t32=mean(mean(T32));T33=double(T33);t33=mean(mean(T33))
T34=double(T34);t34=mean(mean(T34));T35=double(T35);t35=mean(mean(T35))
T36=double(T36);t36=mean(mean(T36));T37=double(T37);t37=mean(mean(T37))
T38=double(T38);t38=mean(mean(T38));T39=double(T39);t39=mean(mean(T39))
T40=double(T40);t40=mean(mean(T40));T41=double(T41);t41=mean(mean(T41))
T42=double(T42);t42=mean(mean(T42));T43=double(T43);t43=mean(mean(T43))
T44=double(T44);t44=mean(mean(T44));T45=double(T45);t45=mean(mean(T45))
T46=double(T46);t46=mean(mean(T46));T47=double(T47);t47=mean(mean(T47))
T48=double(T48);t48=mean(mean(T48));T49=double(T49);t49=mean(mean(T49))
T50=double(T50);t50=mean(mean(T50));T51=double(T51);t51=mean(mean(T51))
T52=double(T52);t52=mean(mean(T52));T53=double(T53);t53=mean(mean(T53))
T54=double(T54);t54=mean(mean(T54));T55=double(T55);t55=mean(mean(T55))
T56=double(T56);t56=mean(mean(T56));T57=double(T57);t57=mean(mean(T57))
T58=double(T58);t58=mean(mean(T58));T59=double(T59);t59=mean(mean(T59))
T60=double(T60);t60=mean(mean(T60));
```

```
RAW=[t0;t1;t2;t3;t4;t5;t6;t7;t8;t9;
      t10;t11;t12;t13;t14;t15;t16;t17;t18;t19;
      t20;t21;t22;t23;t24;t25;t26;t27;t28;t29;
      t30;t31;t32;t33;t34;t35;t36;t37;t38;t39;
      t40;t41;t42;t43;t44;t45;t46;t47;t48;t49;
      t50;t51;t52;t53;t54;t55;t56;t57;t58;t59;
      t60]
```

## APPENDIX D

### MATLAB PROGRAM CAL40.M

```

T0=fitsread('test0.fit');T1=fitsread('test1.fit');
T2=fitsread('test2.fit');T3=fitsread('test3.fit');
T4=fitsread('test4.fit');T5=fitsread('test5.fit');
T6=fitsread('test6.fit');T7=fitsread('test7.fit');
T8=fitsread('test8.fit');T9=fitsread('test9.fit');
T10=fitsread('test10.fit');T11=fitsread('test11.fit');
T12=fitsread('test12.fit');T13=fitsread('test13.fit');
T14=fitsread('test14.fit');T15=fitsread('test15.fit');
T16=fitsread('test16.fit');T17=fitsread('test17.fit');
T18=fitsread('test18.fit');T19=fitsread('test19.fit');
T20=fitsread('test20.fit');T21=fitsread('test21.fit');
T22=fitsread('test22.fit');T23=fitsread('test23.fit');
T24=fitsread('test24.fit');T25=fitsread('test25.fit');
T26=fitsread('test26.fit');T27=fitsread('test27.fit');
T28=fitsread('test28.fit');T29=fitsread('test29.fit');
T30=fitsread('test30.fit');T31=fitsread('test31.fit');
T32=fitsread('test32.fit');T33=fitsread('test33.fit');
T34=fitsread('test34.fit');T35=fitsread('test35.fit');
T36=fitsread('test36.fit');T37=fitsread('test37.fit');
T38=fitsread('test38.fit');T39=fitsread('test39.fit');
T40=fitsread('test40.fit');

T0=double(T0);t0=mean(mean(T0));T1=double(T1);t1=mean(mean(T1));
T2=double(T2);t2=mean(mean(T2));T3=double(T3);t3=mean(mean(T3));
T4=double(T4);t4=mean(mean(T4));T5=double(T5);t5=mean(mean(T5));
T6=double(T6);t6=mean(mean(T6));T7=double(T7);t7=mean(mean(T7));
T8=double(T8);t8=mean(mean(T8));T9=double(T9);t9=mean(mean(T9));
T10=double(T10);t10=mean(mean(T10));T11=double(T11);t11=mean(mean(T11));
T12=double(T12);t12=mean(mean(T12));T13=double(T13);t13=mean(mean(T13));
T14=double(T14);t14=mean(mean(T14));T15=double(T15);t15=mean(mean(T15));
T16=double(T16);t16=mean(mean(T16));T17=double(T17);t17=mean(mean(T17));
T18=double(T18);t18=mean(mean(T18));T19=double(T19);t19=mean(mean(T19));
T20=double(T20);t20=mean(mean(T20));T21=double(T21);t21=mean(mean(T21));
T22=double(T22);t22=mean(mean(T22));T23=double(T23);t23=mean(mean(T23));
T24=double(T24);t24=mean(mean(T24));T25=double(T25);t25=mean(mean(T25));
T26=double(T26);t26=mean(mean(T26));T27=double(T27);t27=mean(mean(T27));
T28=double(T28);t28=mean(mean(T28));T29=double(T29);t29=mean(mean(T29));
T30=double(T30);t30=mean(mean(T30));T31=double(T31);t31=mean(mean(T31));
T32=double(T32);t32=mean(mean(T32));T33=double(T33);t33=mean(mean(T33));
T34=double(T34);t34=mean(mean(T34));T35=double(T35);t35=mean(mean(T35));
T36=double(T36);t36=mean(mean(T36));T37=double(T37);t37=mean(mean(T37));
T38=double(T38);t38=mean(mean(T38));T39=double(T39);t39=mean(mean(T39));
T40=double(T40);t40=mean(mean(T40));
RAW=[t0;t1;t2;t3;t4;t5;t6;t7;t8;t9;
      t10;t11;t12;t13;t14;t15;t16;t17;t18;t19;
      t20;t21;t22;t23;t24;t25;t26;t27;t28;t29;
      t30;t31;t32;t33;t34;t35;t36;t37;t38;t39;
      t40]

```

## APPENDIX E

### MATLAB PROGRAM CAL80.M

```

T0=fitsread('test0.fit');T1=fitsread('test1.fit');
T2=fitsread('test2.fit');T3=fitsread('test3.fit');
T4=fitsread('test4.fit');T5=fitsread('test5.fit');
T6=fitsread('test6.fit');T7=fitsread('test7.fit');
T8=fitsread('test8.fit');T9=fitsread('test9.fit');
T10=fitsread('test10.fit');T11=fitsread('test11.fit');
T12=fitsread('test12.fit');T13=fitsread('test13.fit');
T14=fitsread('test14.fit');T15=fitsread('test15.fit');
T16=fitsread('test16.fit');T17=fitsread('test17.fit');
T18=fitsread('test18.fit');T19=fitsread('test19.fit');
T20=fitsread('test20.fit');T21=fitsread('test21.fit');
T22=fitsread('test22.fit');T23=fitsread('test23.fit');
T24=fitsread('test24.fit');T25=fitsread('test25.fit');
T26=fitsread('test26.fit');T27=fitsread('test27.fit');
T28=fitsread('test28.fit');T29=fitsread('test29.fit');
T30=fitsread('test30.fit');T31=fitsread('test31.fit');
T32=fitsread('test32.fit');T33=fitsread('test33.fit');
T34=fitsread('test34.fit');T35=fitsread('test35.fit');
T36=fitsread('test36.fit');T37=fitsread('test37.fit');
T38=fitsread('test38.fit');T39=fitsread('test39.fit');
T40=fitsread('test40.fit');T41=fitsread('test41.fit');
T42=fitsread('test42.fit');T43=fitsread('test43.fit');
T44=fitsread('test44.fit');T45=fitsread('test45.fit');
T46=fitsread('test46.fit');T47=fitsread('test47.fit');
T48=fitsread('test48.fit');T49=fitsread('test49.fit');
T50=fitsread('test50.fit');T51=fitsread('test51.fit');
T52=fitsread('test52.fit');T53=fitsread('test53.fit');
T54=fitsread('test54.fit');T55=fitsread('test55.fit');
T56=fitsread('test56.fit');T57=fitsread('test57.fit');
T58=fitsread('test58.fit');T59=fitsread('test59.fit');
T60=fitsread('test60.fit');T61=fitsread('test61.fit');
T62=fitsread('test62.fit');T63=fitsread('test63.fit');
T64=fitsread('test64.fit');T65=fitsread('test65.fit');
T66=fitsread('test66.fit');T67=fitsread('test67.fit');
T68=fitsread('test68.fit');T69=fitsread('test69.fit');
T70=fitsread('test70.fit');T71=fitsread('test71.fit');
T72=fitsread('test72.fit');T73=fitsread('test73.fit');
T74=fitsread('test74.fit');T75=fitsread('test75.fit');
T76=fitsread('test76.fit');T77=fitsread('test77.fit');
T78=fitsread('test78.fit');T79=fitsread('test79.fit');
T80=fitsread('test80.fit');

T0=double(T0);t0=mean(mean(T0));T1=double(T1);t1=mean(mean(T1));
T2=double(T2);t2=mean(mean(T2));T3=double(T3);t3=mean(mean(T3));
T4=double(T4);t4=mean(mean(T4));T5=double(T5);t5=mean(mean(T5));
T6=double(T6);t6=mean(mean(T6));T7=double(T7);t7=mean(mean(T7));
T8=double(T8);t8=mean(mean(T8));T9=double(T9);t9=mean(mean(T9));

```

```

T10=double(T10);t10=mean(mean(T10));T11=double(T11);t11=mean(mean(T11))
T12=double(T12);t12=mean(mean(T12));T13=double(T13);t13=mean(mean(T13))
T14=double(T14);t14=mean(mean(T14));T15=double(T15);t15=mean(mean(T15))
T16=double(T16);t16=mean(mean(T16));T17=double(T17);t17=mean(mean(T17))
T18=double(T18);t18=mean(mean(T18));T19=double(T19);t19=mean(mean(T19))
T20=double(T20);t20=mean(mean(T20));T21=double(T21);t21=mean(mean(T21))
T22=double(T22);t22=mean(mean(T22));T23=double(T23);t23=mean(mean(T23))
T24=double(T24);t24=mean(mean(T24));T25=double(T25);t25=mean(mean(T25))
T26=double(T26);t26=mean(mean(T26));T27=double(T27);t27=mean(mean(T27))
T28=double(T28);t28=mean(mean(T28));T29=double(T29);t29=mean(mean(T29))
T30=double(T30);t30=mean(mean(T30));T31=double(T31);t31=mean(mean(T31))
T32=double(T32);t32=mean(mean(T32));T33=double(T33);t33=mean(mean(T33))
T34=double(T34);t34=mean(mean(T34));T35=double(T35);t35=mean(mean(T35))
T36=double(T36);t36=mean(mean(T36));T37=double(T37);t37=mean(mean(T37))
T38=double(T38);t38=mean(mean(T38));T39=double(T39);t39=mean(mean(T39))
T40=double(T40);t40=mean(mean(T40));T41=double(T41);t41=mean(mean(T41))
T42=double(T42);t42=mean(mean(T42));T43=double(T43);t43=mean(mean(T43))
T44=double(T44);t44=mean(mean(T44));T45=double(T45);t45=mean(mean(T45))
T46=double(T46);t46=mean(mean(T46));T47=double(T47);t47=mean(mean(T47))
T48=double(T48);t48=mean(mean(T48));T49=double(T49);t49=mean(mean(T49))
T50=double(T50);t50=mean(mean(T50));T51=double(T51);t51=mean(mean(T51))
T52=double(T52);t52=mean(mean(T52));T53=double(T53);t53=mean(mean(T53))
T54=double(T54);t54=mean(mean(T54));T55=double(T55);t55=mean(mean(T55))
T56=double(T56);t56=mean(mean(T56));T57=double(T57);t57=mean(mean(T57))
T58=double(T58);t58=mean(mean(T58));T59=double(T59);t59=mean(mean(T59))
T60=double(T60);t60=mean(mean(T60));T61=double(T61);t61=mean(mean(T61))
T62=double(T62);t62=mean(mean(T62));T63=double(T63);t63=mean(mean(T63))
T64=double(T64);t64=mean(mean(T64));T65=double(T65);t65=mean(mean(T65))
T66=double(T66);t66=mean(mean(T66));T67=double(T67);t67=mean(mean(T67))
T68=double(T68);t68=mean(mean(T68));T69=double(T69);t69=mean(mean(T69))
T70=double(T70);t70=mean(mean(T70));T71=double(T71);t71=mean(mean(T71))
T72=double(T72);t72=mean(mean(T72));T73=double(T73);t73=mean(mean(T73))
T74=double(T74);t74=mean(mean(T74));T75=double(T75);t75=mean(mean(T75))
T76=double(T76);t76=mean(mean(T76));T77=double(T77);t77=mean(mean(T77))
T78=double(T78);t78=mean(mean(T78));T79=double(T79);t79=mean(mean(T79))
T80=double(T80);t80=mean(mean(T80));

```

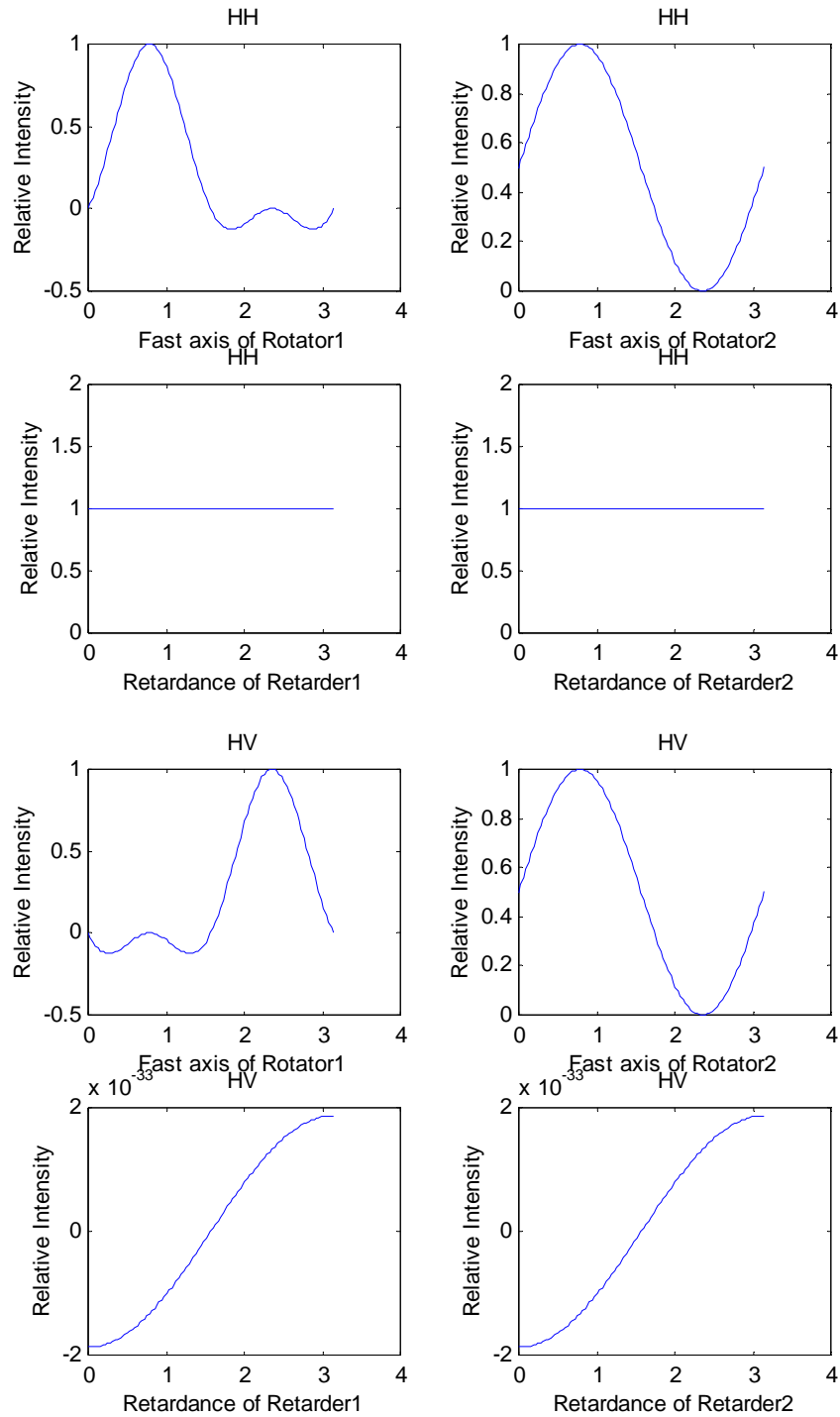
```

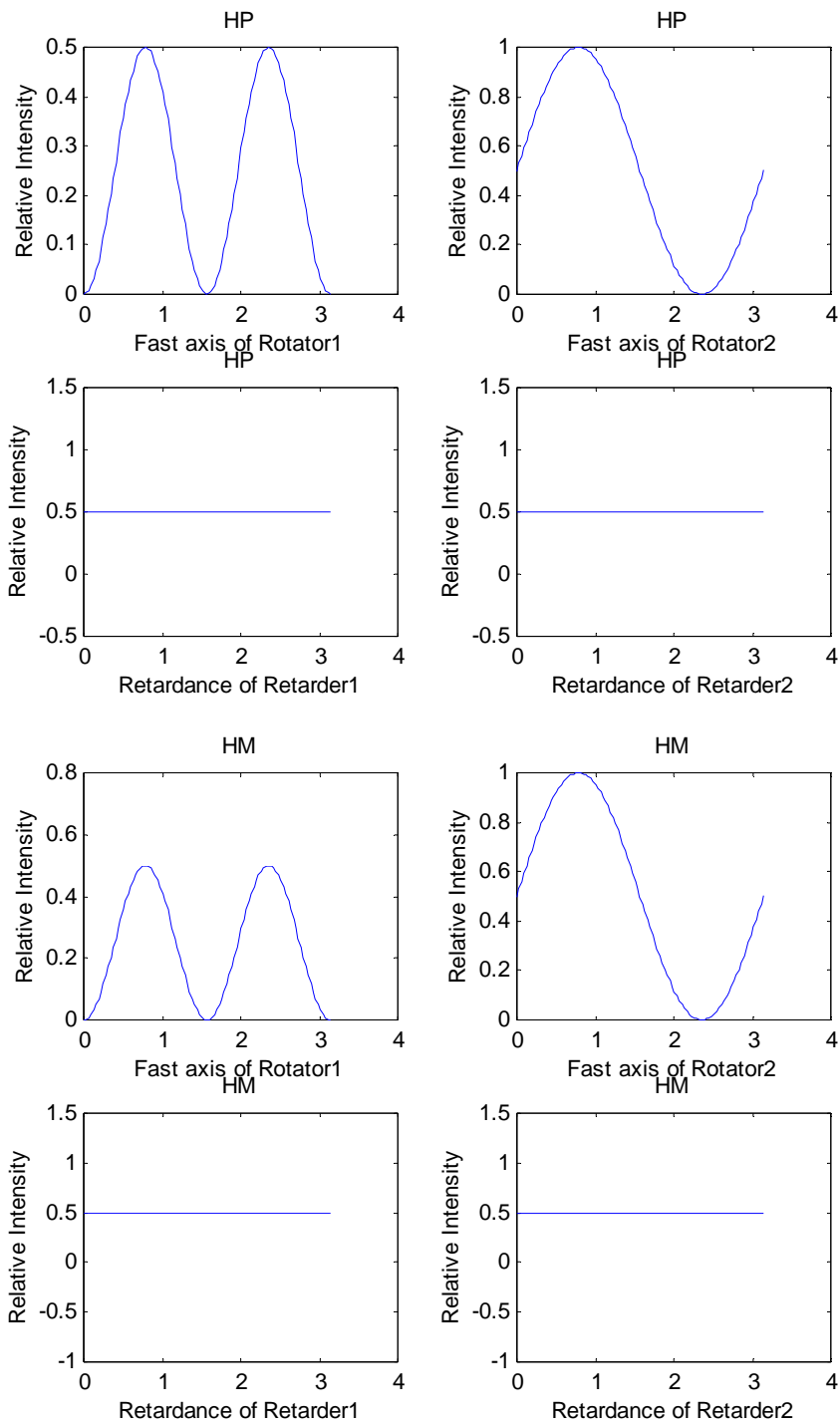
RAW=[t0;t1;t2;t3;t4;t5;t6;t7;t8;t9;
      t10;t11;t12;t13;t14;t15;t16;t17;t18;t19;
      t20;t21;t22;t23;t24;t25;t26;t27;t28;t29;
      t30;t31;t32;t33;t34;t35;t36;t37;t38;t39;
      t40;t41;t42;t43;t44;t45;t46;t47;t48;t49;
      t50;t51;t52;t53;t54;t55;t56;t57;t58;t59;
      t60;t61;t62;t63;t64;t65;t66;t67;t68;t69;
      t70;t71;t72;t73;t74;t75;t76;t77;t78;t79;
      t80]

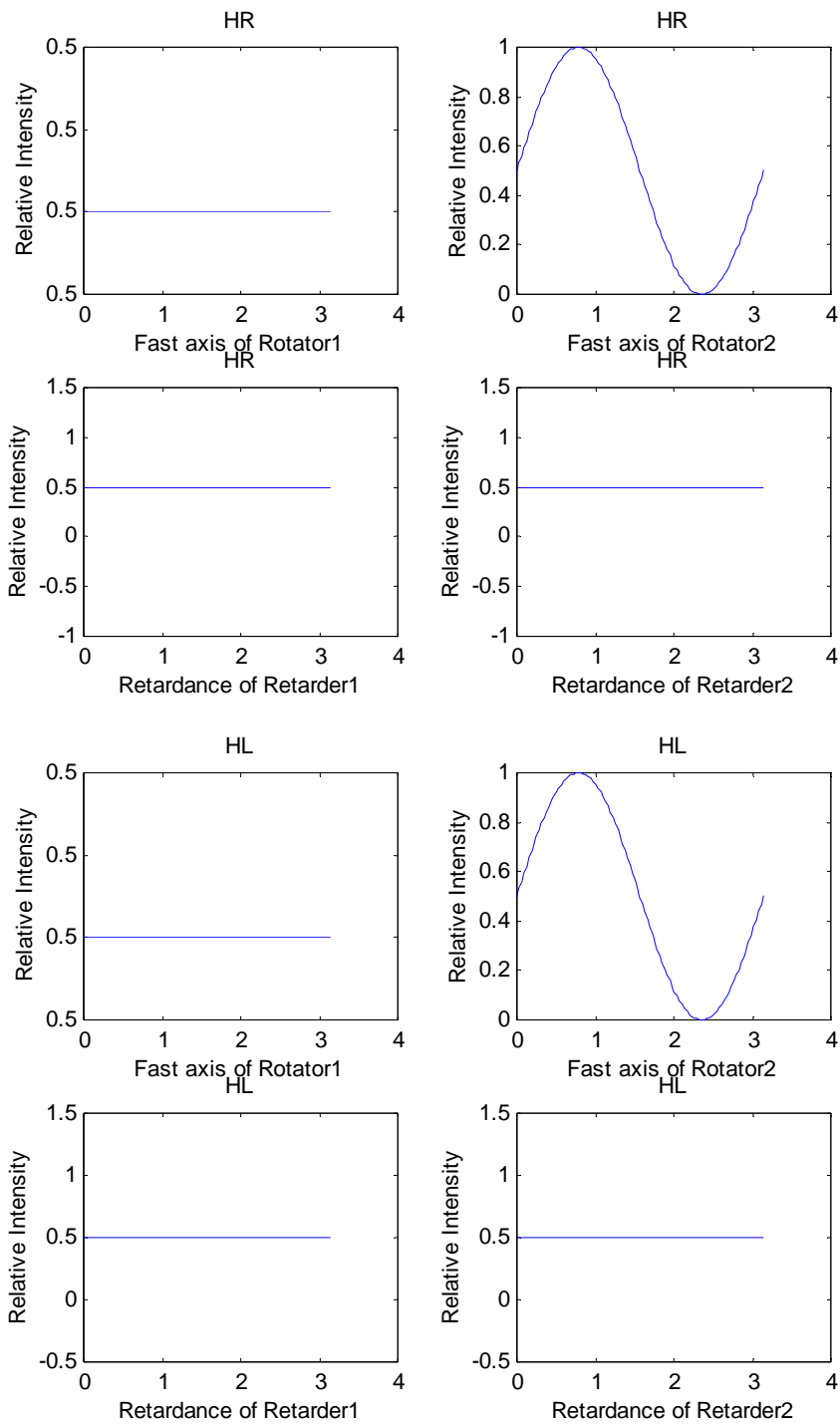
```

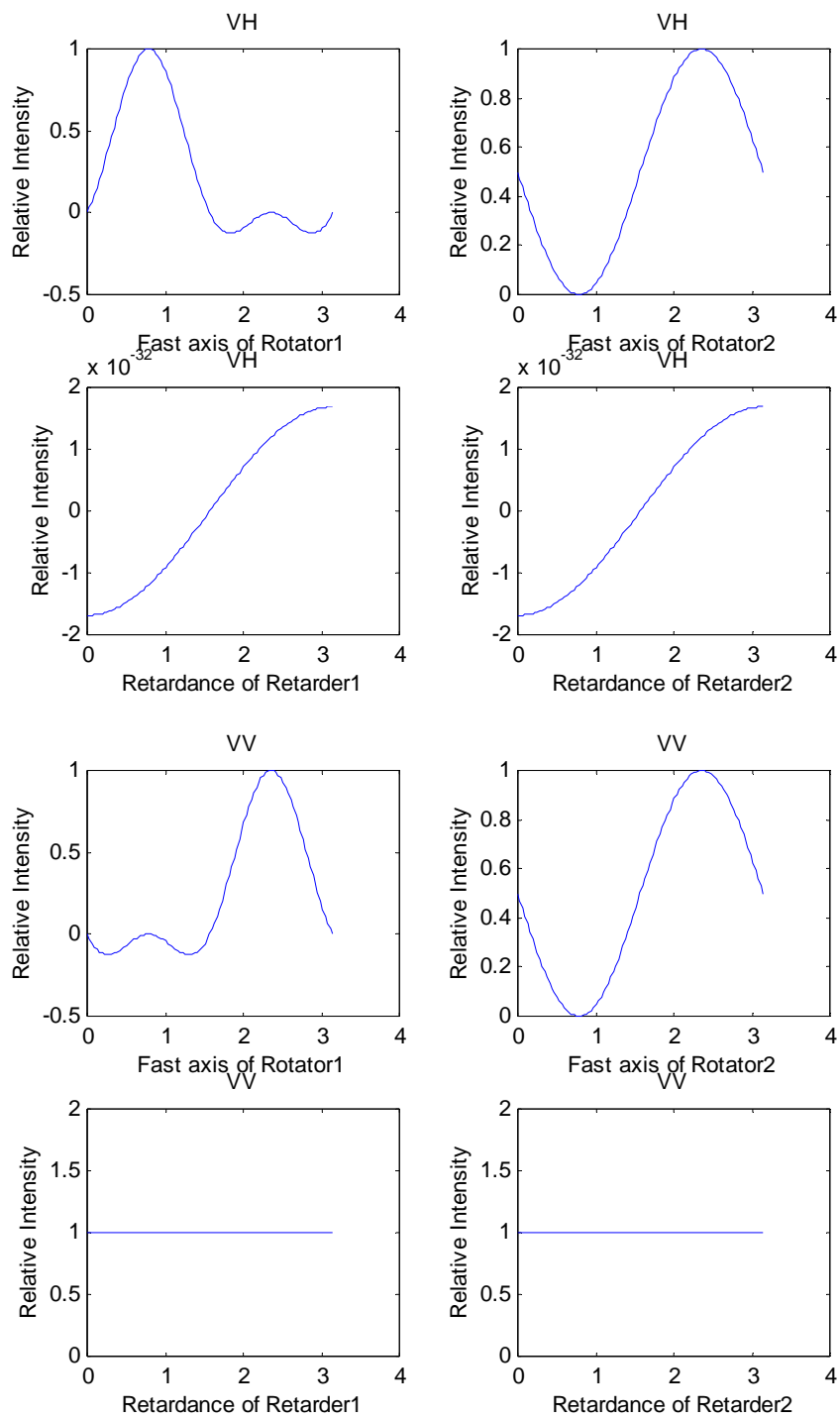
## APPENDIX F

### SYSTEM MODEL PLOTS

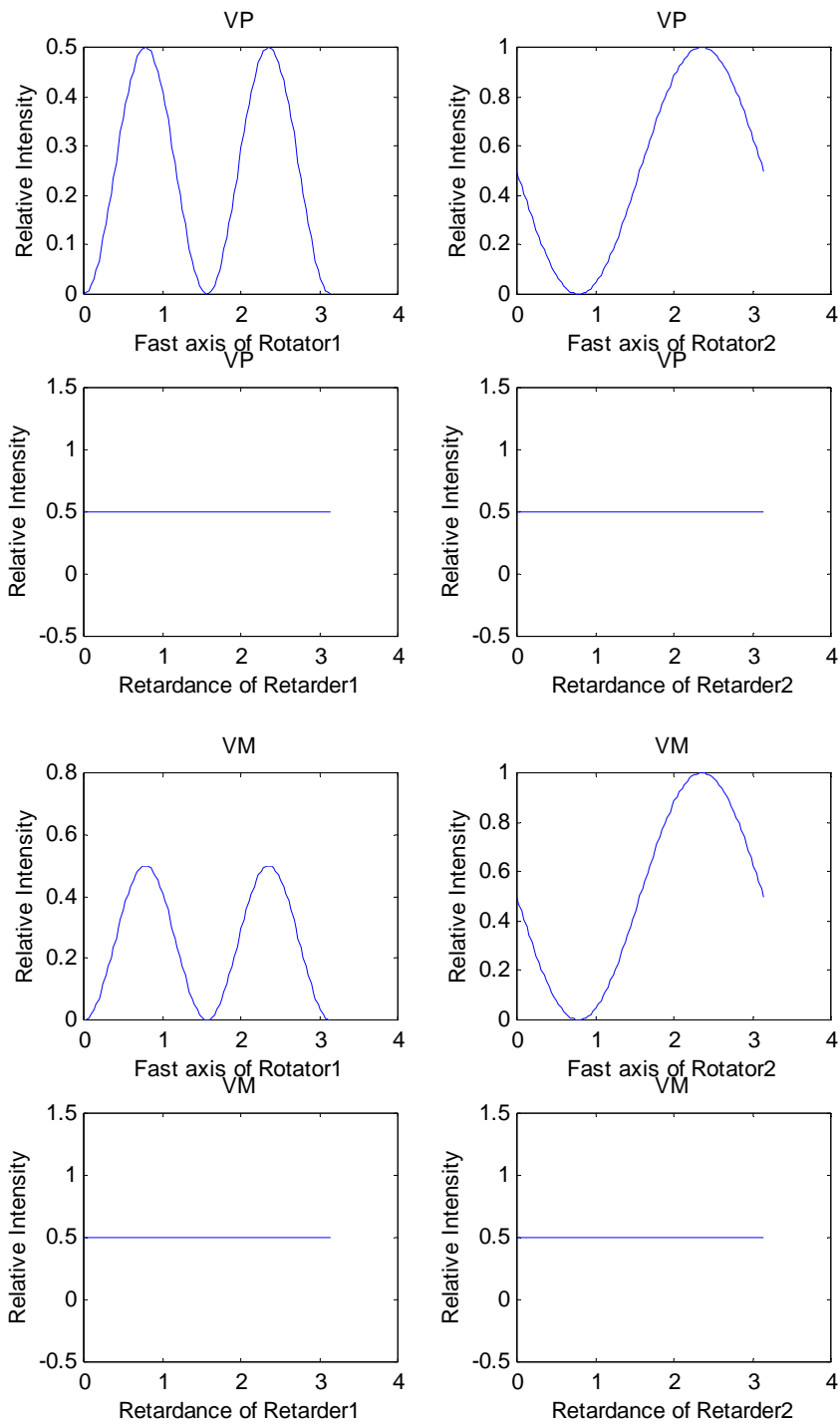


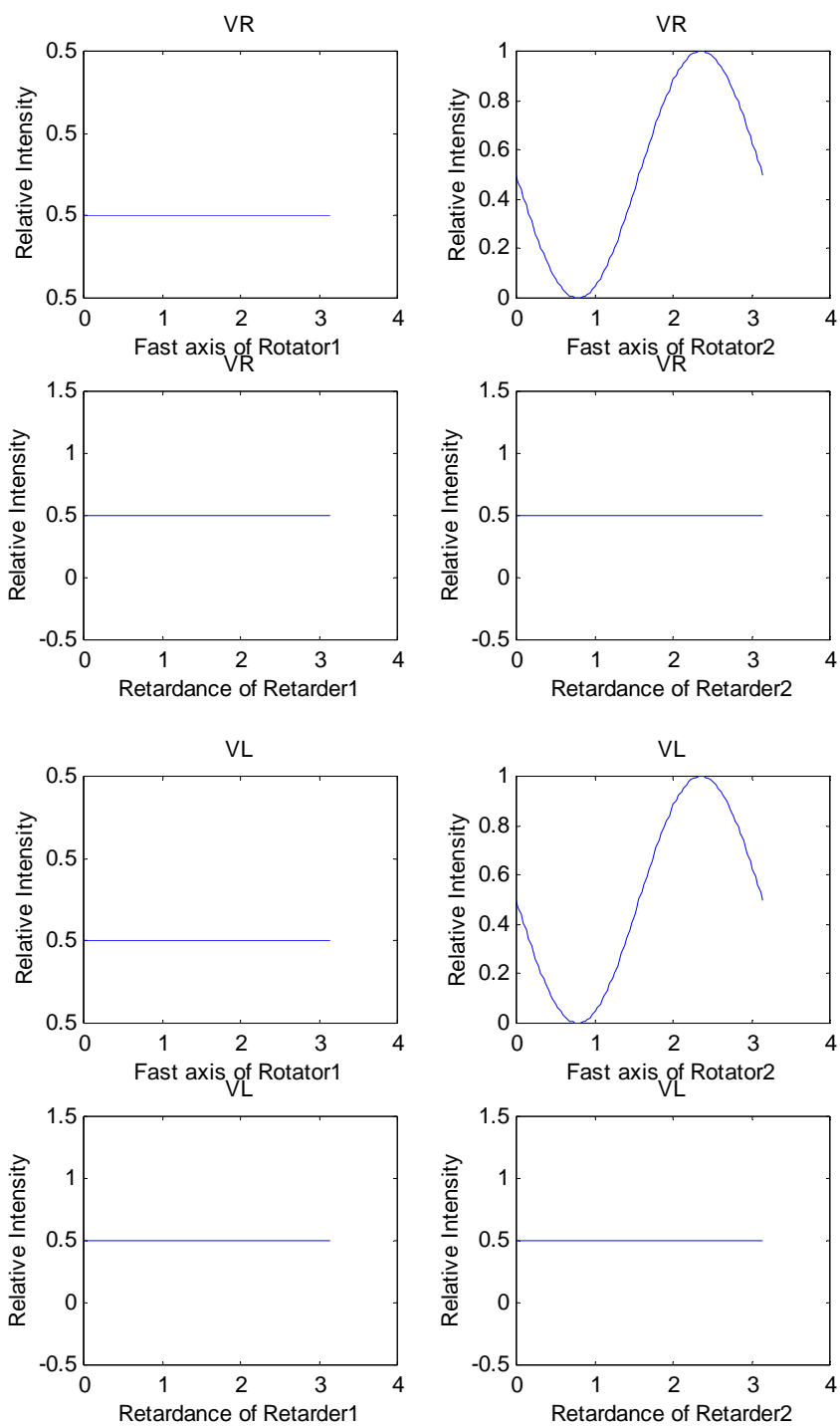


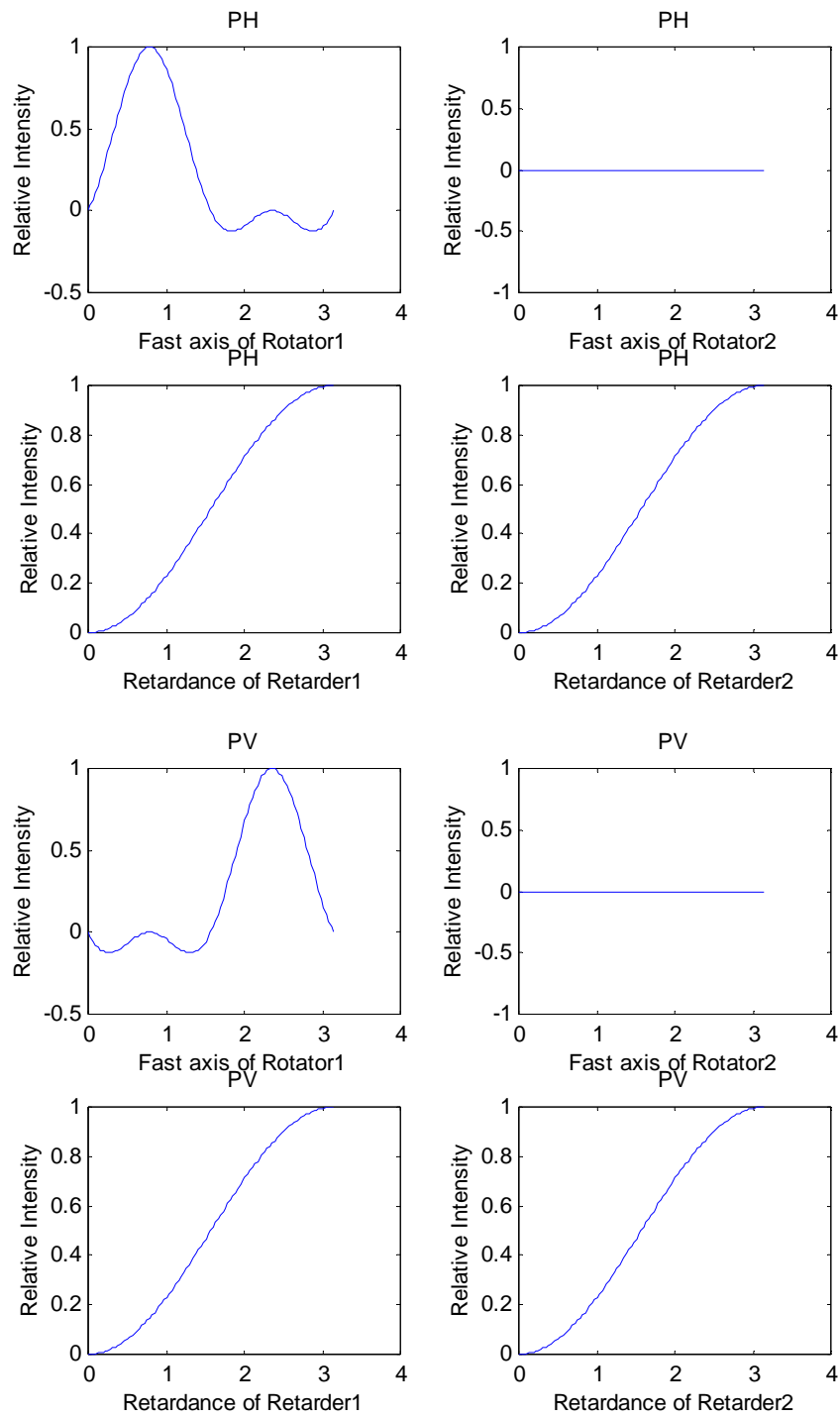


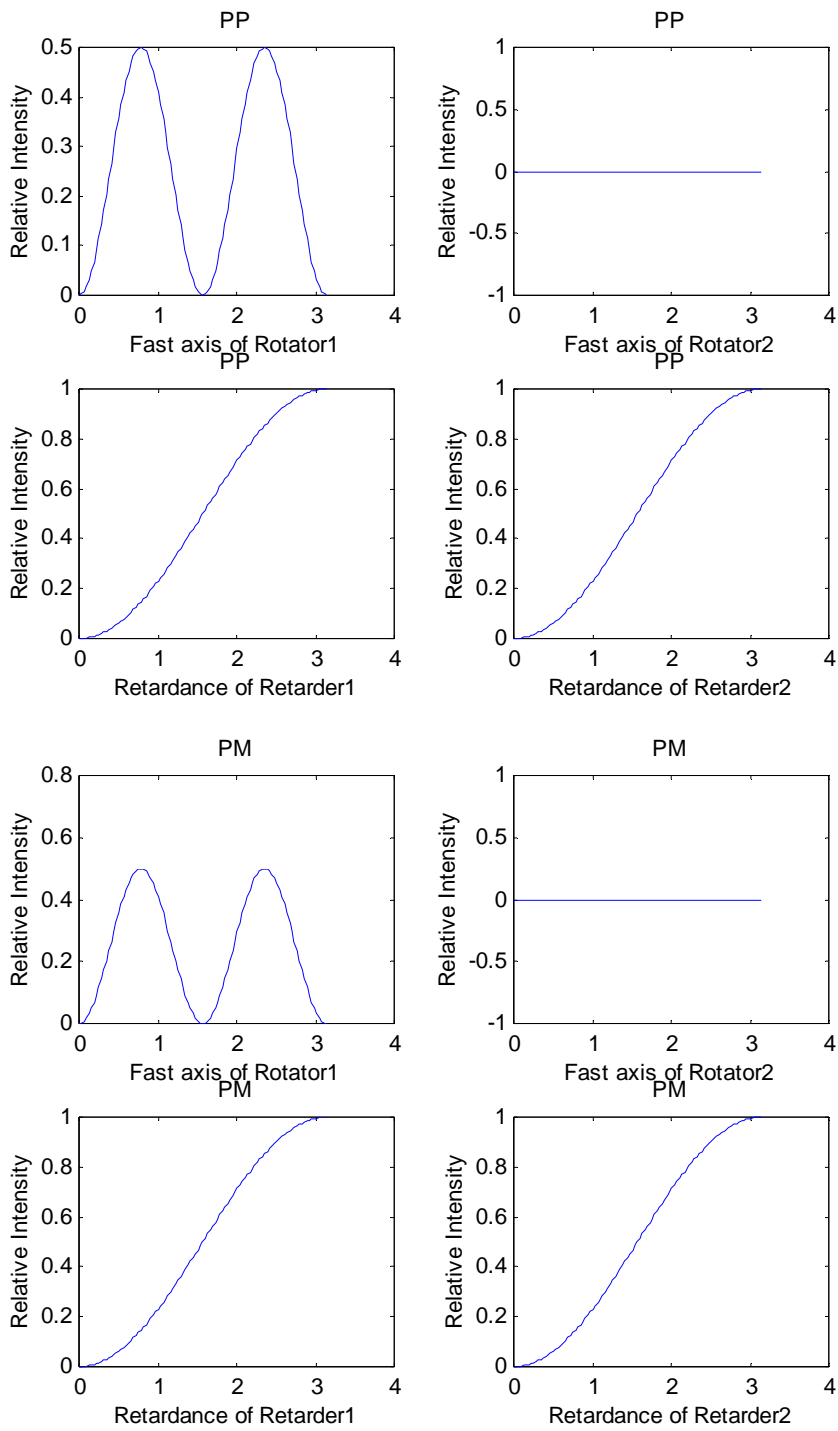


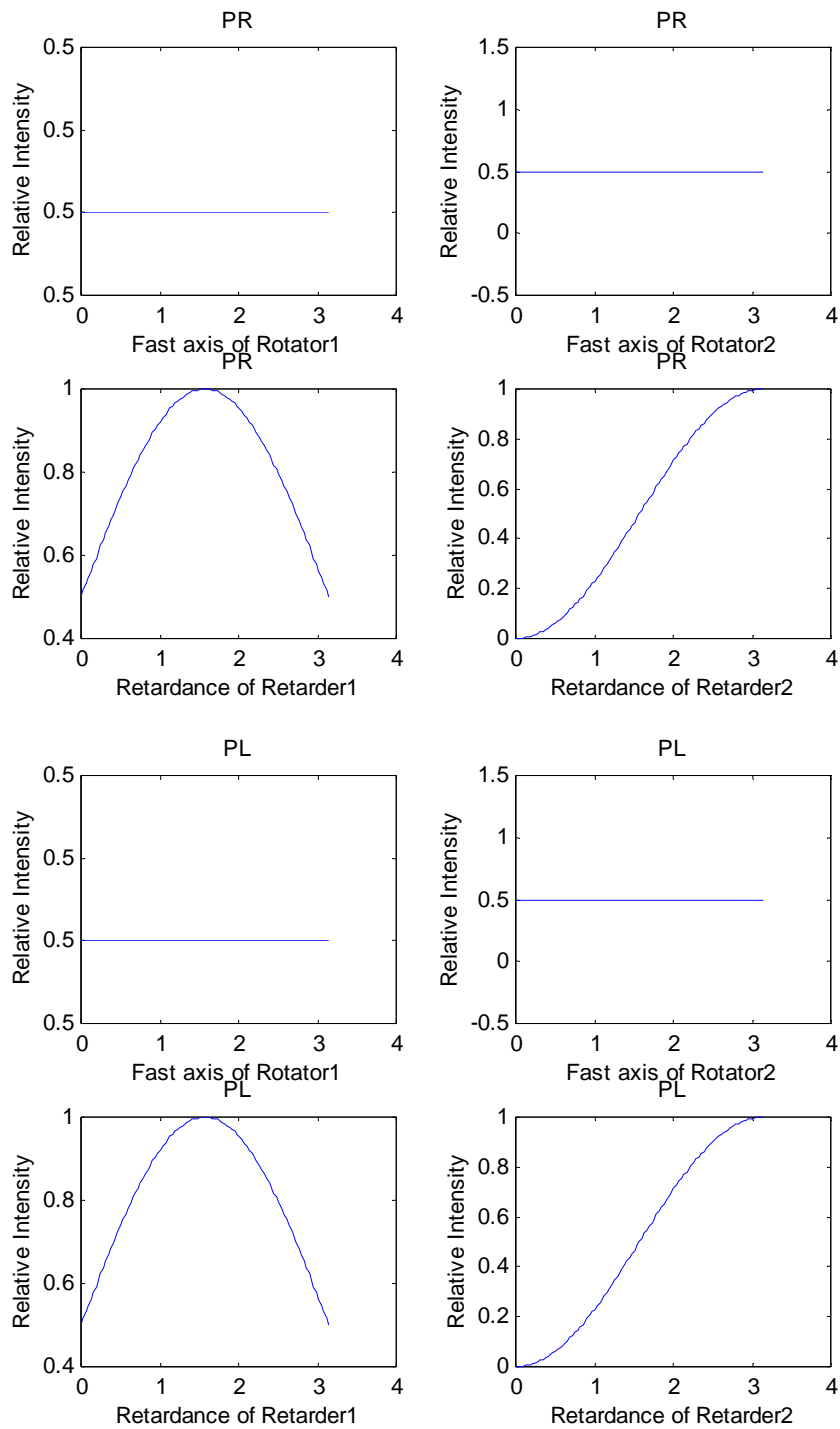


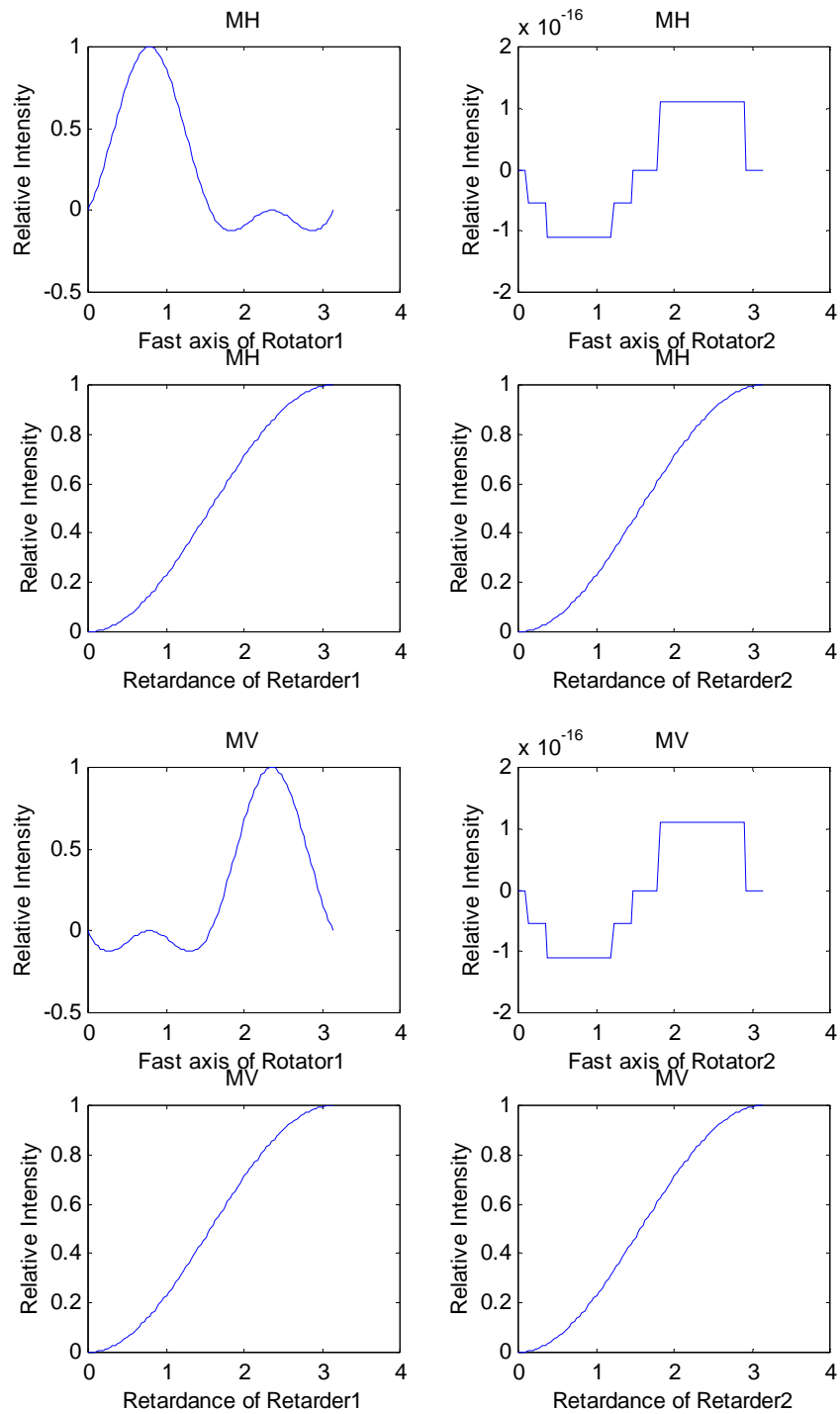


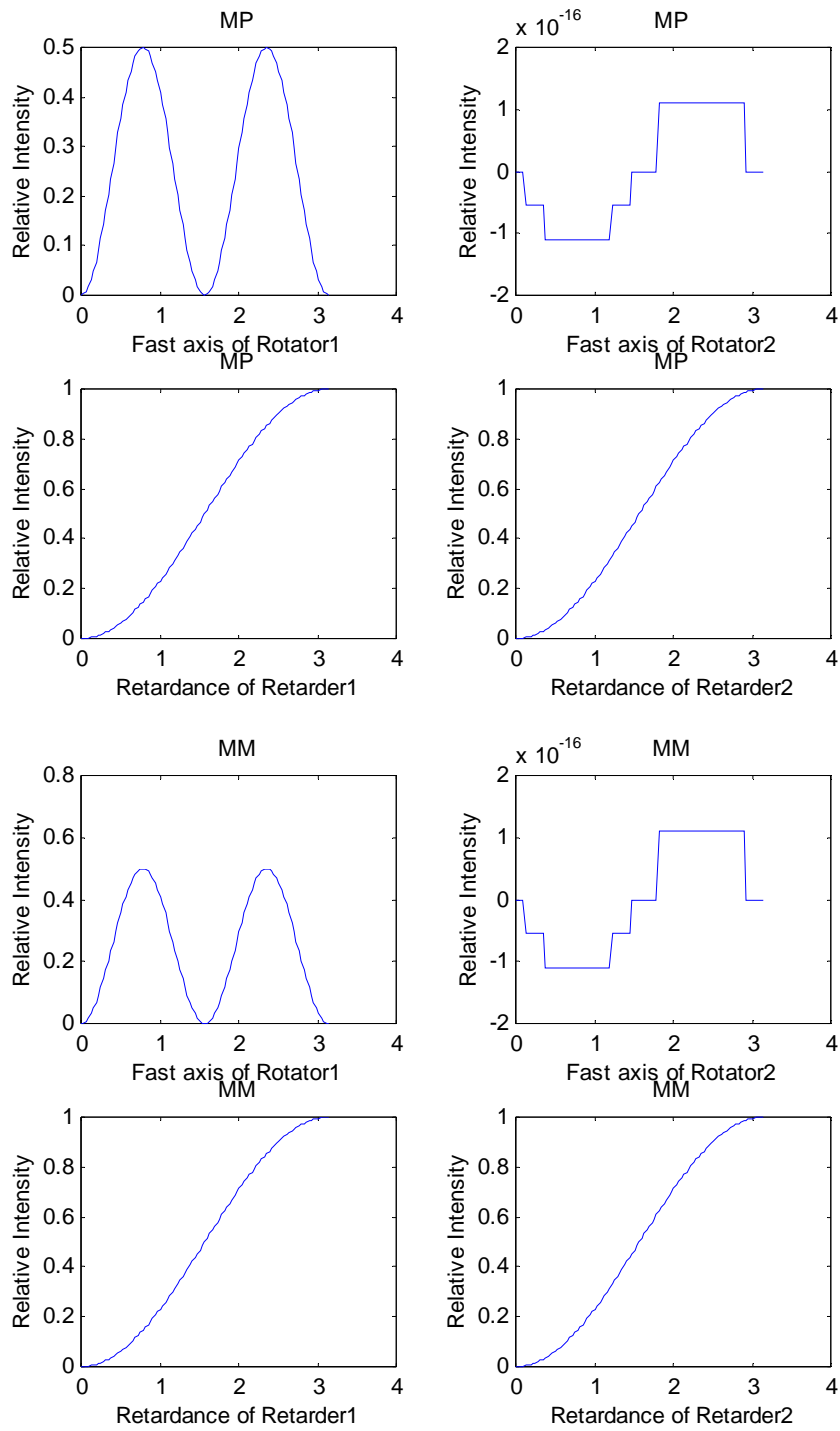


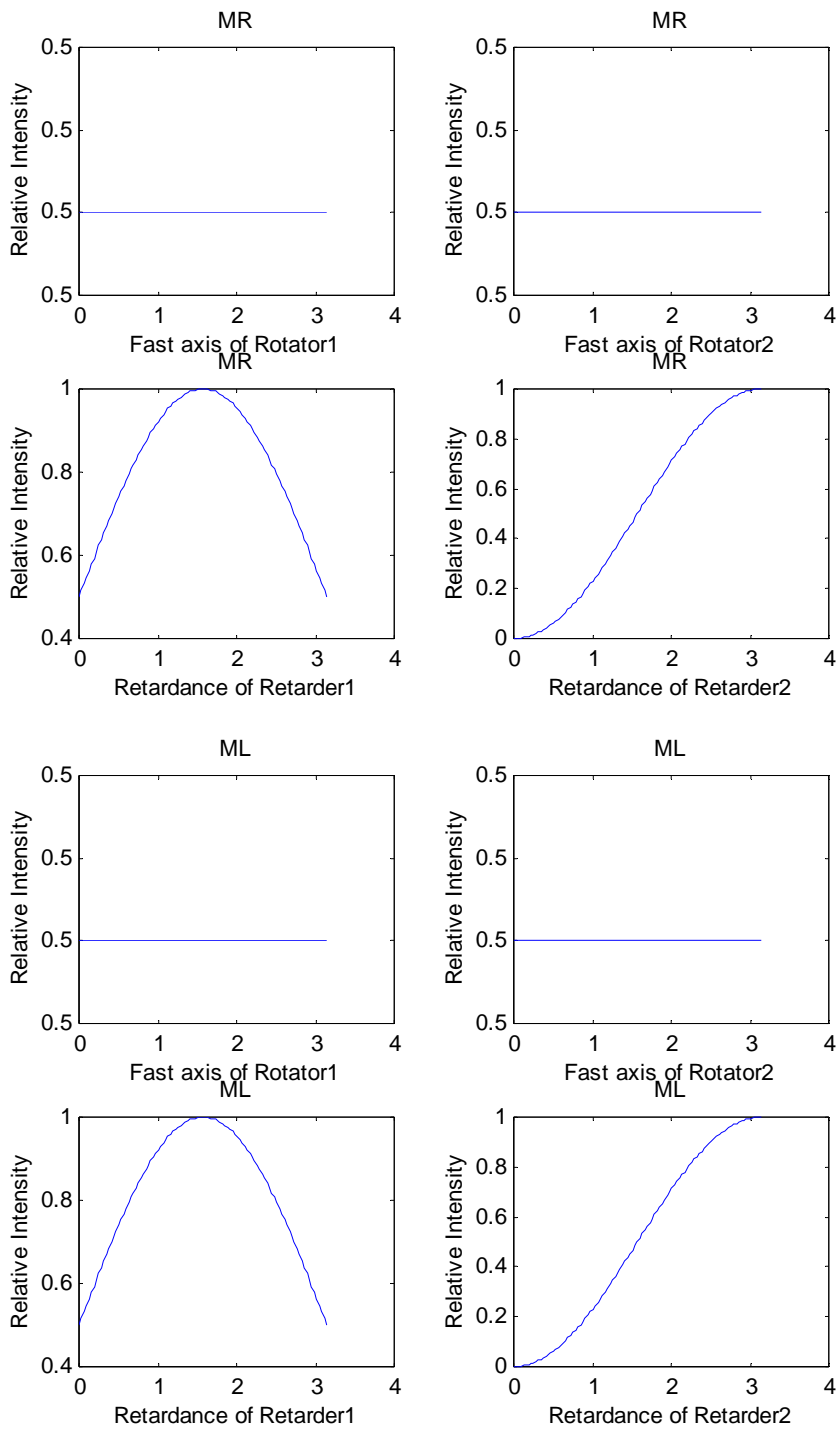




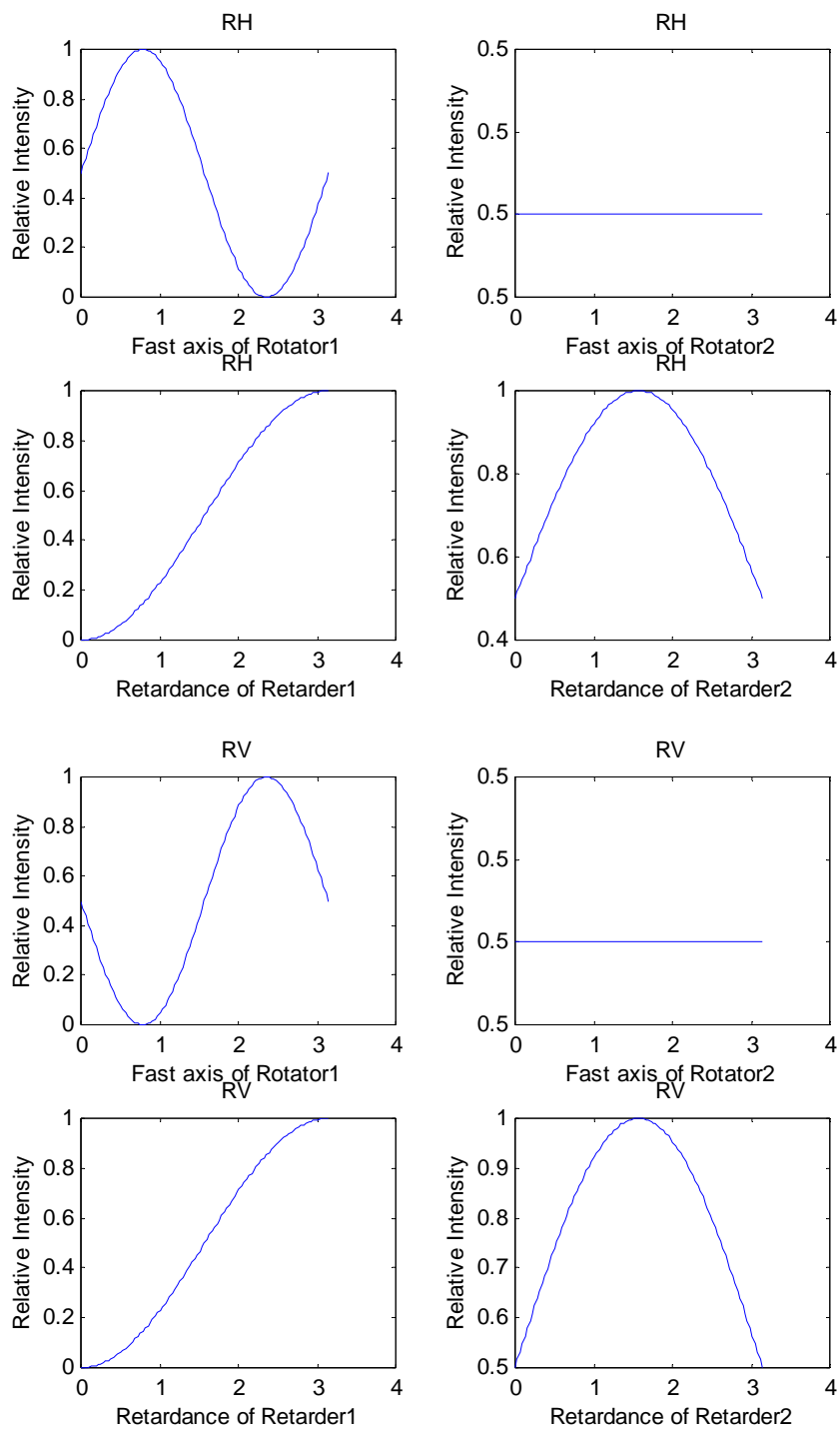


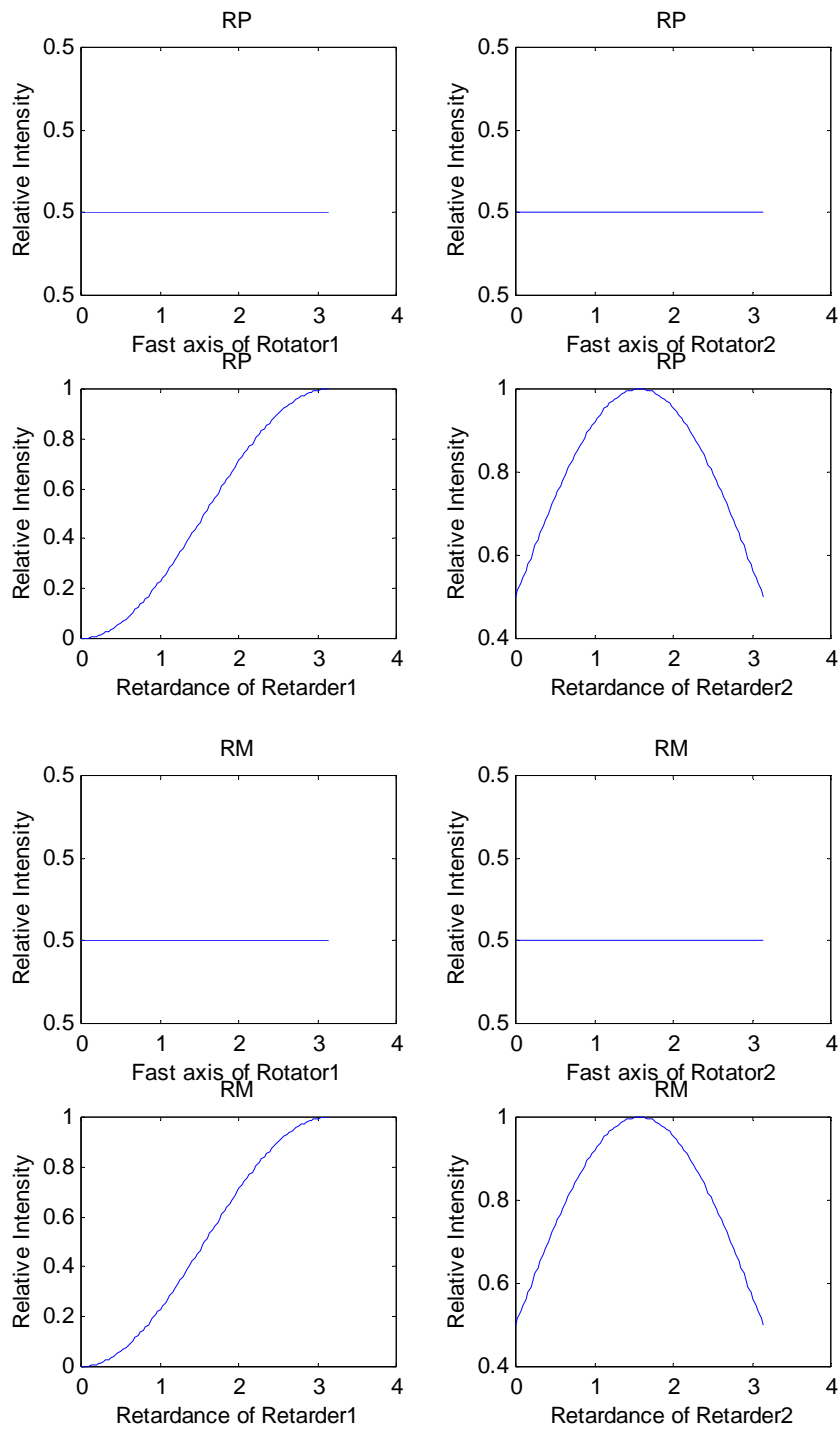


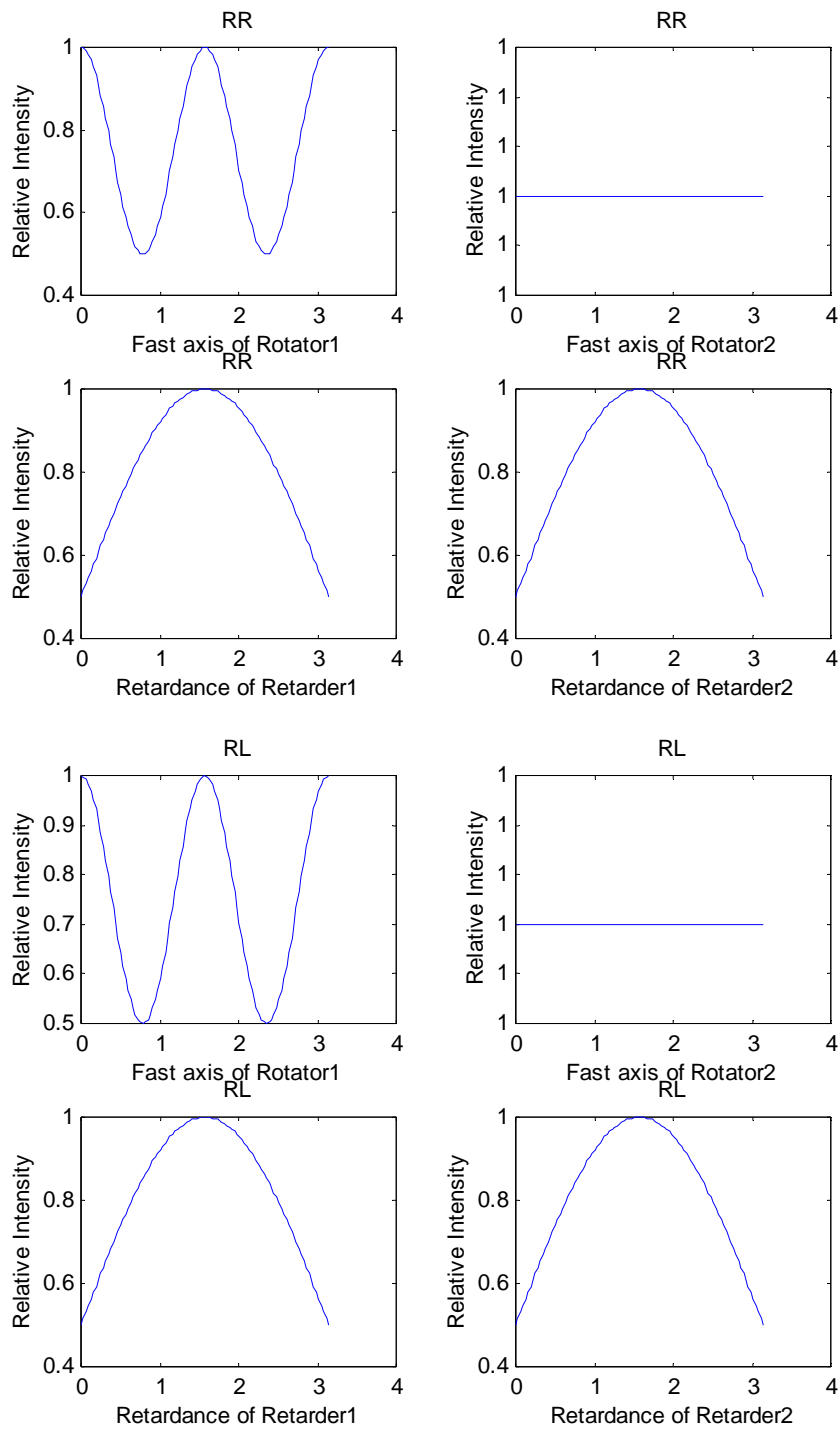


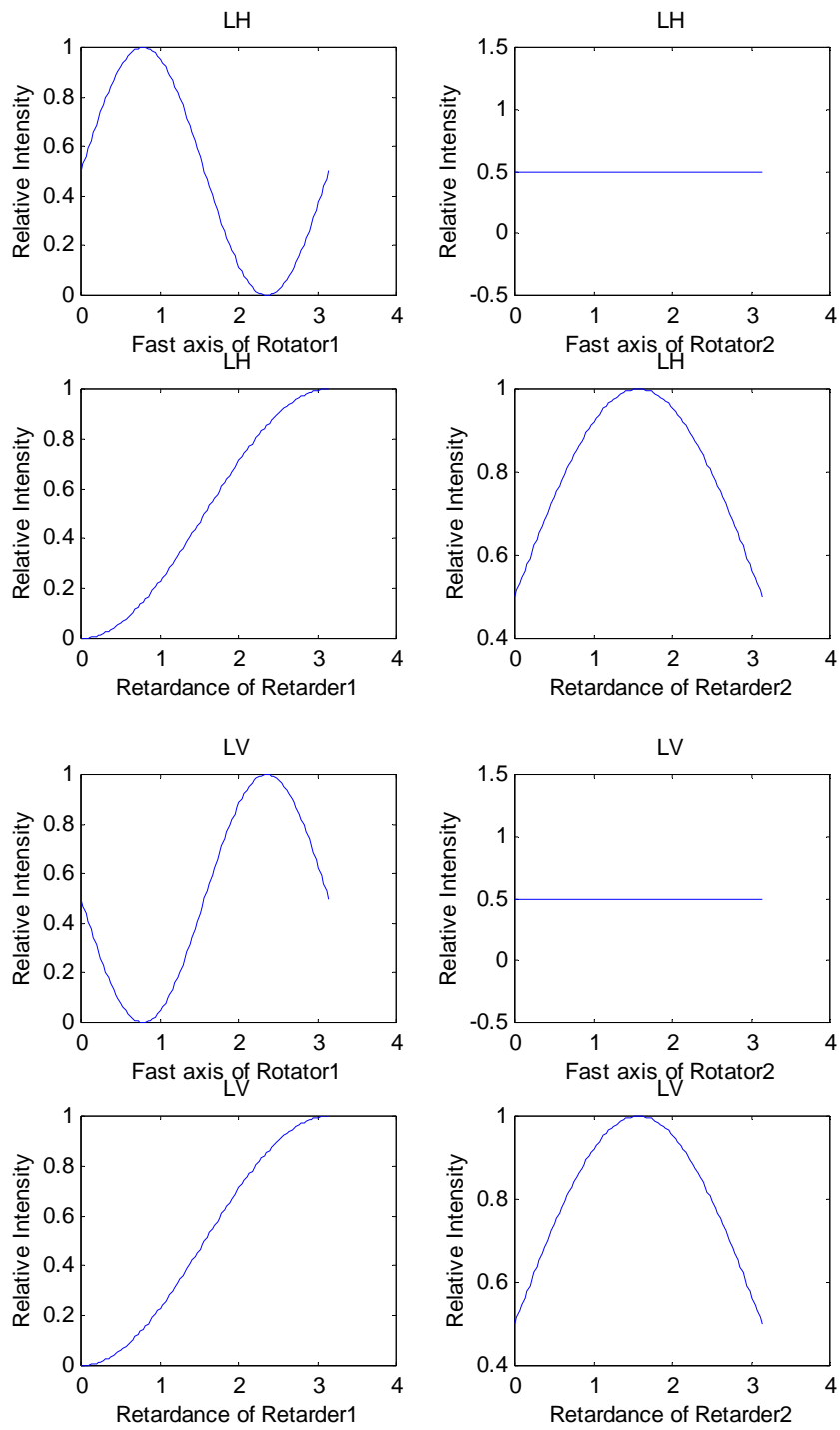


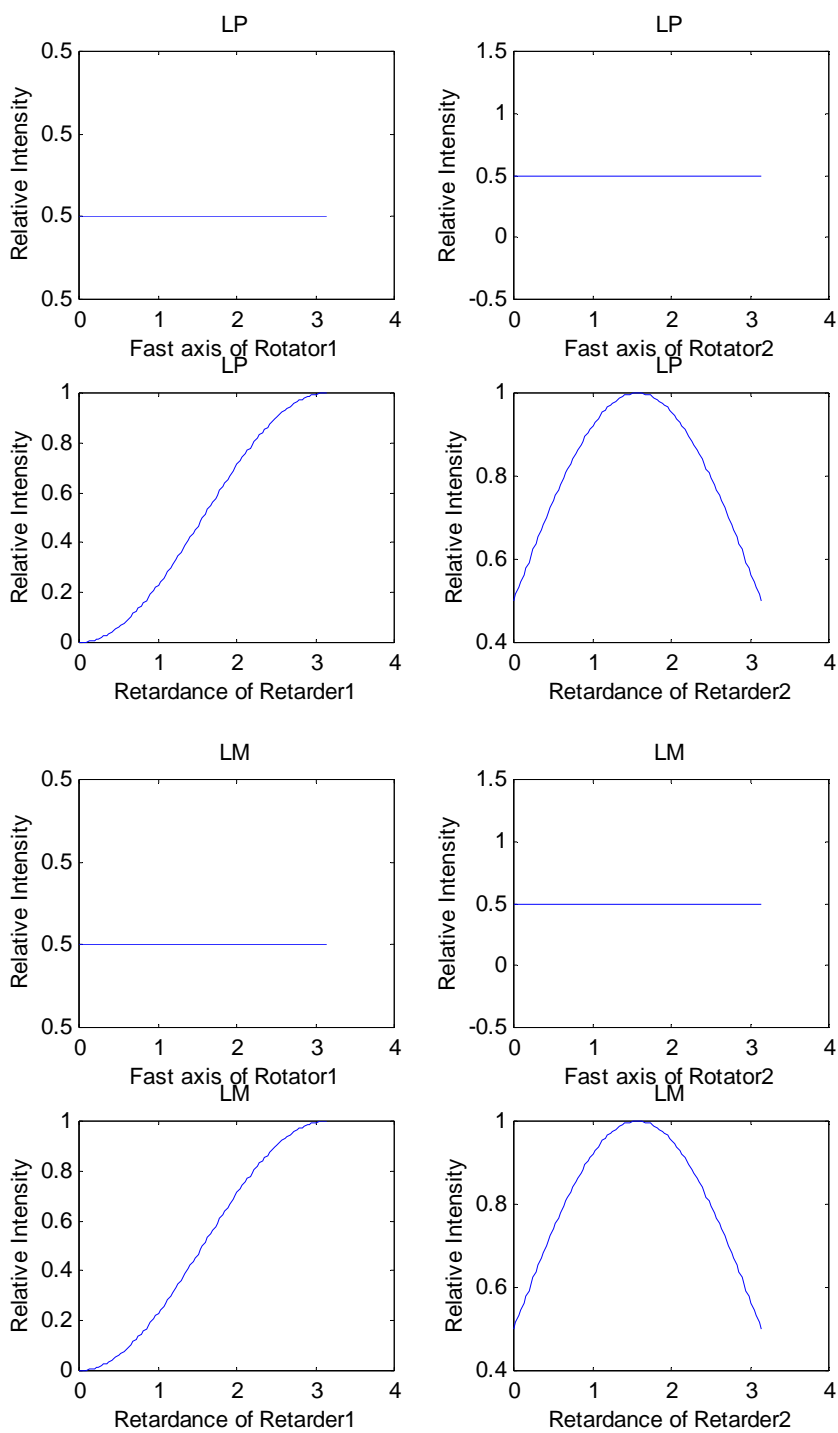


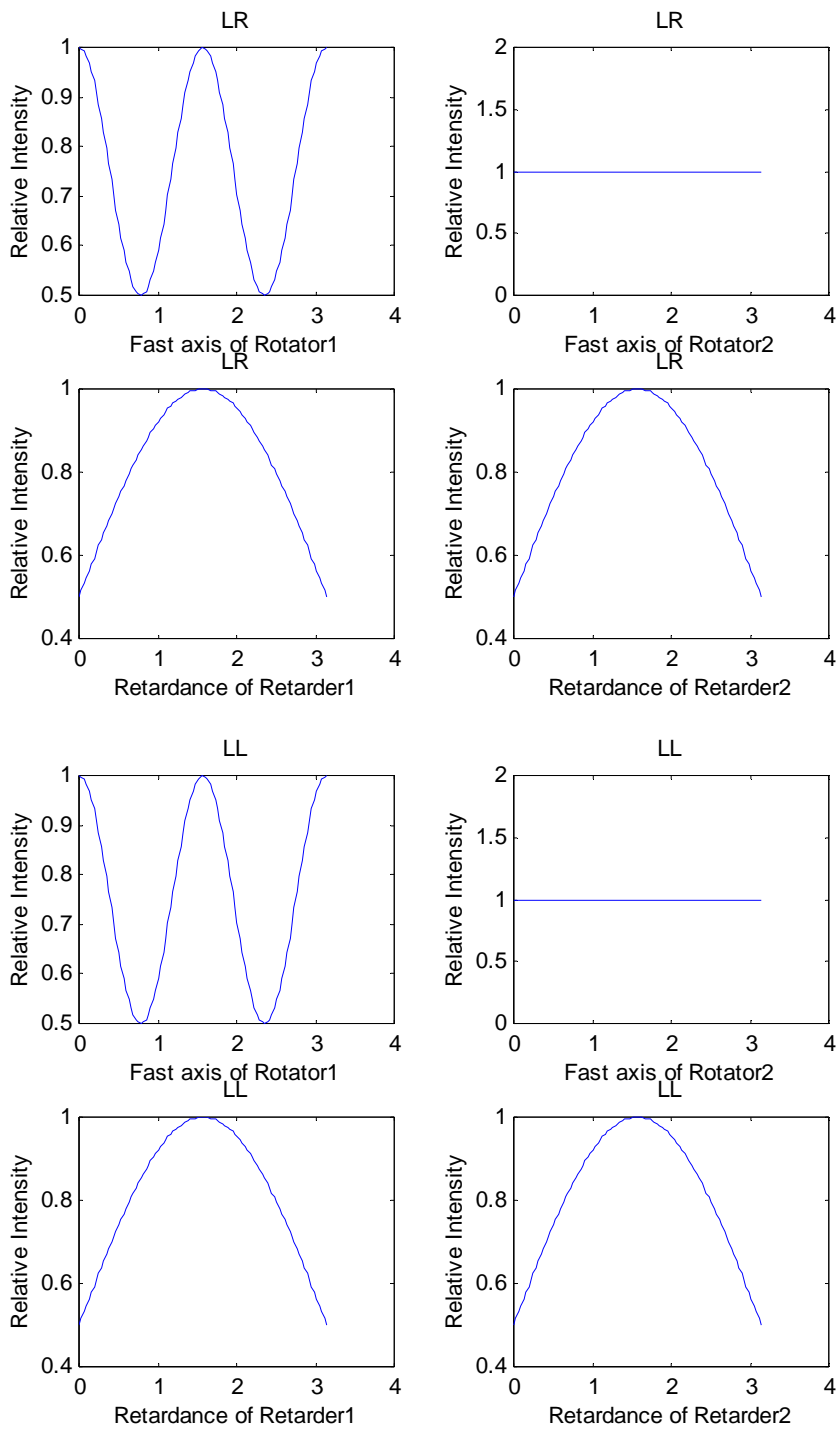












## APPENDIX G

## MUELLER MATRIX IMAGING SYSTEM LABVIEW PROGRAM

## Main Program

KS Application.vi Front Panel \*

Start at: Stop at: Current Image  
 1 36 36

Acquire Images STOP


Time from first to last picture Total Time  
 52.75 0


Raw Intensity Values  
 (after background subtraction)

0	0	0	0	0	0
0	0	0	0	0	0
0	0	0	0	0	0
0	0	0	0	0	0
0	0	0	0	0	0
0	0	0	0	0	0

Mueller matrix

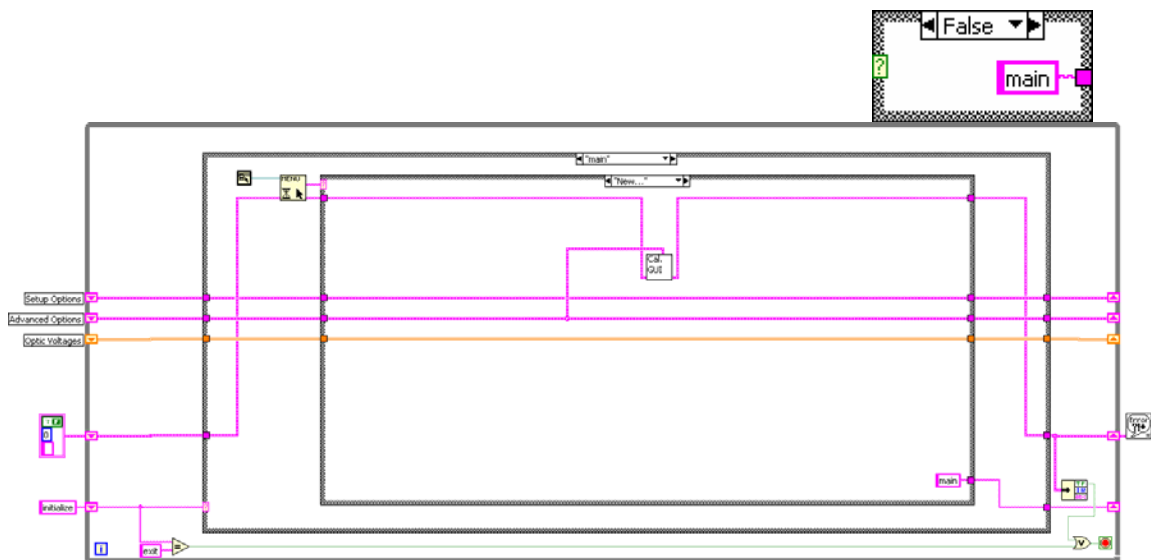
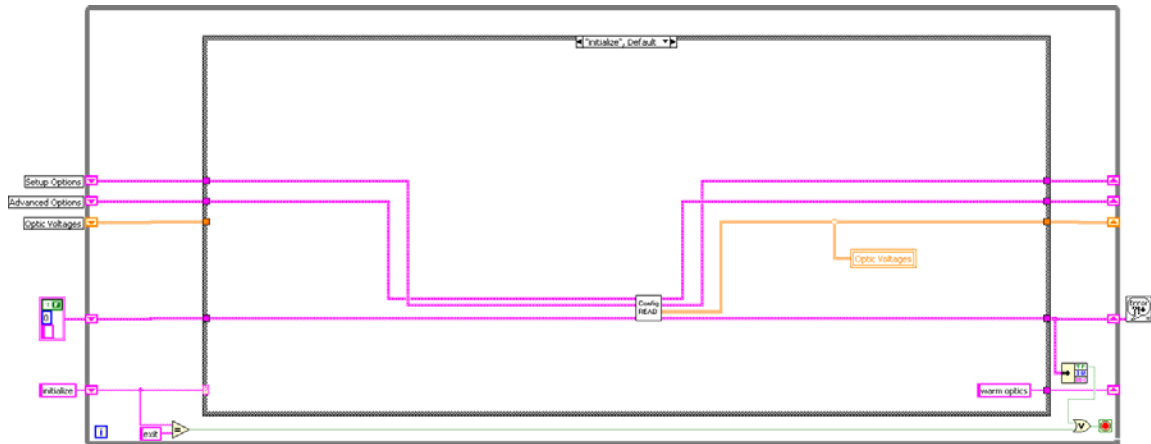
0	0	0	0
0	0	0	0
0	0	0	0
0	0	0	0

Raw Data Filename  
 Save Values?   

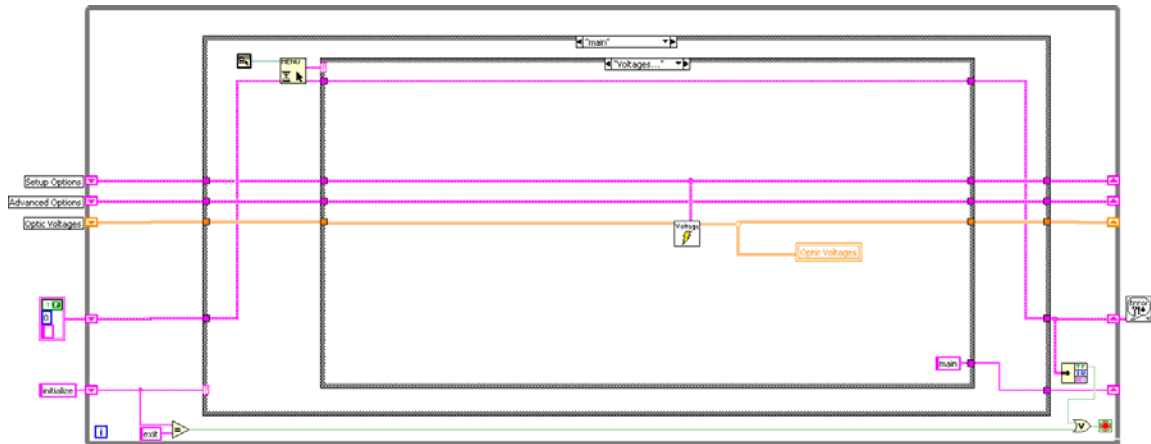
Mueller Matrix Filename  
 

Optic Voltages

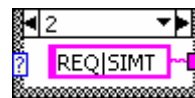
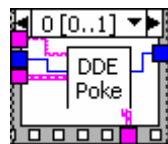
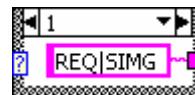
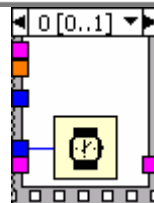
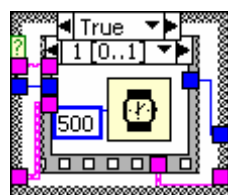
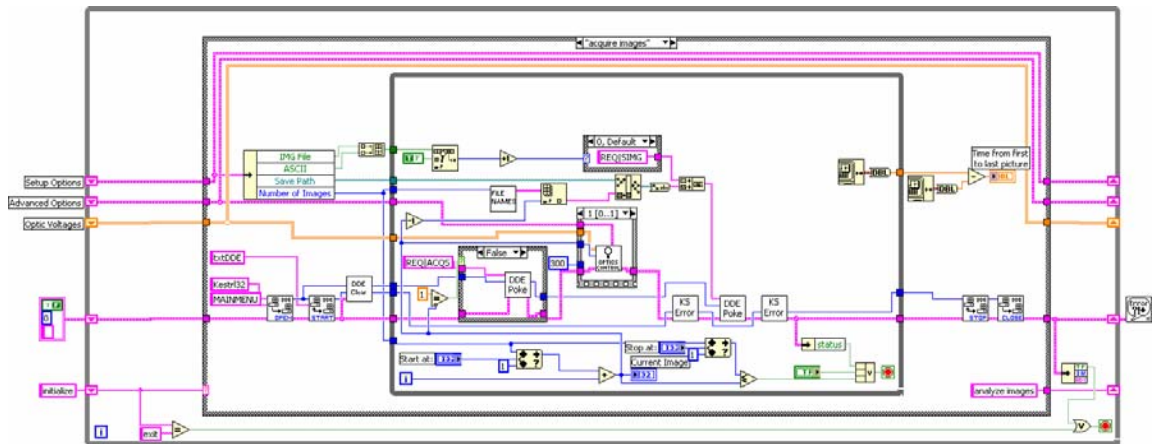
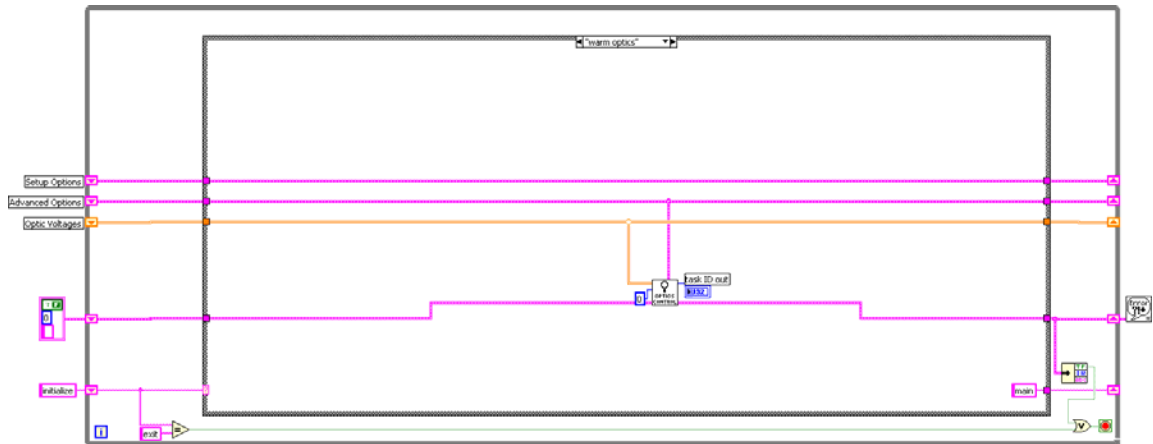
1.310	5.500	5.000	1.310
1.310	5.500	5.000	1.850
1.310	5.500	5.000	1.560
1.310	5.500	5.000	2.240
1.310	5.500	2.760	1.850
1.310	5.500	2.410	1.310
1.840	5.500	5.000	1.310
1.840	5.500	5.000	1.850
1.840	5.500	5.000	1.560
1.840	5.500	5.000	2.240
1.840	5.500	2.760	1.850
1.840	5.500	2.410	1.310
1.580	5.500	5.000	1.310
1.580	5.500	5.000	1.850
1.580	5.500	5.000	1.560
1.580	5.500	5.000	2.240
1.580	5.500	2.760	1.850
1.580	5.500	2.410	1.310
2.210	5.500	5.000	1.310
2.210	5.500	5.000	1.850
2.210	5.500	5.000	1.560
2.210	5.500	5.000	2.240
2.210	5.500	2.760	1.850
2.210	5.500	2.410	1.310
1.840	2.640	5.000	1.310
1.840	2.640	5.000	1.850
1.840	2.640	5.000	1.560
1.840	2.640	5.000	2.240
1.840	2.640	2.760	1.850
1.840	2.640	2.410	1.310
1.310	2.280	5.000	1.310
1.310	2.280	5.000	1.850
1.310	2.280	5.000	1.560
1.310	2.280	5.000	2.240
1.310	2.280	2.760	1.850
1.310	2.280	2.410	1.310

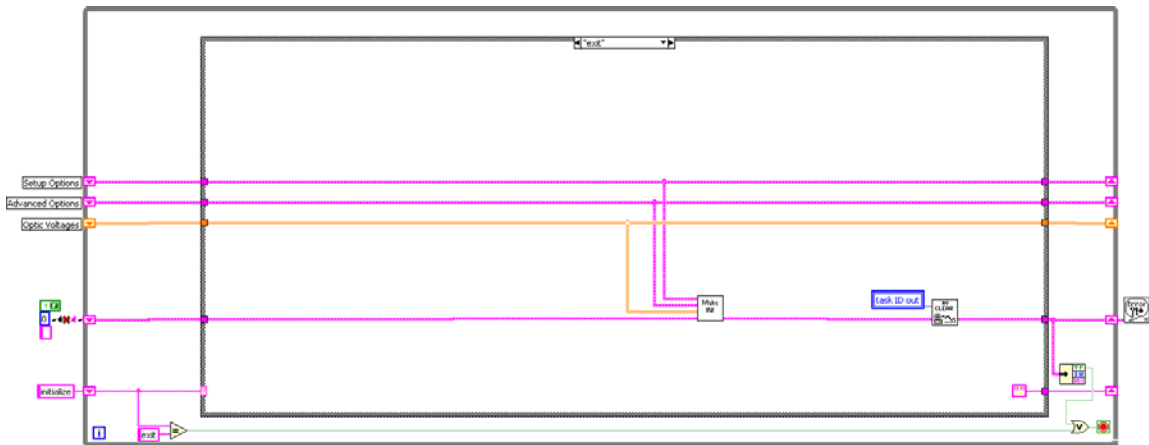
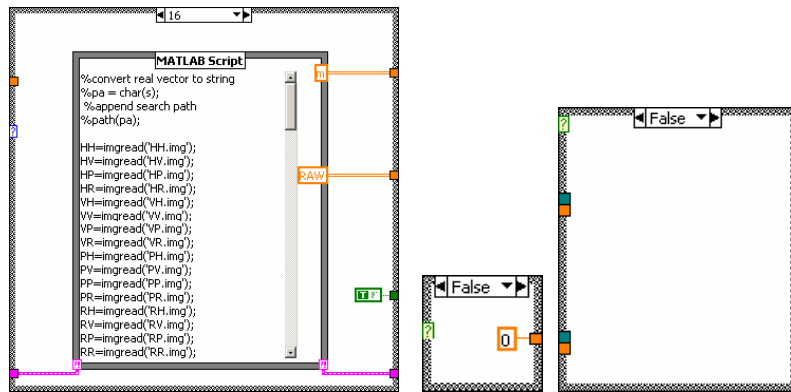
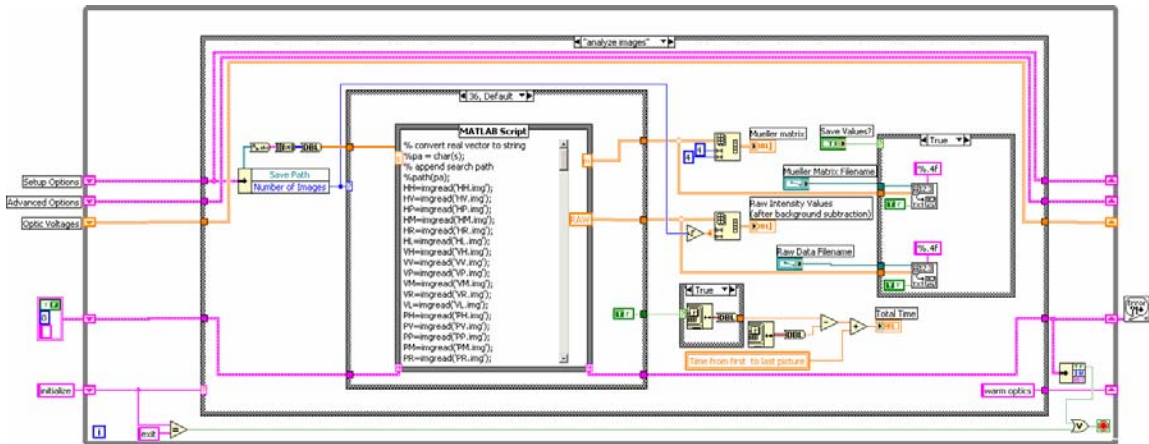




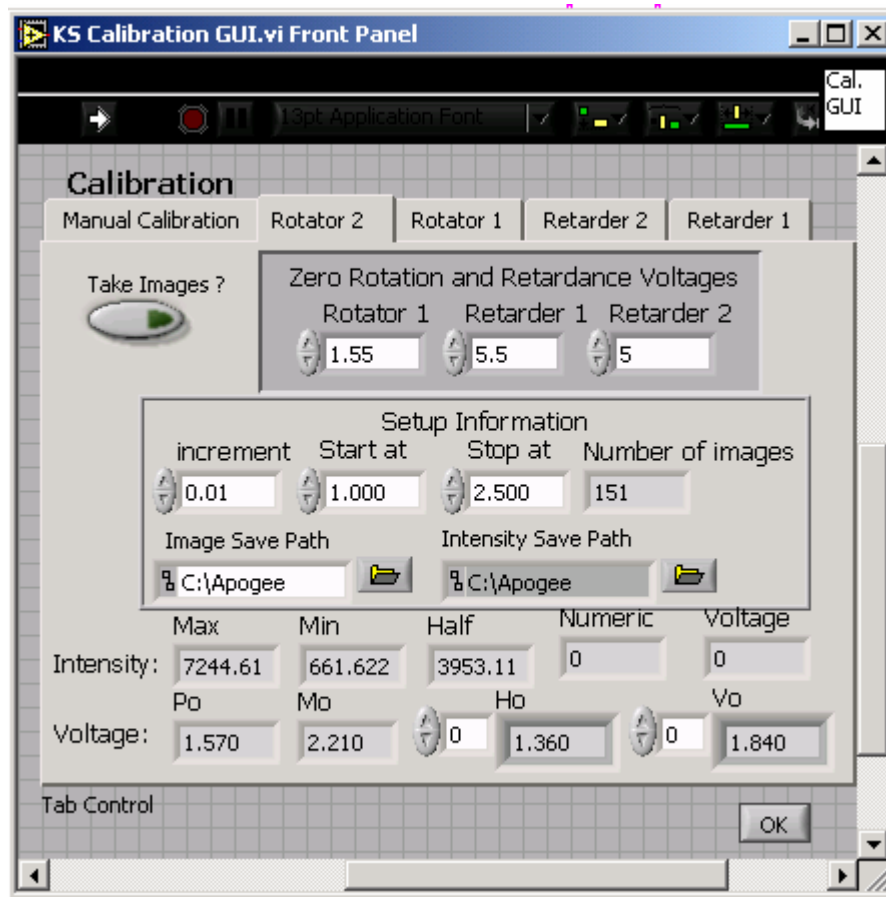


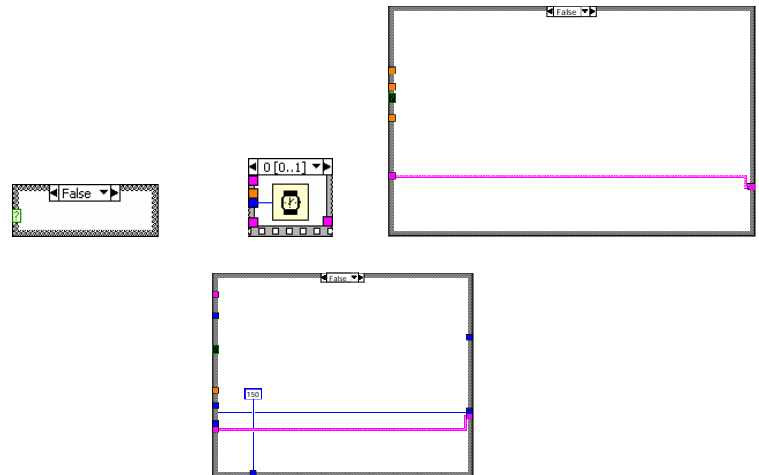
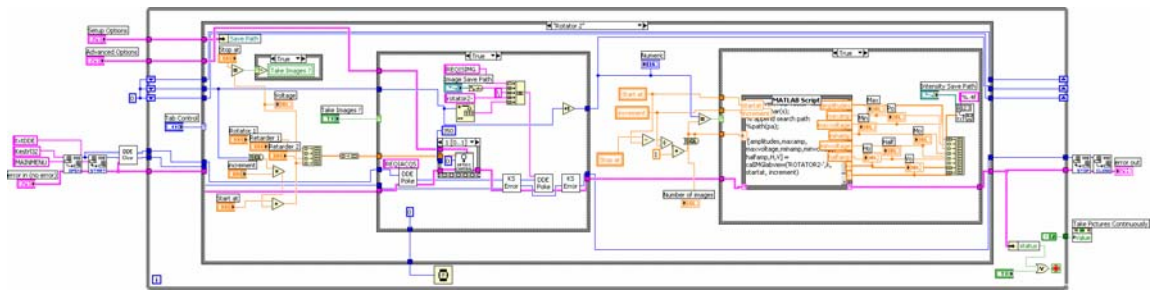
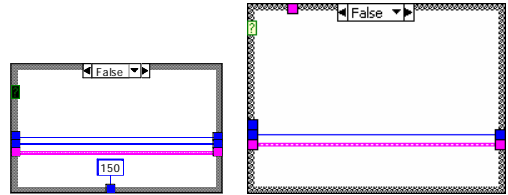
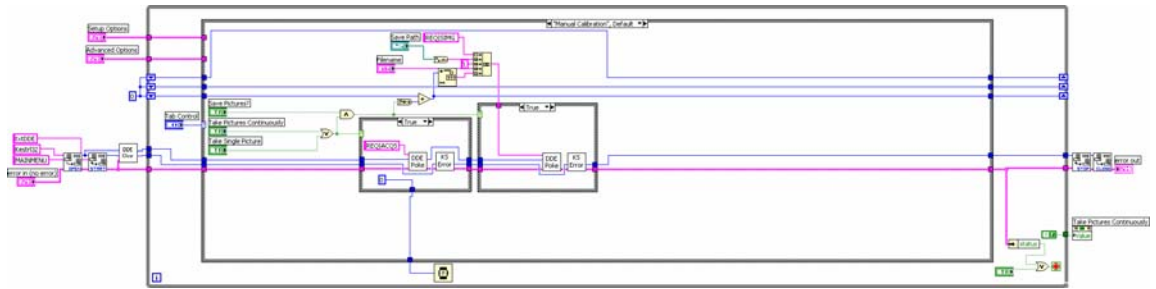


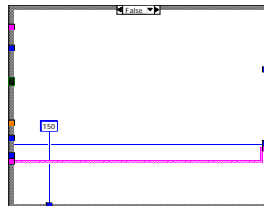
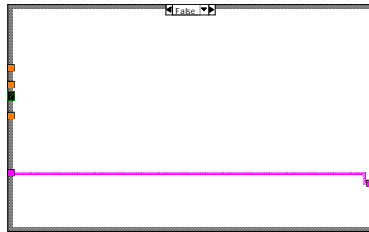
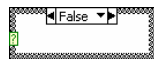
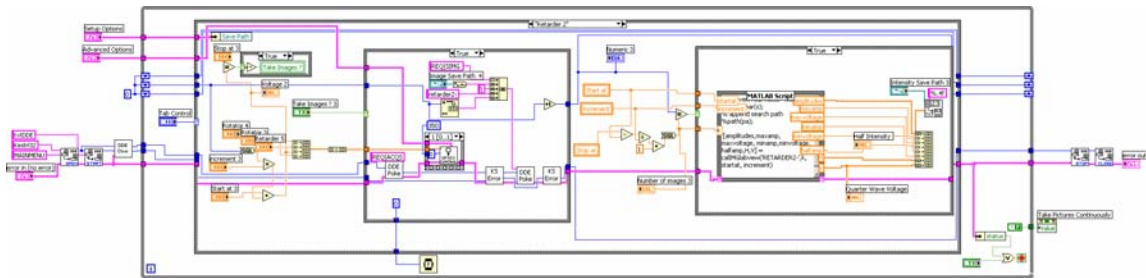
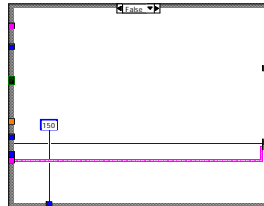
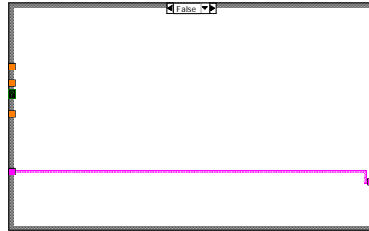
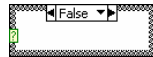
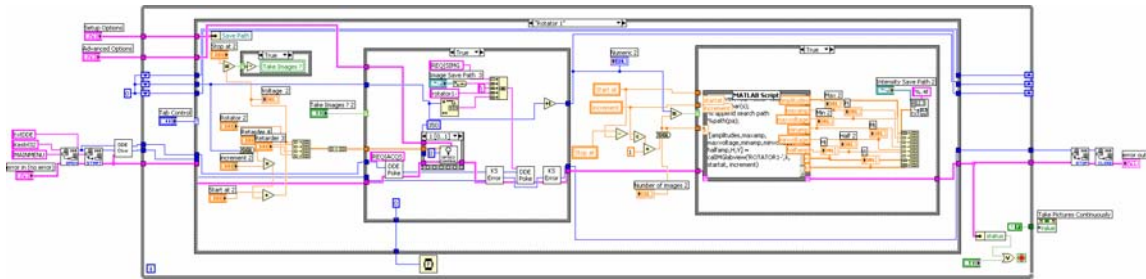


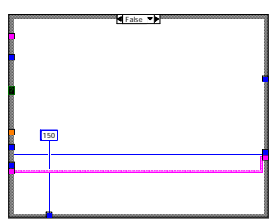
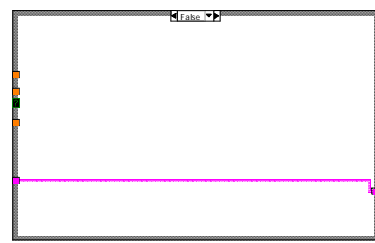
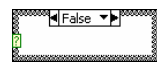
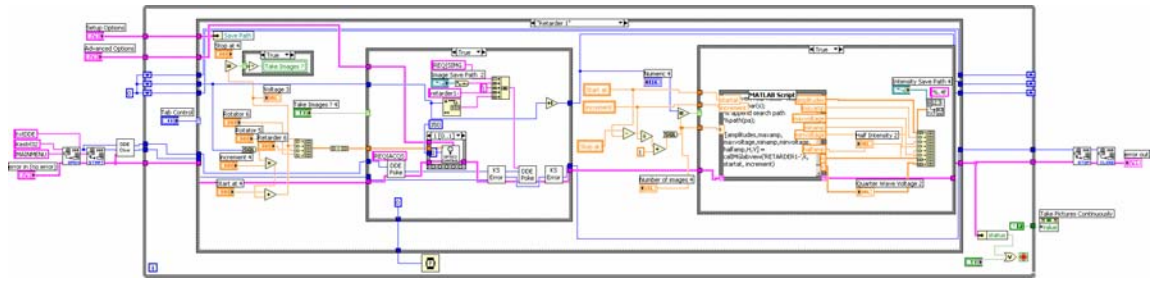


## Calibration Program











## APPENDIX H

### CART OUTPUT FOR IMAGES WITH EXPOSURE TIME OF 4 SECONDS

\*\*\* CART \*\*\*

COPYRIGHT, 1991-1995

SALFORD SYSTEMS, SAN DIEGO, CALIFORNIA, U.S.A.

02-15-2004 14:13

1500000 PREPROCESSOR 8-BYTE WORKSPACE ELEMENTS.

3000000 TREE BUILDING 4-BYTE WORKSPACE ELEMENTS.

BASIC WORKSPACE CLEARED.

VARIABLES IN SYSTAT-FORMAT RECT FILE ARE:

M11TEN	M11TWENT	M11THIRT	M11FORTY	M11FIFTY
M11SIXTY	M11SEVEN	M11EIGHT	M11NINET	M11MEAN
M12TEN	M12TWENT	M12THIRT	M12FORTY	M12FIFTY
M12SIXTY	M12SEVEN	M12EIGHT	M12NINET	M12MEAN
M13TEN	M13TWENT	M13THIRT	M13FORTY	M13FIFTY
M13SIXTY	M13SEVEN	M13EIGHT	M13NINET	M13MEAN
M14TEN	M14TWENT	M14THIRT	M14FORTY	M14FIFTY
M14SIXTY	M14SEVEN	M14EIGHT	M14NINET	M14MEAN
M21TEN	M21TWENT	M21THIRT	M21FORTY	M21FIFTY
M21SIXTY	M21SEVEN	M21EIGHT	M21NINET	M21MEAN
M22TEN	M22TWENT	M22THIRT	M22FORTY	M22FIFTY
M22SIXTY	M22SEVEN	M22EIGHT	M22NINET	M22MEAN
M23TEN	M23TWENT	M23THIRT	M23FORTY	M23FIFTY
M23SIXTY	M23SEVEN	M23EIGHT	M23NINET	M23MEAN
M24TEN	M24TWENT	M24THIRT	M24FORTY	M24FIFTY
M24SIXTY	M24SEVEN	M24EIGHT	M24NINET	M24MEAN
M31TEN	M31TWENT	M31THIRT	M31FORTY	M31FIFTY
M31SIXTY	M31SEVEN	M31EIGHT	M31NINET	M31MEAN
M32TEN	M32TWENT	M32THIRT	M32FORTY	M32FIFTY
M32SIXTY	M32SEVEN	M32EIGHT	M32NINET	M32MEAN
M33TEN	M33TWENT	M33THIRT	M33FORTY	M33FIFTY
M33SIXTY	M33SEVEN	M33EIGHT	M33NINET	M33MEAN
M34TEN	M34TWENT	M34THIRT	M34FORTY	M34FIFTY
M34SIXTY	M34SEVEN	M34EIGHT	M34NINET	M34MEAN
M41TEN	M41TWENT	M41THIRT	M41FORTY	M41FIFTY
M41SIXTY	M41SEVEN	M41EIGHT	M41NINET	M41MEAN
M42TEN	M42TWENT	M42THIRT	M42FORTY	M42FIFTY
M42SIXTY	M42SEVEN	M42EIGHT	M42NINET	M42MEAN
M43TEN	M43TWENT	M43THIRT	M43FORTY	M43FIFTY
M43SIXTY	M43SEVEN	M43EIGHT	M43NINET	M43MEAN

M44TEN M44TWENT M44THIRT M44FORTY M44FIFTY  
M44SIXTY M44SEVEN M44EIGHT M44NINET M44MEAN  
TYPE

BASIC WORKSPACE CLEARED.

RECORDS READ: 19

RECORDS WRITTEN IN LEARNING SAMPLE: 19

PRIORS SET EQUAL

CURRENT MEMORY REQUIREMENTS

TOTAL: 16007 DATA: 3059 ANALYSIS: 12948

AVAILABLE: 3000000

SURPLUS: 2983993

The data are being read ...

19 Observations in the learning sample.

File: angelanew.Systat

CART is running.

Tree 1 of 12

Tree 2 of 12

Tree 3 of 12

Tree 4 of 12

Tree 5 of 12

Tree 6 of 12

Tree 7 of 12

Tree 8 of 12

Tree 9 of 12

Tree 10 of 12

Tree 11 of 12

=====  
TREE SEQUENCE  
=====

Dependent variable: TYPE

Terminal	Cross-Validated	Resubstitution	Complexity
Tree Nodes	Relative Cost	Relative Cost	Parameter

1** 3	0.357 +/- 0.085	0.000	0.000
-------	-----------------	-------	-------

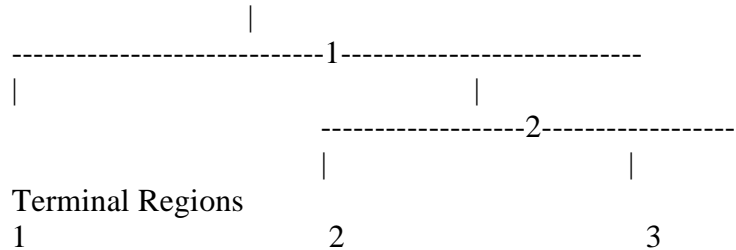
2 1	1.000 +/- 0.000	1.000	0.333
-----	-----------------	-------	-------

Initial misclassification cost = 0.667

Initial class assignment = 1

Tree 12 of 12

```
=====
CLASSIFICATION TREE DIAGRAM
=====
```



```
=====
NODE INFORMATION
=====
```

```

*      Node 1 was split on variable M11TWENT
**     A case goes left if variable M11TWENT <= 5450.000
* *    Improvement = 0.333      C. T. = 0.333
* 1 *
* *    Node   Cases   Class      Cost
**     1     19     1         0.667
*      -1     8     3         0.000
**     2     11     1         0.500
* *
8 11      Number Of Cases      Within Node Prob.
* *      Class Top Left Right      Top   Left   Right
* *      1   4  0  4   0.333   0.000  0.500
---*--- *      2   7  0  7   0.333   0.000  0.500
| | * *      3   8  8  0   0.333   1.000  0.000
| | * *
| 1 | * 2 *  Surrogate      Split   Assoc.  Improve.
| | * *      1 M11SEVEN s   8142.000   1.000   0.333
| | * *      2 M11THIRT s   5981.000   1.000   0.333
| | * *      3 M11FORTY s   6450.000   1.000   0.333
----- *      4 M11FIFTY s   6920.000   1.000   0.333
          *      5 M11SIXTY s   7454.000   1.000   0.333
          Competitor      Split      Improve.
          1 M11THIRT      5981.000      0.333
          2 M11FORTY      6450.000      0.333
          3 M11FIFTY      6920.000      0.333
          4 M11SIXTY      7454.000      0.333
          5 M11SEVEN      8142.000      0.333

```

```

*      Node 2 was split on variable M11TWENT
* *    A case goes left if variable M11TWENT <= 15640.500
* *    Improvement = 0.333      C. T. = 0.333
* 2 *
* *    Node   Cases   Class      Cost
* *      2     11     1         0.500
*      -2     7      2         0.000
* *      -3     4      1         0.000
* *
7 4      Number Of Cases      Within Node Prob.
* *      Class Top Left Right      Top   Left   Right
* *      1  4  0  4  0.500  0.000  1.000
---*--- ---*--- 2  7  7  0  0.500  1.000  0.000
| | | | 3  0  0  0  0.000  0.000  0.000
| | | |
| 2 | | 3 | Surrogate      Split      Assoc.  Improve.
| | | | 1 M11SEVEN s 25219.000  1.000  0.333
| | | | 2 M11THIRT s 18404.000  1.000  0.333
----- ----- 3 M11FORTY s 20481.000  1.000  0.333
4 M11FIFTY s 21988.500  1.000  0.333
5 M11SIXTY s 23553.500  1.000  0.333
Competitor      Split      Improve.
1 M11THIRT      18404.000          0.333
2 M11FORTY      20481.000          0.333
3 M11FIFTY      21988.500          0.333
4 M11SIXTY      23553.500          0.333
5 M11SEVEN      25219.000          0.333

```

=====
  
TERMINAL NODE INFORMATION
  
=====

[Breiman adjusted cost, lambda = 0.333]

Node	N	Prob	Class	Cost	Class	Complexity		Threshold
						N	Prob	
1	8	0.333	3	0.000	1 0	0.000	0.333	
			[ 0.357]	2 0	0.000			
				3 8	1.000			
2	7	0.333	2	0.000	1 0	0.000	0.333	
			[ 0.357]	2 7	1.000			
				3 0	0.000			
3	4	0.333	1	0.000	1 4	1.000	0.333	
			[ 0.357]	2 0	0.000			

3 0 0.000

=====

MISCLASSIFICATION BY CLASS

=====

Class	Prior Prob.	-----CROSS VALIDATION-----			-----LEARNING SAMPLE-----		
		N Mis- Classified	Cost	N Mis- Classified	Cost	N Mis- Classified	Cost
1	0.333	4	0	0.000	4	0	0.000
2	0.333	7	5	0.714	7	0	0.000
3	0.333	8	0	0.000	8	0	0.000
Tot	1.000	19	5		19	0	

=====

CROSS VALIDATION CLASSIFICATION PROBABILITY TABLE

=====

ACTUAL CLASS	PREDICTED CLASS			TOTAL	ACTUAL
	1	2	3		
1	1.000	0.000	0.000	1.000	
2	0.714	0.286	0.000	1.000	
3	0.000	0.000	1.000	1.000	

=====

LEARNING SAMPLE CLASSIFICATION PROBABILITY TABLE

=====

ACTUAL CLASS	PREDICTED CLASS			TOTAL	ACTUAL
	1	2	3		
1	1.000	0.000	0.000	1.000	
2	0.000	1.000	0.000	1.000	
3	0.000	0.000	1.000	1.000	

```
=====
VARIABLE IMPORTANCE
=====
```

	Relative	Number Of	Minimum
	Importance	Categories	Category
-----			
M11TWENT	100.000		
M11THIRT	100.000		
M11FORTY	100.000		
M11FIFTY	100.000		
M11SIXTY	100.000		
M11SEVEN	100.000		
M44MEAN	0.000		
M22FORTY	0.000		
M22FIFTY	0.000		
M22SIXTY	0.000		
M22SEVEN	0.000		
M22EIGHT	0.000		
M22NINET	0.000		
M22MEAN	0.000		
M22THIRT	0.000		
M22TWENT	0.000		
M22TEN	0.000		
M21MEAN	0.000		
M21NINET	0.000		
M21EIGHT	0.000		
M21SEVEN	0.000		
M21SIXTY	0.000		
M21FIFTY	0.000		
M23TEN	0.000		
M23TWENT	0.000		
M23THIRT	0.000		
M24NINET	0.000		
M24EIGHT	0.000		
M24SEVEN	0.000		
M24SIXTY	0.000		
M24FIFTY	0.000		
M24FORTY	0.000		
M24THIRT	0.000		
M24TWENT	0.000		
M24TEN	0.000		
M23MEAN	0.000		
M23NINET	0.000		

M23EIGHT	0.000
M23SEVEN	0.000
M23SIXTY	0.000
M23FIFTY	0.000
M23FORTY	0.000
M21FORTY	0.000
M21THIRT	0.000
M13THIRT	0.000
M13TWENT	0.000
M13TEN	0.000
M12MEAN	0.000
M12NINET	0.000
M12EIGHT	0.000
M12SEVEN	0.000
M12SIXTY	0.000
M12FIFTY	0.000
M12FORTY	0.000
M12THIRT	0.000
M12TWENT	0.000
M12TEN	0.000
M11MEAN	0.000
M11NINET	0.000
M11EIGHT	0.000
M13FORTY	0.000
M13FIFTY	0.000
M13SIXTY	0.000
M21TWENT	0.000
M21TEN	0.000
M14MEAN	0.000
M14NINET	0.000
M14EIGHT	0.000
M14SEVEN	0.000
M14SIXTY	0.000
M14FIFTY	0.000
M14FORTY	0.000
M14THIRT	0.000
M14TWENT	0.000
M14TEN	0.000
M13MEAN	0.000
M13NINET	0.000
M13EIGHT	0.000
M13SEVEN	0.000
M24MEAN	0.000
M31TEN	0.000

M42NINET	0.000
M42EIGHT	0.000
M42SEVEN	0.000
M42SIXTY	0.000
M42FIFTY	0.000
M42FORTY	0.000
M42THIRT	0.000
M42TWENT	0.000
M42TEN	0.000
M41MEAN	0.000
M41NINET	0.000
M41EIGHT	0.000
M41SEVEN	0.000
M41SIXTY	0.000
M41FIFTY	0.000
M41FORTY	0.000
M41THIRT	0.000
M41TWENT	0.000
M42MEAN	0.000



## VITA

Angela Michelle Baldwin was born in Shreveport, Louisiana on February 21, 1980 to Debra and Tad Ryder. She attended elementary and middle school at Walnut Hill and high school at C.E. Byrd Math-Science Magnet in Shreveport, Louisiana. She graduated in the top 5% of her high school class in 1998. In the fall of 1998, she began Louisiana Tech University majoring in Biomedical Engineering. She was a member of the LA Tech cross country team her junior and senior year. During the summer of 2001, she worked as an engineering intern at Kennedy Space Center. She was able to see two space shuttle launches, one rocket launch, and a space shuttle landing. She was given tours of the space shuttles, the launch pads, the crawler, the international space station building site, and was able to meet several astronauts. She graduated with a Bachelor of Science in Biomedical Engineering in May 2002. She then came to Texas A&M in the fall of 2002 and worked in the Optical Biosensing Laboratory under Dr. Gerard Cote. She received her Master of Science degree in Biomedical Engineering in May of 2004.

Mailing Address: 14777 FM 2154

College Station, TX 77845

Permanent Phone Number: 318-512-9453